8-2019

Graphene-Based Nanomaterials in the Design of Nerve Conduits for Regenerative Medicine Applications

Richard Steiner
University of Tennessee, rsteine4@vols.utk.edu

To the Graduate Council:

I am submitting herewith a dissertation written by Richard Steiner entitled "Graphene-Based Nanomaterials in the Design of Nerve Conduits for Regenerative Medicine Applications." I have examined the final electronic copy of this dissertation for form and content and recommend that it be accepted in partial fulfillment of the requirements for the degree of Doctor of Philosophy, with a major in Comparative and Experimental Medicine.

David Anderson, Major Professor

We have read this dissertation and recommend its acceptance:

Mahdu Dhar, Stacey Stephenson, Alex Biris

Accepted for the Council:

Dixie L. Thompson

Vice Provost and Dean of the Graduate School

(Original signatures are on file with official student records.)

Graphene-Based Nanomaterials in the Design of Nerve Wraps for Regenerative Medicine Applications

A Dissertation Presented for the

Doctor of Philosophy

Degree

The University of Tennessee, Knoxville

Richard Conlin Steiner

August 2019

Dedication

To my Mother:

Lori Steiner

and my Father:

Henry-York Steiner

Acknowledgment

I would like to express my deepest gratitude to Dr. David Anderson, for his support and guidance during my 5-year tenure at the UTCVM. I would also like to thank Dr. Alex Biris for his guidance and the opportunity to work at the University of Arkansas Little Rock to provide material essential to the body of work presented here. I would like to thank Dr. Madhu Dhar and Dr. Stacy Stephenson for serving on my thesis committee and for their guidance and assistance in both the *In-vitro* and *In-vivo* experimental setups and executions. I would also like to thank the entire Regenerative Medicine group at the UTCVM for providing their input and assistance in my research. A great thanks also to Tom Masi at the UT medical center, Dr. Robert Donnell at UTCVM's department of histology, and David Harper at the UT Center of Renewable Carbon for their assistance towards my research. I would also like to express my appreciation to the COE/NIFA program thru the UTIA for providing funding for this work.

Abstract

Peripheral neuropathies are a debilitating problem in human and animal patients resulting in diminished the quality of life. The current gold standard methods for repair of critical size peripheral neuropathies have limitations that overall diminish the quality of life for patients. The use of nerve scaffolds composed of synthetic polymer-based materials to heal damaged nerves has become an attractive approach in regenerative medicine research. Studies have shown the biomaterial characteristics of graphene oxide to have potential in applications for regenerating damaged peripheral nerves. Studies have also shown that incorporating Mesenchymal Stem Cell (MSC) therapies into neural scaffold designs can significantly improve the quality of tissue healing as well. The hypothesis of this study is that a novel synthetic thin film composed of electro spun polycaprolactone (PCL) and modified with surface coating of Graphene Oxide (GO) and cultures of Human Mesenchymal Stem Cells (hMSC) will have the potential to regenerate a critical size peripheral nerve defect. The first objective studied the potential cytotoxic effect of graphene surfaces with different oxidative group saturation levels to rat adipose derived stem cell (rADSC) cultures. This objective also manufactured PCL materials of fibrous and smooth surface topographies using both electrospinning and polymer-drop techniques. The second objective assessed the *In-vitro* capabilities of GO surface modifications of both fibrous and smooth surface PCL material templates seeded with adipose derived hMSCs for materials effectiveness in supporting and guiding trans-differentiation of hMSC into a Schwann like cell lineage. The final objective involved the development of an approved critical nerve defect model in Rats to assess the *In-vivo* performance of electro-spun PCL films with GO surface modification and hMSC platform to stimulate nerve regeneration at a critical nerve defect. The degree of nerve regeneration was determined by exogenous detection of gait patterns in the rats during nerve repair and tissue identification/ measurements thru Histology sections. This study to date has shown that neural wraps composed of electro-spun PCL surface coated with GO can support the hMSC in both static and trans-differentiated forms and can stimulate nerve regeneration in a critical nerve defect rodent model.

Table of Contents

Chapter 1: Literature Review 1
1.1 Biomaterial for Biomedical Applications 2
1.1.1 Biocompatibility Assessment 2
1.1.2 Polymers 9
1.1.3 Nerve Conduits 13
1.2 Peripheral Nervous System 19
1.2.1 Peripheral Neuropathy 20
1.2.2 Endogenous Nerve Repair 22
1.3 Graphene 23
1.3.1 Biocompatibility 24
1.3.2 Graphene Neural Conduit Design 32
1.4 Stem Cell Therapy 33
1.4.1 Mesenchymal Stem Cell 34
1.4.2 Neural-Fate Pathways 35
1.5 Summary 38
Reference 39
Chapter 2: PCL Electrospin Film with GO Surface Modification as a Platform for hMSC 42
Abstract 43
2.1 Neural Wrap Manufacturing 44
2.1.1 Introduction 44
2.1.2 3D Fabrication of Neural Wrap 45
2.1.3 Graphene Family Nanomaterial Inclusion 46
2.1.4 Objective 47
2.2 Experimental Neural Wrap 47
2.2.1 Graphene Solution Preparation 47
2.2.2 Air Spray Surface Coating (24-Well Plate) 48
2.2.3 Electrospinning 49
2.2.4 Drop Coating 49
2.2.5 Rat/ Human ADSC Culture 49
2.2.6 MTS Assay 50
2.2.7 Calcein AM, Propidium Iodine Live Stain 50
2.2.8 Immunofluorescence 51

2.3 Results 52
2.3.1 MTS Analysis 52
2.3.2 Live/Dead Calcein AM Propidium Iodine Stain 53
2.3.3 Day 6 Immunofluorescence-Vimentin 54
2.3.4 Day 1 Immunofluorescence-S100β 56
2.3.5 Day 1 S100β Intensity 58
2.4 Discussion 59
2.4.1 Implication/Challenges 61
2.5 Conclusion 64
Reference 65
Chapter 3: Biometric Data Comparison Between Lewis and Sprague Dawley Rats 67
Abstract 68
3.1 Introduction 69
3.2 Methods 71
3.2.1 Tekscan VH4 Specifications 71
3.2.2 Gait Testing Protocol 72
3.2.3 Statistical Analysis 74
3.3 Results 74
3.3.1 Normal Gait Assessment 74
3.3.2 Gait Analysis: Ratio Temporal Parameters 75
3.3.3 Gait analysis: Force and Temporal Parameters 78
3.4 Discussion 83
3.5 Conclusion 86
Reference 88
Chapter 4: Critical Nerve Defect Model using Lewis Rat Subjects to Assess In-vivo Performance of PCL+GO+hADSC Fiber Neural Wrap 90
Abstract 91
4.1 Sciatic Nerve Transection Model 92
4.1.1 Introduction 92
4.2 Methods 94
4.2.1 Electrospinning 95
4.2.2 Animal Surgery 95
4.2.3 VH4 Pressure Sensing Mat Assessment 97
4.2.4 Histology 97

4.3 Results 97
4.3.1 PCL Neural Wrap Extraction 97
4.3.2 Gait Assessment of Lewis Rats During 12-Week Nerve Repair 98
4.3.3 Histology 104
4.3.4 Luxofast Blue Coverage/Myelin Diameter 105
4.4 Discussion 107
4.4.1 Implications/Challenges 109
4.5 Conclusion 111
Reference 113
Chapter 5: Conclusion 114
5.1 Final Remarks 115
Vita 117

List of Tables

Table 1.1 *In-vitro* viability assays 5

Table 1.2 Degrees of Cytotoxicity in the Agar Diffusion and Direct Contact Tests 6

Table 1.3 Degradation properties of synthetic biodegradable polymers 12

Table 1.4 Most current list of FDA approved neural conduit and wraps designs 15

Table 1.5 Design Criteria for Nerve Wrap and Conduits 16

Table 1.6 Nerve Injury Classification 21

Table 3.1 Ratio values for normalized temporal parameters 76

Table 3.2 Values for # of Stance, Gait time, Gait Distance, Gait Velocity, Gait Cycle Time, Cycle min 77

Table 3.3 Values based on specific limbs for both species 77

Table 3.4 Mean values statistical comparison between Sprauge Dawley and Lewis groups based on limbs 83

Table 3.5 Lewis mean value group comparison between limbs 84

Table 3.6 Sprague Dawley mean value group comparison between limbs 85

Table 4.1 Tekscan pressure mat raw data of mean temporal parameters 99

Table 4.2 Mean ratios of hind limbs mean 103

List of Figures

Figure 1.1 Ideal neural conduit design configurations (Physical and Biological cues) 18

Figure 1.2 Peripheral nerve anatomy 19

Figure 1.3 Endogenous peripheral nerve regenerative process 22

Figure 1.4 Intracellular toxicity pathways induced by GFNs 31

Figure 1.5 Current identified pathways for induction of MSC towards neural-like cells 37

Figure 2.1 Common horizontal electrospinning apparatus setup 45

Figure 2.2 Air spray setup for graphene coatings on 24-well plates 48

Figure 2.3 Rat ADSC MTS Analysis on Graphene Iterations 52

Figure 2.4 Calcein AM staining of hADSC cultures on graphene iterations 53

Figure 2.5 Day 7 Calcein AM average area coverage quantification 54

Figure 2.6 Day 6 1µg vimentin/well. Counter cytoplasm stain DiI and nuclear stain DAPI 55

Figure 2.7 Day 1 1µg S100β/well. Counter cytoplasm stain DiI and nuclear stain DAPI 57

Figure 2.8 Day 1 1µg S100β/well 5X magnification 58

Figure 2.9 S100β intensity profile for hADSC 59

Figure 3.1 Tekscan VH4 Pressure-mat system setup 72

Figure 3.2 Tekscan software display 73

Figure 3.3 Mean Body weight distribution between Lewis and Sprauge Dawley Rats 75

Figure 3.4 Ratio temporal and force parameter values 76

Figure 3.5 Analysis of variance of gait variables 78

Figure 3.6 Mean temporal parameter values 82

Figure 4.1 GO+PCL neural wrap repair of 10mm peripheral nerve defect in Lewis rat subject. 96

Figure 4.2 Week 12 neural wrap/conduit removal from Lewis rat subject's post-euthanasia. 98

Figure 4.3 Mean surface area coverage profile of left and right hind limbs for each group 101

Figure 4.4 Normalized mean body weight percentage profile of left and right hind limbs for each group 102

Figure 4.5 Week 12 MCOLL staining 104

Figure 4.6 ImageJ grey scaling of luxofast blue staining of myelin sheath 106

Figure 4.7 Luxofast Blue stain area coverage quantification spanning the neural defect at week 12 106

Figure 4.8 Myelin diameter assessment: tracking for presence of myelin tissue at week 12 107

Chapter 1: Literature Review

1.1 Biomaterials for Biomedical Applications

Our current definition of a biomaterial is a natural or synthetic material intended to interface with biological physiological systems to treat or replace tissue/organ functions in the body [1]. Biomaterials are an essential component that must be incorporated into the design of medical devices so that when such devices interact with surrounding tissue/extracellular matrix (ECM) they stimulate the surrounding native tissue to behave in either a state of regenerative potential or an inert homeostasis. The effectiveness of a biomaterial to stimulate tissue into a regenerative state is based on the materials ability to support proliferation, migration/orientation, and differentiation of cells while ensuring that material structural failure, foreign body signaling, and toxicity are minimized. This can be further characterized by understanding how biomaterial properties like surface chemistry, surface topography, bulk porosity/geometry, and by-products created thru biological degradative processes can stimulate particular cellular chemical and mechanobiological pathways.

There is currently on going and rapidly expanding research in the field of biomaterials to understand how these characteristics of biomaterials can target specific regenerative cellular pathways to become active and how they could further enhance tissue regeneration. Such research has also been discussed for the design of biomaterial scaffolds for the application of regenerating severe peripheral neuropathies in the hopes of improving healing time and the quality of regenerated peripheral nerve tissue [2].

1.1.1 Biocompatibility Assessment

The term biocompatibility is defined by D.F. Williams as *"the ability of a material to perform with an appropriate host response in a specific application"* [3]. The Science community has discussed throughout the conception of biomaterials as to how to characterize biocompatibility of a material and to what degree. Thru decades of research in both *In-vitro* and *In-vivo* models, the term can be subdivided into four individual categories of analysis that must be reviewed for a material to be labeled as biocompatible: toxicology, reaction to extrinsic microorganisms, mechanical effect, and cell-biomaterial interactions [4]. This has led to the development of both *In-vitro* and *In-vivo* methods for the assessment of each subdivision and the development of standardized procedures designed to insure these methods answer with high certainty the public concern that a device or material will improve and ensure public safety. The selection of *In-vitro* methods should consider the type of biomaterial and biological components being assessed for cytotoxicity to determine any potential toxic mechanisms or material property effects due to reaction with the assays involved that could give null or false readings. Most of these procedures are standardized by international agencies such as the International Organization for Standardization (ISO) section 10993 *"Concerning Biological Evaluation of Medical Devices"* and the American Society for Testing and Materials (ASTM)

while other agencies will regulate or enforce these standards such as the United States Food and Drug Administration (USFDA) Code of Federal Regulations (CFR) *Cha 1- Subchapter H* [5].

1.1.1.1 *In-vitro* Models

The evaluation of cytotoxicity in biomaterials can be simplified by observing how target cells or tissue will react in direct or indirect contact with biomaterials. If, under controlled conditions, cells react to the material with normal cell behavior and function such as cell adhesion, proliferation, migration, and differentiation we can conclude that the cell's physiological system is normal or homeostatic. However, if under these same conditions' cells react with behaviors indicative of cell stress, or cell death we can conclude that the material can induce some toxic or stressful effect on the cells. *In-vitro* models have a distinct advantage due to the methods employed and the environments that can be controlled. Under controlled laboratory conditions, specific variables related to cell-material interaction cytotoxicity can be analyzed under reproducible and sensitive conditions. The methods utilized are therefore more precise, accurate, and reproducible to strengthen statistical models. *In-vitro* methods can result in both qualitative and quantitative data. Qualitative methods assess the state of cellular health by evaluating the morphology of cell lines after exposure to the material and grading the health of cells based on the amount of cell death, cytoplasmic granule formations, and the percentage of cells non-adhered to the material. Quantitative methods determine the number of viable cells based on the presence of nucleic acid, metabolic by-products, or the expression of surface adhesion markers. These methods follow ISO standards under section 10993 part 5 which stipulates the different methods for collecting cytotoxicity data *In-vitro* and can be further subdivided into more specific methods of cell-material interactions [5, 6].

In-direct contact method involves either Agar or Filter Diffusion Tests. In both cases, a monolayer cell culture is grown in a culture environment while the physical biomaterial is placed in the same culture environment but is separated by an Agarose gel or cell filtration film as a barrier diffusion model. Over a designated period of culture, the material might diffuse compounds through the Agar membrane into the culture environment where it will make direct contact with the cell line. The purpose is to observe whether the cell lines can be induced towards a cytotoxic state due to direct exposure to potentially toxic material/protein loading components, nanomaterials and the agglomerates, and degradation agents that have leached from the material into the culture environment. The advantage of this system is that it is controlled to look at toxicity of cells specific to the leeched components from the materials, while qualitative and quantitative assays have their additional sensitivity, and accuracy parameters for identifying the specific toxic components responsible. The disadvantage is that it does not include toxic effects due to mechanical trauma, mechanobiological pathways, and cell-material interactions. This must be further analyzed with a direct contact model [5, 6].

Direct contact method involves direct contact of cells with the substrate with no separation of the cell monolayer to the biomaterial. The cell line is cultured in direct contact with the material which adds the variable of cell-material reactivity as a variable in cytotoxicity as well as the physicochemical variables specific to in-direct methods of cytotoxicity analysis. This creates a more complex model of analysis due to the higher degree of variables that can elicit a toxic response to the cell. This may make it more difficult to determine, with certainty, what the exact causes of cytotoxicity are and thus it is often necessary to confirm with additional testing. There is a concern in establishing standard testing methodologies for direct contact methods due to the nature of the materials (3D structure, Bio-resorption, Nano-topography, etc.) being tested and the different cell-lines used, adding even more potential variables of toxicity. The advantage of this method is that it is inexpensive, quick, and sensitive to these toxicity factors. If the material under a direct contact model does not elicit a cytotoxic effect to the cell-lines, then an initial conclusion would be that both the physicochemical and mechanical properties of the material are not cytotoxic to the cell lines. It should be further confirmed with repeated direct contact tests utilizing different cytotoxicity assays, but the potential statistical power of a single direct contact test performed correctly could conclude with high certainty whether a material is cytotoxic or not.

Extract Dilution (Elution) test involve suspending a sample of the material in a physiological solution that will extract elution solvents present in the material during the production phase while minimizing physical and chemical damage to the material as well as being compatible with the cell lines. Elution samples are then added to mono-layered cell cultures for 24-48 hours before toxicity assays are introduced. Very similar to the indirect contact method, this method will often result in a consistent toxicity pattern in cell culture due to minimal variability of elution solvents that are present in the material during production. While a good first approach to determine initial cytocompatibility of the material, it suffers the same disadvantages as an indirect method [5, 6].

Qualitative assessment of cytotoxicity in *In-vitro* studies involve the use of methods that are labeled as categorical variables to determine if cytotoxicity is present in cell-lines. This form of assessment will often use stains for viable and non-viable cells under fluorescent microscopy (FM) as a morphological indicator of cell health. Some of the more common viable stains in use involve high affinity towards specific cell structures such as the nucleotides within the nucleus, ATP and coenzymes in the mitochondria, permeability of the cell membrane, or cytoplasmic proteins/cytoskeletons. The intensity of the stain is correlated to the number of these structures present in the cell and combined with all other stained cells gives an overall indication of viability for the entire culture. Some examples of common viability assays utilized for *In-vitro* assessment of cell biocompatibility of are shown in **Table 1.1**.

Table 1.1 *In-vitro* viability assays

Viability Stains	Stain mechanism	Assessment (live cells/dead cells)
4`,6-diamidino-2-phenylindole (DAPI)	Fluoresces to covalent binding to DNA and RNA sections	Dead cells
7-Aminoacetinomycin D	Fluoresces to covalent binding of cytosine, and guanine sites of DNA	Dead cells
Calcein AM	Intracellular esterases excitation	Live cells
Propidium Iodine	Fluoresces to covalent binding of DNA and chromosome bases	Dead cells
MTT	Bulk tetrazolium salt dehydrogenase with NADPH formazan excitation	Live cells
WST-8	Soluble tetrazolium salt dehydrogenase with NADPH formazan excitation	Live cells
Thymidine [H3]	radioactive neucleoside binding to DNA sections	Live cells

Viability data can also be acquired by observing cell morphology and death or lysis under (FM), light microscopy (LM), or scanning electron microscope (SEM) to determine the viability of cells based on physical cell characteristics such as cell shape size, spreading, or density. Fluorescent stains can also be used for this type of assessment if stains are sensitive enough to differentiate between cell structures such as the use of nuclear stains coupled with cytoplasmic counter stains. Cells suspended in media that exhibit spherical shapes and minimal spreading on surface after 24-48 hours of incubation are often key indicators of apoptotic behavior, while viability stains will confirm whether cell integrity, DNA, and cytoplasmic environments are stable. This type of analysis is often categorized into a graded scale assessment of cytotoxicity. Based on previous research involving similar cell lines, these types of observations can establish a standard scoring system for cell cytotoxicity as the primary method for assessing the health of cells based on cell morphology alone[7]. Other qualitative methods involve real-time tracking of the cells by implanting fluorescent protein or radioactive isotope components or by labeling protein/gene sequence markers using fluorochrome labeled antibodies that bind to these specific markers, which can then be detected and quantified using spectrofluorometric analysis, scintillation to detect radio isotopes, or imaging software.

Table 1.2 Degrees of Cytotoxicity in the Agar Diffusion and Direct Contact Tests

Degree	CYTOTOXICITY	DESCRIPTION OF THE CYTOTOXICITY AREA
0	Absent	Absence of decolorization around or under the sample
1	Slight	Decolorization limited to the area under the sample
2	Mild	The size of the decolorization area from the sample is less than 0.45 cm
3	Moderate	The size of the decolorization area from the sample is less than 0.45 cm and 1.0 cm
4	Severe	The size of the decolorization area from the sample is greater than 1.0 cm, but does not involve the entire plate

Source: Vidal, M. N. P., and J. M. Granjeiro. 2017. "Cytotoxicity Tests for Evaluating Medical Devices: An Alert for the Development of Biotechnology Health Products." *Journal of Biomedical Science and Engineering* 10 (09): 431–43

Caution must be reserved when interpreting qualitative data as it will often introduce debate among experts as to what the cells' morphology indicates about the health of the cells. This also is present when comparing fluorescent stains to control parameters to determine if any specific toxicity pathway or mechanism has activated in the cell-line. This is particularly true for unspecified cell-lines that are capable of differentiating into multiple cell lineages and are thus capable of activating many different cytotoxicity pathways. It is important to model the design of *In-vitro* models to account for statistical errors based on the sensitivity and accuracy of the assays used by including enough replicates to overcome these limitations and to use experts to minimize the risk of bias observations. With a categorical data set, it is often difficult to determine whether a correlation exists between the material and variables for cytotoxicity as compared with continuous data typically acquired during quantitative tests. This is why it is suggested that qualitative data be complemented by quantitative data to detect specific cytotoxic pathways and determine if a correlation exists between the material variables and any cytotoxic mechanisms.

Quantitative assessment of cytotoxicity includes methods that can assess the specific factors related to cell or death. One of the most common forms of qualitative assessment of biomaterials in *In-vitro* models is to count the number of viable cells across a material surface (adherence and proliferation) under normal incubation conditions. Colorimetric assays are a common qualitative method for assessing the proliferation pattern of cells. This method involves the interaction of molecular compounds designed to fluoresce when exposed to the cell that change in response to activated cytotoxicity pathways such as specific enzymes, cell membrane permeability, cell adherence markers, ATP production, co-enzyme production, and nucleotides. The fluorescent labeled cells can then be quantified by counting the number of viable or non-

viable cells through a hemocytometer or flow cytometer. The light intensity of the fluorochrome density in the culture area can be determined using light spectroscopy calibrated to detect the specific fluorescence wavelength given off by the fluorochromes or by imaging software (ex: ImageJ) that can determine the optical properties of images taken by FM. This is possible only if the fluorochromes remain bound to the internal cell structures and minimal leaching out of the cell is observed. One of the most reliable and sensitive calorimetry assays in use today are tetrazolium salt-based assays that bind specifically to mitochondrial enzyme Nicotinamide adenine dinucleotide phosphate (NADP) which reduces tetrazolium salt into a fluorescent protein known as Formazan as an indicator of metabolic activity. Soluble formazan present in the surrounding media can then be detected using a spectrometer apparatus where the fluorescence intensity can be correlated to give an estimated number of viable cells that is within acceptable variations. Each of these assays are labeled as 3-(4, 5-dimethylthiazol-2-yl)-2, 5-diphenyltetrazolium bromide (MTT) with other iterations often removing the extra step of solubilizing the formazan proteins into the media solution (MTS, WST, XTT).

There are certain compromises that should be considered when choosing specific calorimetry assays. Often these assays consist of simple protocols that can be completed with little effort or knowledge in advanced laboratory operating procedures while also providing extremely sensitive and accurate data that correlates to the physical cell numbers. This presents possible limitations to their effectiveness around different cell lineages and any indirect methods of quantifying cell numbers [8, 9]. Some assays could be potentially toxic to certain cell lines and some use radioactive isotopes such as [H^3] Thymidine. Other indirect assays that bind to cellular enzymes and proteins will often not consider other factors that could activate these processes besides apoptotic pathways that will often lead to incorrect interpretation of the data [10]. Biomaterials can also impact the function of these assays by either activating the fluorescence as a false positive or preventing the reagent to bind to its specific target as a false negative. It is therefore essential that the limitations of one assay be supported by the advantages of another assay. This will insure that not only the data is interpreted correctly but will provide a standard guide for different cell-lines and biomaterials of compatible assays that can be utilized *In-vitro*.

Other methods involve detecting and quantifying more precise protein/genetic markers indicative of activated apoptotic pathways such as pro-apoptotic genes (bax, bak, cytochrome c) and anti-apoptotic genes (bcl-2, bcl-xl, Mcl-1). Western blot (WB), quantitative polymerase chain reaction (qPCR), and immunofluorescence (IF) are all methods capable of identifying apoptotic pathways initiated by a specific toxicity profile. The ratio of labeled surface markers, gene sequences, or proteins to the total image area or volume of cell culture can be quantified to indicate whether apoptotic behavior is present along one or more specific pathways.

1.1.1.2 *In-vivo* Models

While *In-vitro* models are a simpler model designed to control experimental variable interactions to determine correlations between them, they are incapable of recreating the same biological/ physiological environment that the implant will be exposed in living organism and there for the full spectrum of measurements of biomaterial performance cannot be assessed. *In-vivo* models are a more complex system in which two or more experimental variables including factors not included in the *In-vitro* model or considered relevant are now exposed. Inflammatory responses, degradation, biochemical kinetics, angiogenesis, and 3D tissue remodeling are complex processes that can only be fully studied *In-vivo*. This can make opportunities to observe and identify associations between variables difficult. The goal of an *In-vivo* model is to not only mimic the physiological conditions of the clinical case but to obtain meaningful data that can be measured and analyzed to find clinically relevant differences in material performance. It is prudent to observe overall physiological reactions and compare them to the current gold-standard (positive control variable) and clinical care to determine the efficacy of the implant towards its intended targeted therapy. This is an essential step in the process of evaluating an implant for clinical assessment and therefore requires careful selection of the model system and variables to control/access depending on the application of the implant and the current standardized guidelines described by both ISO and ASTM protocols for *In-vivo* testing.

The use of mammalian physiological systems can accurately represent most of the conditions that biomaterials will be exposed to under practical clinical applications and is therefore currently the best method for assessing how biomaterials will perform in a physiological system that is to a degree similar to that of a human system. There are variables of *In-vivo* models that we can tightly control such as anatomical location of implant site, size of the implant incision, species, gender, age, sample size, and methodologies for assessing material performance in an attempt to standardize animal models. The design of the model should narrow and strengthen cause/effect relationships of physiological events to the interaction of biomaterials. The controlled variables should also be focused towards answering specific questions related to the assessment of biomaterials in one or all domains of *In-vivo* biomaterial assessments (biocompatibility testing, bioactivity testing, or preclinical testing), while having the ability to translate these control parameters to more complex or different animal models.

In-vivo assessment of biomaterials for neural regenerative applications must therefore fall under the same system of standardization of *In-vivo* models. The number of *In-vivo* studies that have looked at repair of peripheral nerves using scaffolds has created a varied list of the most common animal model designs and methodologies for assessing nerve recovery in an attempt to standardize such studies. A study from 2012 performed a review of the literature on *In-vivo* neural regeneration models using nerve scaffolds and found

that the majority of these studies utilized rat models to assess scaffold performance followed by mouse and rabbits respectively. Of these studies, the majority create defects in the sciatic nerve with most defect gaps between 5-10 mm. The study also reports that within the studies using rat models the most commonly used method to assess nerve healing is through Quantitative Histology analysis, followed by nerve morphometric analysis, electrophysiology, and Immunohistology respectively. The number of animal parameters to consider and the degree of control between model variables has created problems among investigators in establishing a consensus on the best animal model design and methods for assessing nerve recovery.

1.1.2 Polymers

Polymers are a class of biomaterials that has seen an enormous surge in research and in the design of medical devices. Research on polymer incorporation in neural scaffold and conduit implant designs is well represented in the literature, going back as far as the early 1960s. Studies have shown that many polymers are capable of interacting with the native tissue with minimal toxicity. Polymers have a distinct advantage over other commonly used biomaterials in dynamic physiological environments in that they can be designed to incorporate multiple therapies into their design to further improve tissue regeneration success. Polymers can be easily handled and stored at low cost to the manufacture and customer. The methods for synthesizing polymers provide a unique opportunity for exploring a diverse range in polymer combinations and understanding how these new molecular structures impact their physical, chemical, and biological properties. Polymers have also shown an ability to successfully integrate with cells and tissue in *In-vitro*, *ex-vivo*, and *In-vivo* models while maintaining minimal inflammatory and foreign body responses over extended periods of time. Polymers can be further functionalized to express specific traits that are time dependent such as controlled degradation/ inert reactions, drug and protein delivery systems, mechanical integrity in response to thermal and mechanical responses. The traits of certain polymers would correspond to the definition of a biomaterial. Polymers as biomaterials can be organized into two distinct categories: natural and synthetic based polymers.

1.1.2.1 Natural Polymers

Natural polymers have a distinct advantage over other biomaterials due to their natural origin from physiological systems. Since these polymers are composed of organic molecules that are manufactured by physiological processes, they have a higher chance of success when interacting with *In-vivo* physiological systems such as immunomodulation, tissue interaction and reinforcement, and degradation. These polymers also are capable under specific physiological conditions to produce these materials in abundance which has a manufacturing advantage. There are a variety of natural polymers that are capable of being processed into scaffolds of different surface and 3D composite designs with the added benefit of being degraded over time.

Degradation occurs by both hydrolytic and enzymatic processes. Natural polymers are most often compatible with the host extracellular matrix (ECM) which is expected to improve scaffold bio-integration. Some of the most common natural polymers investigated for the development of scaffold designs are polysaccharides (PSA), and poly amino acid chains (PAAC).

(PSA) are a family of naturally occurring monosaccharides cross-linked together with glycosidic linkages (ether bonds) of both human and non-human origin. The most common examples of these types of materials used in biomaterial applications are chitosan, hyaluronic acid, fibrin/fibrinogen, cellulose, alginate/agarose, and dextran. These types of polymers are susceptible to biodegradation and are composed of functional bioactive sites that have been investigated for applications involving controlled drug release, improved cell/tissue interaction by modifying existing scaffold designs, and increased resistance from immune response.

(PAAC) are highly organized collections of either natural or synthetic amino acid chains making them mechanically versatile with little risk of activating adverse immune reactions. Some of the most common (PAACs) under current investigation are polypeptide chains such as elastin, collagen, and blood proteins such as albumin. Similar to PSAs, these constructs are very susceptible to biodegradation through hydrolysis and enzymatic degradation.

1.1.2.2 Synthetic Polymers

Synthetic polymers have been in great demand as an alternative to natural polymers when designing tissue scaffolds. While natural polymers have a higher success of positive bio-interaction with the surrounding tissue and are of a lesser risk of inducing toxicity, synthetic polymers have almost unlimited potential for synthesizing various forms of biomaterial designs without the need to harvest, sterilize, or decellularized native tissue. This makes synthetic polymers a more attractive alternative to natural polymers for creating universally compatible and market feasible scaffolds. The simple and cost-effective means of synthesizing these polymers and their co-polymer iterations allow for excellent quality control during the manufacture phase. Synthetic polymers have many different types of manufacturing and modification processes available for conduit designs. This provides opportunities for careful tailoring of biomaterial variables to improve polymer structure stability during long storage periods at room temperature and incorporation of specific functionality traits that can improve mechanical stability, bioprocessing, and bio-interactions in physiological systems. Such examples for manufacturing physical features include electrospinning, mold casting, gas or solvent evaporation, sputtering, and printing while surface modifications include covalent grafting, oxidation, plasma etching, and surface hydrolysis.

Synthetic polymers composed of α-ester-based functional groups are the most utilized material for designing synthetic polymer scaffolds with controlled biodegradation. These aliphatic polymers are more susceptible to hydrolytic, and oxidative degradation due to the hydrophilic regions of the ester groups reacting with polar molecules and reactive oxygen species (ROS) resulting in successful scission of ester bonds in physiological systems. This will often reduce the polymer chains into α-hydroxy acid monomers (ex: lactic acid, glycolic acid, carboxylic acid, hyaluronic acid (HA)) of minimal toxicity and removed through renal excretion. Examples of these types of aliphatic ester polymers include poly(lactic acid) (PLA), poly (L-lactic acid) (PLLA), poly(glycolic acid) (PGA), poly(lactic acid-co-glycolic acid) (PLGA), poly(ε-caprolactone) (PCL), poly(3-hydroxybutyrate-co-3-hydroxyvalerate) (PHBV), polydioxanone (PDS), polyethylene glycol (PEG) and certain forms of polyurethanes composed of ester and carbonate groups as isocyanates (poly(ester urethane) (PEU), and poly(carbonate urethane) (PCU)) [11–13]. These polymers are often labeled as hydrophilic which describes the ease in which water molecules can react to the polarizing regions of the polymer ester-chains. In the presence of oxidative redox reactions these hydrophilic regions can become more polarized to be further susceptible to hydrolytic and enzymatic degradation. Oxidative reduction may take place in the form of redox reactions usually involving hydrocarbon section of polymer chains that are hydrophobic regions. This will involve oxidative species such as carbonyl, carboxylic, peroxide, and hydroxyl groups that will actively oxidize the material, thus polarizing the material to create hydrophilic regions [14]. Polymer degradation can also occur from enzymatic reduction in the form of both hydrolases and oxidoreductase pathways such as depolymerase, peroxidase, and mono or di-oxygenase.

The degree of access to these reactive regions in the polymer chain to enzyme, oxidative groups, and polar molecules will result in different polymer absorption profiles as described in **Table 1.3** as the most common degradation products and rates determined in these polymers. The degradation profile in these polymers are subject to scrutiny as the degradation rate can change by a large degree in physiological systems when considering dynamic temperature, ph., ROS, enzyme and polymer degradation product concentrations *In-vivo* [15,16]. Other forms of biodegradation such as chemical functionalization, light exposure, microbial interaction, mechanical stimulus, sterilization techniques, and architectural modifications to the material should be considered as they can also have a significant effect on the degradation profile of biodegradable polymers [15,17].

Table 1.3 Degradation properties of synthetic biodegradable polymers

Polymer	Degradation product	Degradation period (months)	Reference
PLLA	L-lactic acid	6-24	Garlotta, 2001; Zilberman et al., 2005; de Tayrac et al., 2008; Armentano et al., 2010
PGA	Glycolic acid	3-6	Wen and Tresco, 2006; Armentano et al., 2010
PLGA	D, L-lactic and glycolic acids	3-12	Lu et al., 1999, 2000; Armentano et al., 2010
PCL	caproic acid	18-36	Nair and Laurencin, 2006; Pena et al., 2006
POE	cyclohexane dimethanol propionic acid 1,6 hexane diol pentaerythitol dipropionate Pentaerythitol	6-34	M.S. Tatlor, 1994
PHBV	crotonic acid butyric-2 isopropyl-2	6-39	Muhamad et al., 2006 Xiang et al., 2016
PDS	glycoxylate glycine	6-12	Ray et al., 1981
PEG	peroxides glycolic acid monoalkyl ethers ethylene glycol	9-18	Guo et al., 2012 Webb et al., 2013 Andersen et al., 1999
PEU	hyaluronic acid groups Urea Urethane	N/A	Ravi et al., 2009 Blais et al., 1990 Szycher et al., 1991
PCU	Carboxylic acid groups Urea Urethane	N/A	Ravi et al., 2009

Source: M.E. Marti, A.D. Sharma, D.S. Sakaguchi, and S.K. Mallapragada. 2013. "Nanomaterials for Neural Tissue Engineering." In Nanomaterials in Tissue Engineering Fabrication and Applications, edited by A.K. Gaharwar, S.Sant, M.J. Hancock and S.A. Hacking, 275–300. 56. 1518 Walnut Street, Suite 1100, Philadelphia, PA: Woodhead Publishing Limited.

Additional Table content added by the Author

The other category of synthetic polymers is characterized as non-degradable, biostable carbon chains that are able to resist hydrolytic, oxidizing, or enzymatic processes due to the stable configurations of the carbon bonds and prevention of access to the sensitive polar regions of the polymer structure. This labels these polymers as hydrophobic which describes the difficulty in which polar molecules can react to the polarizing regions of the polymer chain, resulting in extremely slow or negligible absorption profiles that are often characterized as having inert reactions to physiological systems. Such examples include Polytetrafluoroethylene (PTFE) with carbon-carbon bonds surrounded by stable fluorine atoms, or poly (vinyl alcohol) (PVA) with carbon-carbon bonds surrounded by stable hydroxyl groups. Polyurethanes (PU) are most often utilized in inert or biostable medical device applications. By selecting specific polymers that can be used as soft segments (polyols) and hard segments (diisocyanates) the creation of biostable urethane and block chains can be created with mechanical ratios between stiffness and elasticity. PU can be tailored to be more biodegradable by introducing ester-based polyols for the soft segment component such as PLA, PGA, or PCL resulting in a variety of different biodegradation profiles.

These polymers are categorized under FDA regulations as non-degradable polymer substrates that are highly resistant to bio-resorption making them overall inert to cell/tissue interactions and highly resistant to immunomodulation processes *In-vivo*. This makes inert polymers excellent for blood or cerebral fluid contact, mechanically intensive, or drug delivery applications. However, this presents limitations with successful integration with target tissues and the potential for foreign body reactions due to the inability of cell/tissues to recognize the material as a native material making long duration use of these materials *In-vivo* difficult.

1.1.3 Nerve Conduits

The development of neural scaffolds has been researched as a potential solution to improving the quality of nerve tissue regeneration over extended regeneration distances. Both natural and synthetic polymer scaffolds by themselves still underperform when compared to the current gold standard for PN defects greater than 3 cm. To address this challenge, many studies have begun to look at combining multiple TE techniques together in polymer scaffold designs such as stem cell support, anisotropy surface architecture, and surface coatings to improve the limitations of synthetic scaffolds [18]. The majority of these *In-vivo* studies show a significant improvement in neural repair, with successful bridging of neural defects up to 3 cm in length being reported. A current gap in neural scaffold development is determining the optimal biomaterial design that can facilitate peripheral neuron and Schwann cell adhesion and orientation that is biomimetically similar to the surrounding (ECM) but remains structurally stable over long durations of implantation. This involves investigating the potential cytotoxic and neuro-regenerative effects with different conduit materials and their different design/functionalities thru *In-vitro* and *In-vivo* assessment.

The goal of which is to create a material engineered to a specific design that will maximize neuro-regenerative output in clinical cases. The following section will highlight techniques investigated in the design of nerve conduits and the current observations regarding their potential for regenerating peripheral nerves compared with the quality expected of the current gold standard (autologous graft).

Materials investigated for the development of neural conduits have consisted of both natural and synthetic materials. Natural materials as structural components in neural scaffold designs have focused primarily towards polysaccharides of both human and non-human origin. Currently type 1 collagen and small intestinal submucosa-based scaffolds are the only FDA approved natural material nerve scaffolds available. Synthetic materials that have currently been explored for potential in neural scaffold designs include silicone, ceramics, carbon-based, and polymer materials with few polymers being FDA approval for use in clinical applications of severe neuropathies (PVA, PGA, PLCL).

The vast majority of peripheral nerve scaffolds have designs that are rigid hollowed-out tubes or films wrapped into tubular structures of varied lengths and sizes as needed to bridge the defect site. This type of design is most effective in bridging the two PN ends across the gap with minimal tension. The concept is to fully encapsulate the site of injury for more controlled guidance of nerve healing. Such encapsulation provides opportunities for more direct appliance of targeted therapy techniques such as culturing support-cells to the interior scaffold structure, mechanical and physical ques from tissue interaction with the scaffold material, and controlled drug elution/ transport. Over the years, neural scaffolds have undergone extensive design changes that now incorporate components that are specifically designed to further stimulate controlled nerve growth by careful selection of material properties, geometric and surface features, and the ability to integrate with surrounding tissue resulting in higher rates of successful nerve rehabilitation outcomes. The current market of FDA approved neural conduits and neural protectants/wraps composed of both natural and synthetic polymers are listed in **Table 1.4** [19].

Table 1.4 Most current list of FDA approved neural conduit and wraps designs

Available FDA approved nerve guide conduit devices

510K approved	FDA clearance date	Product name	Material	Degradation	Diameter	Length	Company
K983007	22nd March, 1999/1995	Neurotube®	Polyglycolic acid (PGA)	3 months	2.3-8 mm	2-4 cm	Synovis® Micro Companies Alliance Inc., www.synovismicro.com
K011168	22nd June, 2001	NeuraGen®	Type I collagen	36-48 months	1.5-7 mm	2-3 cm	Integra Life Sciences Corp., www.integra-Is.com
K012814	21st Sept, 2001	Neuroflex™	Type I collagen	4-8 months	2-6 mm	2.5 cm	Collagen Matrix Inc., www.collagenmatrix.com
K012814	21st Sept, 2001	NeuroMatrix™	Type I collagen	4-8 months	2-6 mm	2.5 cm	Collagen Matrix Inc. www.collagenmatrix.com
K031069	15th May, 2003	AxoGuard™ Nerve Connector	Porcine small intestinal submucosa (SIS)	3 months	1.5-7 mm	10 mm	Cook Biotech Products, www.cookbiotech.com
K032115/K050573	10th October, 2003/4th May, 2005	Neurolac®	Poly (DL-lactide-ε-caprolactone); PCL	16 months	1.5-10 mm	3 cm	Polyganics B.V., ww.polyganics.com
K100382	5th August, 2010	SaluTunnel™ Nerve Protector™	Polyvinyl Alcohol (PVA)	Non-absorbable	2-10 mm	6.35 cm	Salumedica™ L.C.C., www.salumedica.com/

Available FDA approved absorbable nerve cuff/protectant wrap devices.

510K approved	FDA clearance date	Product name	Material	Degradation	Diameter	Length	Company
K002098	24th November, 2000/2001	Salubridge™	Polyvinyl Alcohol (PVA)	Non-absorbable	2-10 mm	6.35 cm	Salumedica™ L.C.C., www.salumedica.com/
K031069	15th May, 2003	AxoGuard™ Nerve Protector	Porcine SIS	3 months	2-10 mm	2-4 cm	Cook Biotech Products, www.cookbiotech.com
K041620	16th July, 2004	NeuraWrap™	Type I collagen	36-48 months	3-10 mm	2-4 cm	Integra Life Sciences Corp., www.integra-Is.com
K060952	14th July, 2006	NeuroMend™	Type I collagen	4-8 months	4-12 mm	2.5-5 cm	Collagen Matrix Inc. www.collagenmatrix.com

Source: Kehoe, S., X. F. Zhang, and D. Boyd. 2012. "FDA Approved Guidance Conduits and Wraps for Peripheral Nerve Injury: A Review of Materials and Efficacy." *Injury* 43 (5): 553–72.

1.1.3.1 Conduit Designs

The development and assessment of a variety of neural conduits and wraps has provided the foundation for what criteria should be considered when designing such devices to ensure that the device will perform at a level that meets or exceeds the clinical standards for acceptable peripheral nerve repair (autographs), while minimizing incidences of both mechanical and physiological failure during the course of repair. The current design criteria considered to be essential for successful neural conduit and wrap implementation is described in **Table 1.5** [20]. The majority of peripheral nerve conduit designs both on the market and under research investigation conform to a simple hollow cylinder structure. This design resembles the peripheral nerve anatomy to its most simple geometric shape making it easy to manufacture with minimal variations between completed products depending on the material used (natural or synthetic). Functionally it can fulfill the basic requirements expected of a neural conduit or wrap design for repair of critical defects. This includes bridging the two ends of the proximal and distal stumps, holding its shape and mechanical stability for the duration of nerve growth, allow for permeability of nutrients and waste from the repair site, and support neural cell adhesion and guidance. However, the most recent developments in both natural and synthetic neural conduits and wraps is that they must also incorporate both mechanical and chemical cues into the design to achieve the neural regenerative potential of autographs.

Table 1.5 Design Criteria for Nerve Wrap and Conduits

Ideal properties	*Description*
Biocompatibility	Material should not harm the surrounding tissues
Degradation/ porosity	Degradation rate should complement nerve regeneration rate; conduit should allow nutrient diffusion and limit scar tissue infiltration
Anisotropy	An internal scaffold or film should provide directional guidance
Protein modification/ release	Laminin/fibronectin coating for increased cellular adhesion; controlled/sustained growth factor release
Physical fit	Conduit should have a large enough internal diameter to not "squeeze" the regenerating nerve; wall thickness limited
Support cells	Schwann cells/stem cells capable of delivering neurotrophic factors to the site of regeneration
Electrically conducting	Capable of propagating electrical signals

Source: Nectow, Alexander R., Kacey G. Marra, and David L. Kaplan. 2012. "Biomaterials for the Development of Peripheral Nerve Guidance Conduits." *Tissue Engineering. Part B, Reviews* 18 (1): 40–50.

The majority of peripheral nerve conduit designs both on the market and under research investigation conform to a simple hollow cylinder structure. This design resembles the peripheral nerve anatomy to its most simple geometric shape making it easy to manufacture with minimal variations between completed products depending on the material used (natural or synthetic). Functionally it can fulfill the basic requirements expected of a neural conduit or wrap design for repair of critical defects. This includes bridging the two ends of the proximal and distal stumps, holding its shape and mechanical stability for the duration of nerve growth, allow for permeability of nutrients and waste from the repair site, and support neural cell adhesion and guidance. However, the most recent developments in both natural and synthetic neural conduits and wraps is that they must also incorporate both mechanical and chemical cues into the design to achieve the neural regenerative potential of autographs.

Mechanical modifications to neural conduits have focused primarily on maintaining mechanical stability and improving cell adhesion and guidance during nerve regeneration. Micro-scale modifications to date have involved internalizing parallel channels, filament, or ECMs that are more similar (biomimetic) to the peripheral nerve structure. These can be even further modified with the additions of nano-scale surface modifications to change the degree of cell adhesion, cell guidance, diffusion of nutrients and waste through the conduit, and degradation rate. Micro-channels and nano-groove pattern surface modifications appear to perform the best at adhering and guiding neural and Schwann cells [21]. Multipotent cell-lines such as neural and mesenchymal stem cells have also shown improved potential for neural differentiation on these types of architectural modifications as well. From a mechanical perspective, modifying the surface to increase the diffusion rate across the devices surface such as by creating porous or creating nanofiber or ECM meshes will increase the rate of degradation causing the conduit or wrap to fail at an earlier time. However, this can be negated by careful selection of the conduit material.

Chemical modifications are often used to either alter the bulk design of the conduit to attach and release organic compounds intended to enhance nerve healing, or surface alterations to improve cell-material interactions [22, 23]. Some of the most well-known forms of chemical alterations have been oxidizing or PEGylation to material surfaces, or adding nanoparticles designed to resist microbials and improve electrical conductance on the material. Biological modifications involve the attachment of either proteins, cell, or protein motifs that can better simulate the physiological conditions needed to enhance nerve regeneration. The most common techniques utilized have been to bind specific neurotrophic factors necessary for nerve regeneration to take place such as nerve growth factors (NGF), brain-derived neurotrophic factors (BDNF), and glial-derived neurotrophic factors (GDNF), or incorporate stem cell therapies to enhance nerve regeneration by modulating inflammation, releasing appropriate growth factors, or differentiation toward specific neural lineages (**Figure 1.1**) [2].

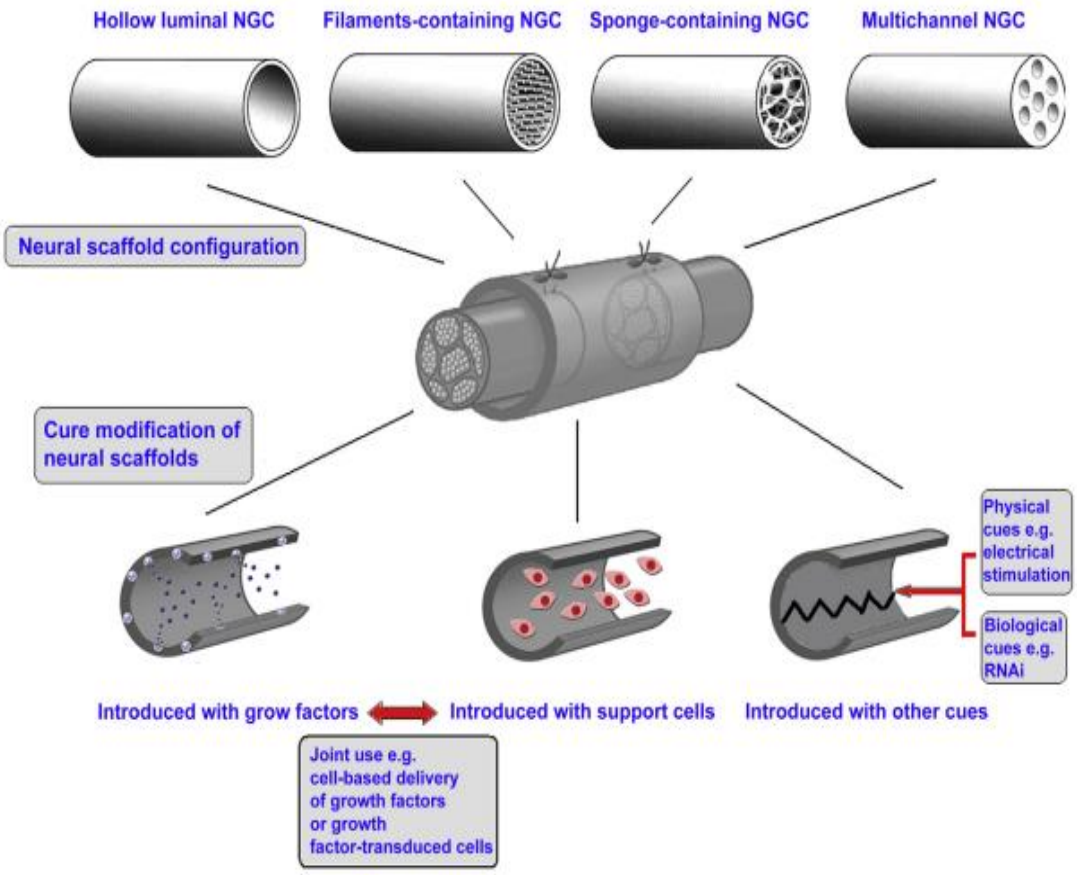

Figure 1.1 Ideal neural conduit design configurations (Physical and Biological cues)

Source: Gu, Xiaosong, Fei Ding, and David F. Williams. 2014. "Neural Tissue Engineering Options for Peripheral Nerve Regeneration." *Biomaterials* 35 (24): 6143–56.

1.2 Peripheral Nervous System

The Peripheral Nervous System (PNS) is a major component of the nervous system that serves to process and transport stimulus signal from peripheral sensory receptors to the Central Nervous System (CNS), and then relay the appropriate motor response to all appropriate target tissues remote from the CNS. The PNS can be subdivided into sensory nerves (afferent) and motor nerves (efferent). Efferent nerves can be further subdivided into autonomic and somatic motor divisions. Autonomic nerves control the motor responses of soft tissue components (i.e. soft muscle, cardiac muscle, gland secretion), while somatic nerve components are more responsible for skeletal muscle functions. In this work, we focus on the sections of the PNS that are distal to the spinal cord where the configuration and organization of the PNS in human models are similar and consistent with other mammalian models. All PNS distal to the spinal cord consist of neurons bundled together and divided into specific sections known as fascicles, which are wrapped around a thin sheet of endoneurium connective tissue composed of elastic and collagen fibers. These fascicles are then bundled together by perineurium connective tissue composed of reticular and collagen fibers. The fascicle regions combined with the neural blood vessels that support PNS are then held together using the outer epineurium connective sheet that tightly compacts the components into the peripheral nerve segment (**Figure 1.2**) [24].

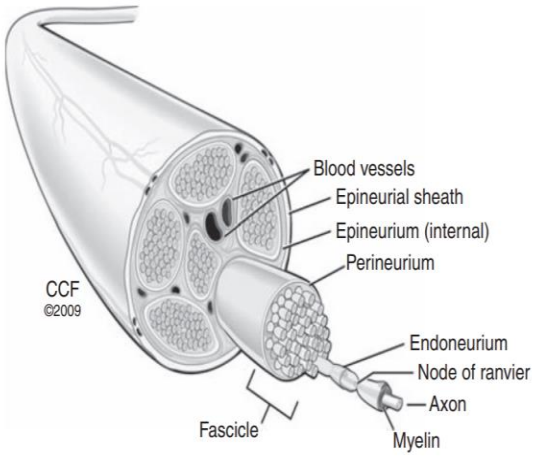

Figure 1.2 Peripheral nerve anatomy

Source: Siemionow, Maria, and Grzegorz Brzezicki. 2009. "Chapter 8: Current Techniques and Concepts in Peripheral Nerve Repair." *International Review of Neurobiology* 87: 141–72

Neurons are the primary cellular units of the PNS responsible for transducing chemical neurotransmitter signals into electrical signals that can propagate across the cell body to their intended location and vice versa. Dendrites will receive neurotransmitter signals from neighboring cells. This will cause Na^+ channels on the cell body to open, causing a graded potential to occur across the cell membrane at the region where the cell body integrates with the axon known as the axon hillock. If the summation of potential difference is great enough to succumb the potential threshold, the Na^+ channels on the axon membrane will depolarize to allow in-flow of Na^+ ions into the axon. Afterwards, the axon membrane will depolarize by out-flow of K^+ ions. This ion channel exchange will insure propagation of the membrane potential difference across the axon membrane until it reaches the synapse site at the opposite end of the axon. Membrane potential will then excrete the appropriate neurotransmitter that will bind to the post-synapse of the adjoining neuron thus continuing neuron communication thru both chemical and electrical synapses thru the physiological system until the signal reaches its intended target synapse.

The other primary cellular component of the PNS are the Schwann cells, whose primary role is to unsheathe the neurons and provide neurotrophic factors essential for neuron survival and regeneration. Most Schwann cells will layer themselves across the neural axon segments as a myelin sheath, ensuring that ionic potentials are guided and have fast conductance across the axons. non-myelinated Schwann cells are primarily used for production of neurotrophic factors necessary to maintain normal PNS functions, and repair of damaged nerves. The last cellular component are the stromal connective tissues that isolates the axons from the ECM and mechanically support the length of the axons. This is divided into three subsections of connective tissues as previously discussed (endoneurium, perineurium, and epineurium). During PNS repair, other connective tissues like fibrinogen and laminin will support Schwann cells during the reinnervation of the damaged nerve section (Bands of Bungner).

1.2.1 Peripheral Neuropathies

Peripheral neuropathy (PN) is a condition of the peripheral nervous system that currently affects over 20 million US citizens, with a prevalence of 3% in all trauma patients showing some form of PN. Most forms of PN can be attributed to mechanical, thermal, or infection damage. PN will often present itself with either swelling that blocks the neural conduction (neuropraxia), disruption of the axon or myelin sheath due to stretching or crushing stressor (axonotmesis), or tearing or complete separation of the nerve section (neurotmesis). The Sunderland Nerve Injury Classification Scheme (SNICS) is the most commonly used method for clinical evaluation of the severity of peripheral nerve injuries after physical traumas is induced. neurotmesis is the most severe type of peripheral injury where the nerve segment is completely transected cutting off the action potential to all sensory and motor functions. Often classified as a type 4 or 5 on the Sunderland nerve injury classification scheme (**Table 1.6**) [26–28].

Table 1.6 Nerve Injury Classification

Sunderland	Seddon	Features
Type 1	*Neuropraxia*	Damage to the local myelin only
Type 2	*Axonotmesis*	Division of intraneural axons only
Type 3	*Axonotmesis*	Division of axons and endoneurium
Type 4	*Axonotmesis*	Division of axons endo and perineurium
Type 5	*Neurotmesis*	Complete division of all elements including epineurium
Type 6	*Mixed*	Combination of types 2-4

Source: Grinsell D, Keating CP. Peripheral nerve reconstruction after injury: a review of clinical and experimental therapies. Biomed Res Int. 2014;2014: 698256

Patients with neurotmesis will often experience symptoms of both acute and chronic motor and abnormal sensory sensations that overall diminish the quality of life for people [29]. Almost all neurotmesis injuries require surgical intervention to insure the nerve heals properly to regain its functionality. Severe neurotmesis involves significant gaps (>2 to 3 cm) that require surgical placement of neural grafts to serve guidance of axons as they grow across the gap [30].

Currently, the gold standard for repair of severe neurotmesis is the use of nerve segments taken from the patients (autografts) [25, 31]. However, this method is limited in the degree of healing possible at the damage site [32]. Surgical protocols require precise matching and orientation of the graft at the two ends of the gap which is difficult and requires skilled microsurgery. The suturing of the graft can rupture or pierce the perineurium around the fascicles, causing scar tissue to form which can cause further problems at the site as iatrogenic peripheral neuropathy. The outcome of this strategy usually involves the following implications: donor-site morbidity, sensory loss, scarring at the donor site, neuroma formation, pain, and in the case of allografts long periods of host immunosuppression [27, 33]. The low quality of recovery for neurotmesis cases results in patients affected by chronic peripheral neuropathy symptoms. This contributes to an overall decrease in the wellbeing of the population and an increase in the health care costs utilized for repair and management of these symptoms. Currently, healthcare costs associated with PN injuries is estimated at around $150 billion annually. This presents a stressing need to research new alternative strategies to autografts for nerve repair that addresses these limitations while minimizing the onset of new ones.

1.2.2 Endogenous Nerve Repair

If the nerve segment sustains 20-30% of axon damage then collateral branching will most likely be the primary mechanism of recovery, however if over 90 % of the axons are damaged then axonal regeneration will be the most likely mechanism of repair [25]. The Wallerian degeneration process begins approximately 24-48 hours post time of injury and will last for a week depending on how severe the injury is. During this time, Schwann cells will begin to express pro-inflammatory and neurotrophic factors that will increase macrophage intrusion to the site and stimulate surrounding Schwann cells to further activate appropriate neurotrophic growth factors or to differentiate prolific Schwann cells to remove cellular debris and break down the nerve segment at both proximal and distal ends until the closest stable neuron body is reached in a process known as Wallerian- degeneration [34]. The result is a proximal and distal nerve stump created by granulation of Schwann cells that concludes the Wallerian degeneration step. The next step is axonal regeneration which first breaks down the nerve stumps thru a form of apoptosis which sees a large uptake in Ca^{+2}. At the same time, non-myelinating Schwann cells will migrate and orient themselves on laminin and fibronectin chains with the endoneurial tubes at the distal end to create a tubular banded structure known as the bands of Bungner. These non-myelinating Schwann cells continue to promote axon regeneration by secreting neurotrophic factors that will promote growth cone formation, filapodia probing, and stimulate pro-myelinating Schwann cells to orient themselves into myelin sheaths. This will continue until the regenerating axon growth cone reaches and assembles with the distal nerve section for complete reinnervation to take place. (**Figure 1.3**) [35].

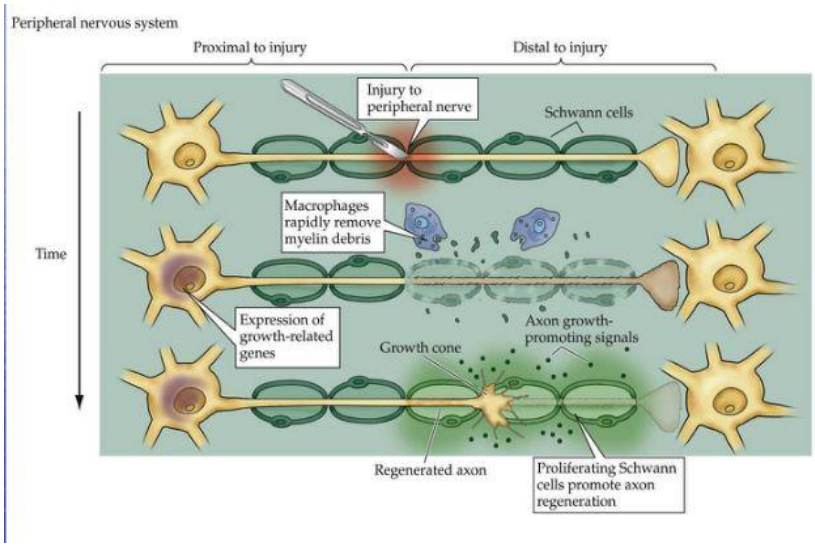

Figure 1.3 Endogenous peripheral nerve regenerative process

Source: Dale Purves, G. J.-S. (2008). Neuroscience. Sunderland MA: Sinauer Associates Inc.

The chance for successful reinnervation to take place with this form of nerve healing is depended on the severity of the injury itself. We can determine this by assessing if the endoneurial tubes are intact, the length of the defect, and the presence of lesion or scar tissue. In the case of neurotmesis injuries with critical size defects the chances of successful reinnervation are practically impossible without surgical intervention. The difficulty is being able to maintain a stable Band of Bunger structure which becomes much less stable as the defect size increases. This makes it difficult to guide axonal growth and often it will lead to loss of nerve functionality due to scar tissue formation and misalignment of axon bundles to the appropriate distal axon bundles. Another issue to consider is the amount of time it will take for full reinnervation to be complete for end organ functions to return. While some sensory neuron end-plates can last for many years before succumbing to atrophy, motor neuron end-plates begin to undergo atrophy in 3 weeks post injury and can last for up to a year before irreversible damage to the endplate incurs leading to complete loss of muscle function. The need to create stable neural scaffolds for prolonged stability and axon guidance is therefore apparent in order answer these limitations that are apparent in endogenous repair of critical neural defects.

1.3 Graphene

Graphene in its pristine form (PG) is a continuous SP2 Hybridized carbon film one atom thick, with carbon atoms organized in a hexagonal lattice configuration that resembles a honeycomb structure. The carbon atoms lateral to each other are held together by both single and double covalent bonds, while all atomic bonds perpendicular to the film are weak Van Der Waals forces. The configuration of the carbon atoms gives the material a unique conductance, mechanical, and bonding profile when combined with organic-based compounds that rivals other competing materials. The usage of Graphene Family Nanomaterials GFN's has been used primarily as an additional component to improve the mechanical, thermal, and electrical conductance of medical devices used in research. However, GFN's have been discussed to have potential in cell integration and differentiation of numerous cell lines much of which has not been fully understood to date. This has naturally led to the discussions of whether GFNs might have potential as a conduit platform to assist in the regeneration of damaged tissue *In-vivo*. Research to date would indicate that GFNs can be constituted as a biomaterial that in both *In-vitro* and *In-vivo* assessments has shown to be capable of supporting positive tissue regeneration for a variety of different tissue phenotypes while retaining acceptable biocompatibility traits over extended periods of time. This section discusses the current findings for carbon–based materials as a potential biomaterial option and its potential as a component in the design of neural scaffolds.

1.3.1 Graphene Biocompatibility

Carbon based materials have been investigated as a component for implanted medical therapies for more than half a century, and in this time have resulted in our further understanding of the properties of carbon and how they interact with carbon atoms and organic compounds resulting in the prodigious development of different carbon-based biomaterials to date. *In-vitro* studies on GFN coated substrates have consistently shown evidence to support that GFNs can act as a bioactive surface coating that can support the adhesion and maturity of a variety of cell-lines, including pluripotent cell-lines. In this section we will focus on the primary evidence to support GFN biocompatibility involving its potential for stable adhesion of cell lines, and its niche properties for controlled differentiation of pluripotent cells.

1.3.1.1 Adhesion

Adhesion of cells to a biomaterial surface is a critical event needed for successful application of biomaterial therapies. Successful adhesion of cells to any biomaterial surface can be characterized as the integration of a cell to the extracellular matrix, bioactive surface, or neighboring cells present on the material surface. This is essential for cells to stimulate a positive regenerative environment by regulating correct cell communication, mobility, differentiation and stability. Previous *In-vitro* studies have assessed the surface characteristic of different GFN's and have found that they are capable of absorbing cells lines of both immortal and multipotent cell lines in the form of electrostatic attraction, integrin binding, and focal adhesion binding pathways. The degree of adhesion varies based on the surface characteristics of GFN such as particle size, topographic features, geometric configuration, surface potential, and molecular bonding sites of the GFN surface. GFN surfaces can be modified for specific protein and cell adhesion profiles in a number of ways depending on the intended function of the device. Such alterations create additional protein anchors and changes to the biomaterial zeta potential that are most ideal for cell adhesion and ECM proteins absorption. *In-vitro* cell adhesion studies involving graphene oxide (GO) coated films have shown the potential for absorption of adhesion-specific proteins on the surface of biomaterials when placed in plasma and serum conditions. One study reported *In-vitro* to yield 25% protein absorption from a specified volume of serum on GO surface coated films compared to 8% absorption on Pristine Graphene coated surface films of similar surface area. The majority of these studies have found that exposing GFN's of different iterations to different protein solutions will create different protein absorption profiles allowing for the design of specific biomaterial protein coronas that can potentially improve the adhesion, communication, and mobility behavior specific cell lineages.

Studies have also found that GFN's has the potential to minimize the adhesion of specific cells that could potentially impact the speed and quality of tissue regenerated. As noted in the previous paragraph, non-adhesion of specific cell lines can also be tailored by altering the surface properties of GFN materials. Thru surface modifications, GFN surfaces can minimize the adhesion of microbials, granulation and fibrous tissue, platelets, and lymphocytes specific to foreign body reactions. Studies have found that modifying the surface of GFN's have improved antibacterial resistance by modifying the surface with antibacterial nanoparticles or altering the lateral dimensions and surface area of carbon-films. Common nanoparticle modifications to Graphene surfaces include Silver (Ag) Gold (Au) Titanium oxide (TiO) and zinc oxide (ZnO), while Graphene films of higher surface areas have less toxicity towards microbials compared to films with lower surface area[36–38]. Chemical modifications such as PEGylation or oxidation have been shown to decrease the proliferation of macrophages and lymphocytes, giving GFN's the ability to minimize foreign body reactions.

1.3.1.2 Differentiation

Both *In-vitro* and *In-vivo* studies have consistently shown that GFN's have the ability to not only support multipotent cell lines conducive to improved tissue healing but also induce these cell lines towards specific differentiation phenotypes simply by integrating with the material surface or internalization of the material into the cell. Interest has been focused primarily on the ability of GFN's to differentiate cells with multipotency potential (progenitor cells). While the specific pathways and cellular processes involved with differentiation of stem cell integration with GFN are still misunderstood, the most current research into GFN have been able to narrow down certain stem cell niches most likely responsible for differentiation towards specific lineages, giving researches an idea of what pathways and cellular processes to further investigate.

GFN surface properties have been found to be a key component in guiding differentiation of specific phenotypes in stem cells. This involves not only the interaction of stem cells with the biochemical properties of the material (cell-cell, ECM mesh, surface proteins) but also the physical features such as surface stiffness, topography, surface patterning, and orientation[39,40]. It has been established in previous *In-vitro* studies that biomaterials with surfaces of higher modulus (greater stiffness) have a higher capacity for osteogenesis in cells of mesoderm origin while surfaces of lower modulus have a higher capacity for neurogenesis in cells of ectoderm origin. This is most likely regulated by specific integrin and focal adhesion kinase (FAK) mechanotransduction pathways designed to differentiate between mechanical stresses brought on by cell interaction with the surface. The addition of GFN as a surface coating will often modify the surface to be stiffer which has resulted in a higher density of mesoderm origin cells to differentiate toward osteogenesis by simply being in contact with the GFN surface. Studies have also found

that specific surface patterns can not only initiate cytoskeletal remodeling but are also important in guiding differentiation of cells towards specific lineages through specific mechanotransduction pathways (anisotropy)[39]. Studies have shown how PG coatings patterned in parallel line patterns can initiate osteogenesis in hMSCs, while surfaces coated with GO in a grid pattern array are able to stimulate a higher yield of hMSCs to differentiate towards neural-like lineages than without said pattern. This is further supported by studies that have shown ectoderm origin cell lines to differentiate towards neural lineages when adhered to GFN surfaces.

Chemical stimulation by GFNs to guide specific differentiation in multipotent cell-lines has been investigated with clear indications that different GFNs exposed to different multipotent cell-lines will result in different neural phenotype outcomes. Many of these studies have found that when neural stem cells (NSC) are exposed to simple GO or rGO films that they will naturally differentiate towards glial derived tissue, while PG and carbon nanotubes (CNT) do not elicit any neural potential at all. However, when GO or rGO films are exposed to embryonic stem cells (ESC) they differentiate towards neuron derived tissue instead. There is a clear need to further study these interactions as we do not yet fully understand the exact stimulant or pathways responsible for neural differentiation in these multipotent cell-lines. It is also not clear as to how other factors involved in peripheral nerve repair will impact the differentiation of multipotent cell-lines *In-vivo* (Co-seeding multipotent cell-lines with Schwann cells and macrophages, presence of proinflammatory and growth factor compounds, etc.).

While guidance of neural differentiation can be controlled to some degree by adding GFN's it is still difficult to determine what pathways are being regulated by the material and whether or not complete differentiation has occurred, and if so, identifying what phenotype the cell has differentiated towards. In most cases, the material will only achieve partial differentiation in the cells, resulting in only a few of the traits required to ID a particular neural phenotype to express. These cells are often labeled as neural-like cells instead and thus we cannot expect them to provide the same form of repair expected of true neural cells. The best indications for the type of chemical stimulus that GFN's will induce in multipotent cells is from the results indicated in toxicity studies. Toxicity studies have consistently found that GFN's can support multipotent cell-line growth and mobility that is essential for neuron and glial transport and spreading. It is also known that certain GFNs will induce oxidative stress due to interference of normal metabolic activities that will then activate inflammatory and apoptotic pathways. These pathways have been found to also be present during endogenous repair of peripheral nerves, particularly when digesting, guiding, and differentiating Schwann cells during the early phases of repair [41]. If GFN's can stress cells to a threshold that will releases pro-inflammatory and apoptotic signals into the ECM, then it could

potentially further stimulate neuron and Schwann cells towards regenerative behaviors or guide multipotent cells towards a specific neural-like phenotypes.

The biocompatibility of GFNs towards different cell lines and the potential to co-functionalize with other therapeutic techniques has created interest in incorporating it as a structural component or surface coating in 3D neural conduit designs. The toxicity of Graphene in physiological systems is still under investigation due to the current literature that supports the presence of cytotoxic behaviors and varying bio distributions of different graphene iterations in specific biological environments. It is also clear that there is still insufficient data to make conclusions on the cellular mechanisms related to cytotoxicity when graphene interacts with native cells. Current toxicity studies have identified specific properties of graphene-based materials that are most responsible for influencing toxicity in both *In-vitro* and *In-vivo* systems.

1.3.1.3 Concentration

Numerous studies have shown that GFN have a dosage-dependent toxicity effect. The concentration of GFN attached to the cell membrane and/or taken up by the cell through endocytosis is correlated to increased cellular stress causing activation of specific Apoptosis/Necrosis, and inflammatory cellular pathways. Similar studies have also looked at different aspects of cell stress with respect to GFN concentrations, such as metabolic stressors, genotoxicity, and cell membrane disruption. *In-vitro* studies that looked at varied concentrations of different GFN iterations have found that cell viability will decrease as concentrations of GFN increase. The concentration of GFN particles needed to observe cell death varies based on the format and size of GFN particles, functionalization/chemical preparation, and the cell phenotype tested. Another degree of variability to consider is that certain cell stressors will be more profound based on the GNF type and concentration tested. Studies have shown how Reduced-Graphene Oxide (rGO) iterations of the same size and format showed no significant production of metabolic stressor metabolites in human umbilical vein endothelial cells (HUVEC) at 10µg/ml concentration but did show significant cell membrane disruption at the same concentration [42]. However, current studies indicate that regardless of the graphene tested there appears to be a Graphene iteration concentration threshold for every cell line that is detrimental to the cell's health.

In-vivo studies are difficult in assessing the dosage-dependency toxicity of GFN at injury sites due to the absorption rate of GFN's and the conduit platforms they are bound to, and the difficulty of tracking GFN in real-time. This however, is suitable for assessing the migration and stimulation of GFN towards acute and chronic toxicity over specific tissues/organs for extended periods of time. *In-vivo* studies have looked at GFN concentrations present in large tissue/organs and excretions over extended periods of time. One study found that mice subjects injected with GO solutions at concentration of 0.4mg had large quantities of

graphene compounds located at the lungs, liver, and kidneys at 30 days [43]. The PI's observed lung granuloma formations and intense inflammation in the kidneys indicating difficulty in cleansing the system of graphene residuals, thus leading to chronic toxicity resulting in almost 50% of subjects to die. All lower GO concentrations tested showed no clinical toxic symptoms with no mortalities in any of the mice subjects over a 30-day period. The study did not indicate any blood toxicity or the ability of graphene to bypass the blood-brain barrier after tail vein injection in any of the graphene concentrations during the duration of the study. This most likely could be attributed to the size of the graphene films, which could not pass the blood-brain barrier or the nuclear membrane of most cells. This would indicate that the lateral dimension of these films is between 100 – 40 nm which is sufficient to passively bypass the cellular membrane.

The conclusion is that there is still no consensus on the GFN dosage required to elicit toxic effects in *In-vitro* or *In-vivo*. When we factor in size, conformity, and functionalization we create different GFN iterations that elicit their own degree of toxicity as the dosage increases. The lack of a standard operating procedure for preparing, storing, and validating different GFN iteration concentrations makes supporting or contradicting studies of similar aims more difficult as the current literature shows. These problems are mirrored when dosages used in *In-vitro* studies are translated to estimated dosages for *In-vivo* models. Most researchers agree that as the concentration of GFNs increases (regardless of the iteration) a threshold for toxicity is reached that will result in declining cell viability *In-vitro* and chronic inflammation and scar tissue formation apparent in lungs, liver, and kidneys *In-vivo*. Studies focused on assessing immunomodulation, genotoxicity, and blood compatibility have also noted this dosage trend which makes standardizing studies that use carbon-based materials a primary concern for finding safe dosages.

1.3.1.4 Size/Morphology

Graphene can conform to a multitude of different formats and sizes, many of which have been studied in physiological systems. There is consensus that the size and type of graphene has a profound effect on the toxicity of GFN. The dimensions of GFN have been found to be most important in facilitating whether films of a certain size can be internalized into the cell, while the morphology of GFN is found to be more responsible in the amount of stress that is induced inside the cells [44]. Studies have found that graphene films of large lateral dimensions and surface area show a greater degree of plasma-membrane adhesion due to a greater concentration of bonding sites for electrostatic and ECM protein bonding. Such large dimensional films are capable of bypassing the plasma membrane by disrupting the membrane integrity by puncturing through at the asperities sites on GFN films. Such disruption of the plasma membrane could potentially disrupt membrane and cytoskeleton associated proteins for maintaining membrane integrity, such as Actg2, Myosin, Tubb2a, and Nebulin. Studies have shown that GFNs deposited on the cell membrane are able to activate membrane receptors that initiate potential cytotoxic-pathways, such as toll-

like receptors (TLR) and transforming growth factor beta (TGFβ) surface receptors for pro-inflammatory and apoptotic induction.

Graphene samples of smaller lateral dimensions can be taken up much more easily into the cell by diffusion, and passive, or active mechanisms (endocytosis, ionic channel pumps, pinocytosis, and phagocytosis). As the lateral dimension of graphene films decreases, we begin to see increased uptake into the cell's cytoplasm where subsequent pathways for production of metabolic stressors, and inflammatory cytokines become more active. Even smaller graphene particle sizes have the potential to bypass the nuclear membrane, resulting in genotoxicity. GFN films with sizes between 100 – 40 nm lateral dimensions are capable of passively bypassing the cellular membrane, while GFN films of 40-35 nm lateral dimensions can passively bypass the nuclear membrane. All other GFN films smaller than 35 nm are capable of bypassing the blood brain barrier. This behavior in cells can relate to how certain sizes of graphene are more prone to elicit certain cellular responses that are indicative of cytotoxicity.

1.3.1.5 Surface Charge/Physiochemistry

PG and its different forms have a hydrophobic surface due to the covalent bonding of carbon atoms that present few areas on the surface for hydrogen atoms and other polar based molecules to interact with graphene. When organic compounds covalently or electrostatically bind to a material's surface that adds or changes the surface properties, we refer this chemical modification as functionalization. GFN's can have their surfaces modified in this way to create hydrophilic surfaces more capable of cell adhesion and interacting with physiological molecules. The most common examples of this are PG films functionalized with oxygen-based groups like hydroxyl (OH-), carboxylic (COOH-), and carbonyl (CO) groups to create modified GFN's like GO and rGO. These groups are usually created thru Hummer's method that can exfoliate the ends of the graphene films using powerful acids like sulfuric or nitric acid to bind to an oxidizing reagent such as potassium permanganate. The presence of these oxidative groups changes the charge density and zeta potential of the graphene surface making it negatively charged and more susceptible to reactions with other polar molecules and making the surface more hydrophilic. This creates a platform well suited for cell-adhesion molecules (CAM) to adsorb to the surface. Graphene films highly saturated with (CAMs) have a greater success of establishing integrin binding on the surface of cells for controlled adhesion and migration. These functional groups can also act as anchor points for attaching polar proteins, lipids, antibodies and drug components as a drug delivery platform for targeted or systemic control over physiological systems to improve tissue regeneration outcomes. However, preparation of certain functional groups could also potentially modify the toxicity of GFNs to make them more toxic to cell lines from both an *In-vivo* and *In-vitro* perspective. Great care should be taken to ensure that these types of modifications do not alter normal cell physiology or elicit toxic responses. Such examples include GO which has been

observed to increase oxidative stress due to its high concentration of bound oxygen species, or the toxicity attributed to impurities created during surface modifications.

In-vitro studies used to evaluate cytotoxicity of GFNs in immortalized cell lines have found that PG films are more likely to localize on cell membranes rather than internalize into the cell due to the strong electrostatic attraction of the hydrophobic graphene surface to the negatively charged phospholipid cell membrane. It is here that films of large lateral dimensions could interfere with normal cell functions by overlapping cell surface binding sites, which can initiate toxicity pathways by preventing cell nutrients and waste processes, increase intracellular reactive oxygen species (ROS) concentrations, or immobilizing the cell. GFNs can also activate pro-inflammatory receptors such as Tumor Necrosis Factor (TNF), Toll-Like Receptors (TLR), and Transformation Growth Factor-Beta (TGF-β). These receptors will follow pro-inflammatory and apoptotic pathways such as nuclear factor kappa B (NF_KB), extracellular signal–regulated kinases (ERK), mitogen-activated protein kinase (MAPK), and Caspase-3. These pathways will often secrete pro-inflammatory cytokines such as Interlukin-1,6,12 (IL-1,6,12), Tumor Necrosis Factor-alpha (TNF-α), monocyte chemoattractant protein 1 (MCP-1), and Interferon gamma (IFN-g) that will further cell death. PG films of smaller dimension and size are more capable of internalizing into the cell cytoplasm thru endocytosis and phagocytosis (**Figure 1.4**: A, B)[45].

In-vitro studies have consistently reported that high concentrations of GFNs internalized into the cell bodies will increase ROS radicals as a result of GFNs interacting with cellular mitochondrial processes. This increase in intracellular ROS levels will often activate apoptotic and pro-inflammatory pathways in the form of oxidative stress that will eventually lead to cell death if the stress is prolonged. The tricarboxylic acid (TCA) or “Krebs cycle” is a component of aerobic metabolic processing in mitochondria necessary to store chemical energy in the form of ATP from reduced proteins, fat, lipid, and carbohydrates in all eukaryote cells. It has been suggested that GFNs could act as an electron donor that could add electrons to redox enzymes at specific points during the Krebs cycle. This form of interference is more likely to occur with redox co-enzymes such as nicotinamide adenine dinucleotide (NAD) that can accept electrons from hydrophilic (GFN) surfaces. A byproduct of redox reactions is ROS which are the primary source for intracellular oxidative stress and at critical concentrations will activate pro-inflammatory, apoptotic, necrotic, and autophagy pathways. Other studies have looked at indirect forms of detecting increases in ROS such as detecting dynamic changes in lactate dehydrogenase (LDH) enzyme secretions as a direct correlation with changes in ROS levels.

These studies have also reported that the degree of metabolic stressors released internally is dose, size, and conformation dependent. Surface area, degree of functional group saturation, and the orientation of functional groups on GFN surfaces will also affect the amount of internal metabolic stressors produced (**Figure 1.4**) [45]. In the case of GO or rGO, *In-vitro* reports indicate a greater degree of metabolic disruption compared to pristine graphene iterations due to the presence of oxidative radicals on the materials surface. These radicals and the impact that it has on normal mitochondrial processing can increase the number of ROS in the cytoplasm which presents a greater severity of toxicity due to ROS reactions with cellular components such as protein synthesis, tubulin structure, and mitochondria/nuclear membrane integrity. These changes not only disrupt cell function but also induce genotoxicity or epigenetic damage.

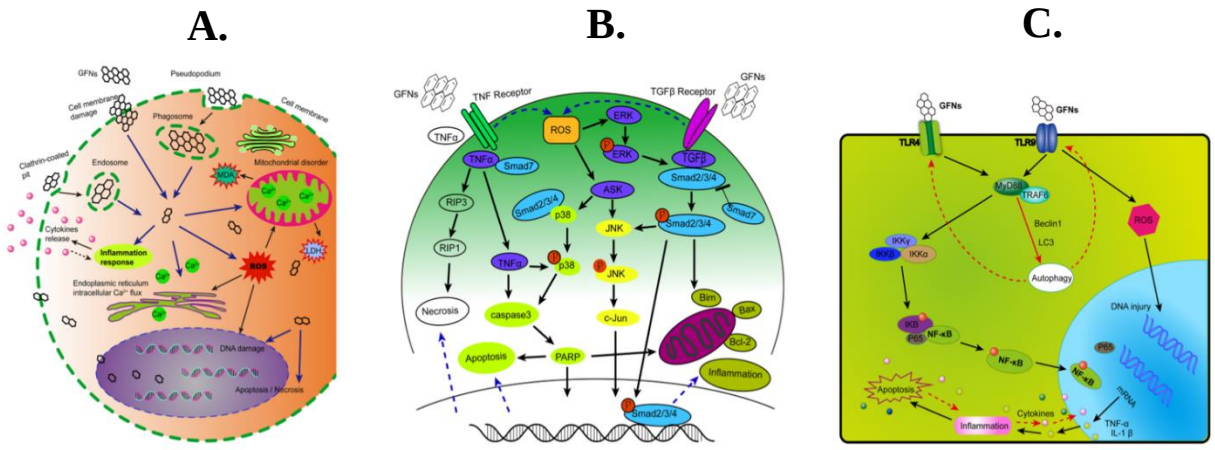

Figure 1.4 Intracellular toxicity pathways induced by GFNs

Note: (A) TLR4,9 pathway activation by GFN's resulting in upregulation pro-inflammatory factors. (B) MAPKs, TGF-beta and TNF-α dependent pathways involved in activation of apoptotic factors caspase3 and necrosis caused by GFN's. (C) Passive transport of GFNs across cell membrane with subsequent ROS, LDH, and MDA generation.

Source: Ou L, Song B, Liang H, Liu J, Feng X, Deng B, et al. Toxicity of graphene-family nanoparticles: a general review of the origins and mechanisms. Part Fibre Toxicol. 2016;13: 57.

1.3.2 Graphene Neural Conduit Designs

Based on the current consensus on GFN biocompatibility/toxicity and the pursuit to design neural conduits that can address the current debilitation brought about by severe cases of peripheral neuropathies, GFNs have been introduced as a material component that could potentially improve current neural scaffold functionality [46]. GFNs have been used in the design of neural scaffolds primarily to improve upon the mechanical integrity, neural conduction dynamics, and thermal stability of polymer based neural scaffolds. However, over the last decade there has been a growing interest to understand how this material can integrate with the ECM and cells used in neural regenerative applications and whether as a biomaterial by itself can stimulate endogenous neural repair. This has furthered our understanding of GFN as an attractive candidate as the primary component in neural scaffolds devices resulting in a variety of GFN neural scaffolds designs. The inclusion of GFNs into previous neural scaffold designs have shown improvement in nerve conduit and wrap performance by enhancing the devices in regards to the specific design criterions previously discussed (Sec 1.1.3.1).

One of the most studied and often utilized GFN iteration used for improving the performance of nerve conduit and wrap designs is GO or rGO substrates (graphenes oxidized with oxidative groups). As previously discussed, GO and rGO coated surfaces can not only support neuronal and multipotent cell-lines but can direct multipotent cells towards specific neuronal lineages, where as other GFN iterations are not as effective or have no effect in directing neurogenesis. It is for this reason that these GFN's are often used to modify the surfaces of these types of constructs, specifically those surfaces in direct contact to the nerve under repair [47]. Apart from the proven benefit of being able to support neural and stem cell therapies, these modifications will alter the physical and chemical properties of the construct surface in a variety of expected ways that are further advantageous to nerve repair. This includes surface stiffness increase, neurogenic anisotropic properties, slightly higher hydrophilic surface charge, electrical conductance potential, and further tailored functionality for absorption of neurogenic positive compounds. This makes GO, and rGO excellent contenders as surface coatings for enhanced nerve conduit and wrap performance.

Despite these neurogenic positive properties of GFN, a nerve conduit capable of meeting or surpassing the degree of repair achieved by autologous scaffolds has not yet been achieved. Implications involving the potential toxicity of GFN's and the misinformation regarding what pathways are activated or negated when multipotent and neuronal cells are exposed to GFN's *In-vivo* has created uncertainty as to the materials ability to meet the clinical standards for successful nerve repair and whether it will produce adverse effects in a clinical setting. This is why to date, there is currently no clinical peripheral nerve conduit or wrap device with GFNs that has been successfully brought to market.

1.4 Stem Cell Therapy

Stem cells are a family of cells that are specifically characterized as undifferentiated cell lines capable of self-renewal over long periods of time until exposed to specific environmental conditions that will induce the cells towards specialized cell lineages. A common hierarchy of stem cells, starting with the most potent stem cell form is to start with totipotent stem cells. These cells are usually present during the early stages of embryonic development. Such examples include spores or zygotes, which are capable of differentiating into any tissue type possible in the body. After successful fertilization, a culture of these totipotent cells is created which will then differentiate into pluripotent cells. Differentiation potential of these cells is limited to any three germ layers, these being endoderm, ectoderm, and mesoderm lineages. Endoderm differentiation includes lung and gastrointestinal tissue. Ectoderm differentiation includes epidermal and neural system tissues. Mesoderm differentiation includes muscle, bone, and blood tissues. Once pluripotent cell begins to differentiate towards either of these three pathways, they will further differentiate towards progenitor cells that have the potential to differentiate towards multiple discrete cell types, further characterized as multipotent cells. An example of this concept are multipotent cells that develop from a mesodermal origin that will differentiate towards bone, chondrocyte, or adipose tissue often referred to as mesenchymal stem cells (MSC).

When isolated from adult tissues, multipotent cells have the potential to improve the outcome of tissue healing when directly applied to the site of injury or when pre-differentiated towards its intended cell type before being applied. Recent studies have directed interest towards incorporating multipotent cell lines into the design of scaffolds to improve regeneration, tissue quality, and cell-material interaction [48]. The scope of these types of studies has focused primarily on answering the question of which type of multipotent cell line should be used, what form of stimulation is most effective in differentiating cells to express the intended therapy, the time and duration of administration *In-vivo*, survivability, and tracking of the cells *In-vivo*.

Investigations using multipotent cell lines for improved neural tissue healing has shown promising results in both *In-vitro* and *In-vivo* models, particularly when used in collaboration with nerve scaffolds that can act as a platform for stable cell growth, cell protection, and elicit its own biomaterial cues to guide cell differentiation. The most commonly investigated multipotent cell lines for nerve healing applications have been embryonic stem cells (ESC), induced pluripotent stem cells (IPSC), and adult somatic stem cells (ASSC). Although ESC and IPSC have shown potential for nerve tissue healing, there are concerns from a clinical standpoint due to greater cellular sensitivity towards immunological processes, ethical implications involved in using these cell lines, and the technical difficulty in isolating these cells. This makes the use of ASSC a more attractive stem cell therapy option for healing extensive nerve damage. A number of ASSC

have already been investigated for their potential in nerve repair including ones of both mesoderm and ectoderm origins. There is a greater consensus towards using ASSC of mesoderm origin due to its prevalence in certain tissue locations and the ease of accessibility to those locations as compared to ectoderm origin cell-lines. Although this origin cell-line best represents the tissue being regenerated at the site of injury, they are very difficult to isolate making them non-feasible to use from a clinical standpoint. Neural crest stem cells (NCSC) and MSC are multipotent cell lines of mesoderm origins that have received interest in nerve repair. Their ease of accessibility, simple isolation techniques, and current results have shown potential to express cellular structure and behaviors similar to that of ectoderm origin cell lines but not exact in every aspect which is termed by many researchers as neuron-like cells.

1.4.1 Mesenchymal Stem Cells

MSC are a type of multipotent progenitor cell line that is capable of self-renewal and differentiating into specific cells of a mesoderm lineage such as chondrocytes, osteoblast, and adipocytes [49–51]. A type of non-hematopoietic adult stem cell line, MSCs are produced in both fetal and adult tissues in most mammal species to assist in the repair and maintenance of specific tissues of mesoderm origin such as cartilage, bone, fat, skeletal muscle, and tendon. MSCs have been isolated from a variety of fetal and adult tissues with bone marrow, adipose tissue, and umbilical cord blood, and Warton's jelly being the most common source due to their high MSC content. The most common natural reservoirs used for collecting MSCs from a clinical standpoint are cells derived from bone-marrow or adipose tissue. While both forms of these multipotent cell lines have been used to repair nerve with mixed results to date, there are specific advantages observed that puts preference of using one form over the other for nerve repair.

From a clinical stand point adipose tissue is more readily available, adipose tissue is easier to remove, and it is easier to isolate MSCs from adipose tissue compared to bone-marrow tissue. This makes adipose derived stem cells (ADSC) a more attractive multipotent cell choice compared to bone marrow derived cells (BDSC). Furthermore, once ADSCs are isolated from adipose tissue the yield of healthy ADSC is much greater and can survive for longer lengths *In-vitro* than BDSC isolated from bone-marrow tissue. From a therapeutic stand point both cell types have immunogenic properties and have shown to expressing neural and glial cell markers such as S100B, GFAP, P75, and Tuj-1 and are able to release neurotrophic factors such as GDNF and BDNF. *In-vitro* studies have shown both cell types have a higher potential to differentiate towards Schwann-like cells when exposed to chemical inductions geared towards neural differentiation. *In-vivo* performance of these cells in peripheral nerve injuries have shown promising results with the majority of studies reporting a significant improvement in nerve repair as opposed to neural grafts without MSC inductions. Considering the advantages of combining MSCs to neural grafts for neve repair,

if this should be translated to clinical assessment ADSC appears to be the more preferred choice for nerve repair.

1.4.2 Neural-Fate Pathways

Human MSC (hMSC) have shown the potential for induction into cells that exhibit characteristics often found in cells of the ectodermal lineages [52]. Investigations have found that, under the right chemical induction parameters, *In-vitro* hMSCs can express surface markers, ectodermal protein and gene modulation, and re-orient their cytoskeletal structures to resemble that of neuron, astrocyte, or glial cells. Neural differentiation of hMSCs can be further modulated through mechanical niches stimulated by both physical and topographical cues presented on the surface of surrounding tissues and biomaterials. While these cells will resemble certain traits of neuronal cells, to date there is no protocol developed that can differentiate mesoderm cell lines into functional neuronal cells, which is a major limitation for using mesoderm cells for repair of peripheral nerves.

1.4.2.1 Biochemical Induction

The ability of multipotent cell lines to differentiate towards multiple cell types is in part regulated by the activation of specific intracellular pathways at different intensities and at varying stages during their development into specialized cells. Specific intracellular pathways are essential in regulating the neural fate of multipotent cells. Activation of these pathways can guide multipotent cells, not designed to differentiate towards neural lineages (MSCs, NCSCs) towards neural-like cell lineages [53].

Cyclic-adenosine-monophosphate (cAMP) a common intracellular messenger protein responsible for regulating the activation of protein kinase A (PKA), cAMP has been found to be an essential component in regulating the modulation of genes present in neural development such as c-fos, brain derived neurotrophic factor (BDNF), or tyrosine hydroxylase (TH) in MSC cell lines. Use of PKA inhibitors to induce neural-like differentiation in hMSC have been shown to be ineffective in successful neural differentiation, while the use of compounds that will upregulate PKA pathways would result in neural-like differentiation of hMSCs. This would indicate that regulation of PKA pathways are a considerable factor involved with directing MSCs towards neural lineages. Induction of the PKA pathway has been mitigated by either increasing cAMP production using forskolin, or 8-bromo-cAMP, or by preventing cAMP break down by inhibiting phosphodiesterases using dibutyryl-cAMP (db-cAMP), or 3-isobutyl-1-methylxanthine (IBMX). This method has shown evidence of early morphology changes observed in neurons such as cytoskeleton reorientation, and cells expressing proteins for neural markers associated with neuronal development such as βIII-tubulin (Tuj-1), neuron-specific enolase (NSE), microtubule-associated protein-2 (MAP-2) and glial fibrillary acidic protein (GFAP). However, a lack of other early markers expected during neuron

development such as growth factor protein- 43 (GAP-43), and minimal presence of neurotransmitters or voltage-dependent Na^{+}, P^{+}, or Ca^{+2} cations leads many to conclude that neurite formation is not authentic and is a result of culture conditions rather than activation of a differentiation process.

Retinoic acid (RA) is a metabolite created through retinol dehydrogenase (RoDH) of retinol. RA will bind specifically bind to cellular RA binding protein (CRABP) which will regulate primarily Hox gene activation, which is thought to be an important gene sequence for modulating anterior/posterior neural mapping during fetal development. A study compared the neural stimulation of MSC by activating cAMP pathways to that of activating RA pathways. The results found that both cAMP and RA stimulation would differentiate MSCs to positively express neurogenic surface markers NSE, Tuj-1, and GFAP. It is also shown that using these two stimulants together can result in higher expression of these markers, including expression of normal resting potentials and increases in calcium concentrations to that of native neural cells. This form of stimulation has also shown potential to express electrophysiological changes in multipotent cells has shown in a study involving neural stimulation of dental pulp stem cells (DPSC) that expressed active sodium voltage-gated ion channels, which could be an essential component for differentiating mesoderm cells towards functional neurons.

Neurotrophic growth factors (NGF) are essential in maintaining normal neural cell functionality and survival, while under certain forms of stress can be upregulated to guide neural cell fate in neural stem cells. This family of proteins involve NGF, BDNF, GDNF, and neurotrophins (NT- 3, 4, 5, and 6). NGF and neurotrophins have a high affinity towards tyrosine kinase receptors A, B, C (TrkA, TrkB and TrkC), GDNF affinity towards GDNF family receptor alpha-1(GFRα) and RET proto-oncogene (RET), and NGF and BDNF affinity towards P75 receptors. Signal transduction will then follow one of three pathways: mitogen-activated protein kinases (MAPKs), phospholipase C (PLC), or phosphatidyl-inositol-3-kinase (PI3K). These pathways will further phosphorylate towards PKC, protein kinase B (PKB), or ERK which will transcript gene sequences that will regulate neuronal development, health, and synaptic functions. By themselves, neurotrophic factors will initiate neural differentiation in neural stem cells while initiating neural-like cell differentiation in Mesodermal cell lines to varying degrees. Combined with other neural pathways will further enhance expression of neural traits in mesodermal cell-lines.

Wnt pathway involves proteins that are involved in regulating homeostasis in adult tissue and early stages of tissue development during embryogenesis. This includes early neural development from neuronal stem cells by regulating stem cell fate, proliferation, and survival as neuronal cells. Wnt proteins will first activate Frizzled (Fzd) G-coupled proteins on stem cell surfaces which will then trigger β-catenin accumulation in

the cytoplasm which will then regulate T-cell specific transcription factors (TCF) gene sequences specific to the type of stem cell. This pathway is geared to differentiate stem cells based on their respective phenotype, where mesoderm stem cells will most likely be guided toward smooth muscle and endothelial cell fates neural stem cells will be guided towards neuron cell fates. By its self, the Wnt pathway cannot successfully initiate differentiation of MSC towards neuronal fates. However, when combined with other stimulation pathways previously discussed will express other neuron markers such as Ngn1, NeuroD, and Brn3a when used in combination with forskolin and IBMX (PKA pathways) (**Figure 1.5**).

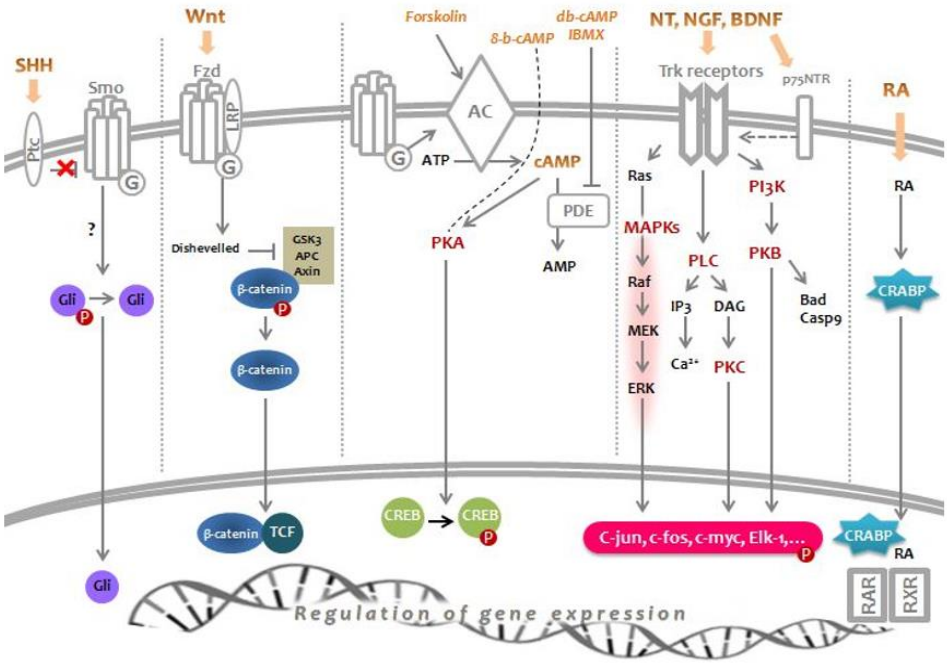

Figure 1.5 Current identified pathways for induction of MSC towards neural-like cells

Source: Neirinckx, Virginie, Cecile Coste, Bernard Rogister, and Sabine Wislet-. 2013. "Neural Fate of Mesenchymal Stem Cells and Neural Crest Stem Cells: Which Ways to Get Neurons for Cell Therapy Purpose?" In *Trends in Cell Signaling Pathways in Neuronal Fate Decision*, edited by Sabine Wislet-Gendebien. InTech

1.5 Summary

The topics discussed in this chapter provide the frame work for understanding peripheral neuropathies and the methods for repairing critical size nerve defects and their limitations. It is also discussed the approaches of using both biomaterial and stem cell therapies together as a potential novel alternative method for repair of critical size nerve defects. Biomaterial conduits or wraps arranged as an open tube structure are the most commonly studied alternative repair option for severe neurotmesis. It is clear that the addition of stem cell therapies can improve the quality of neural tissue growth along the scaffold channel by introducing immunomodulatory effects and promoting axonal growth and minimizing muscle atrophy by expressing neurotrophic growth factors at the site of injury. While GFNs are currently under investigation for their toxicity in physiological models, *In-vitro* and *In-vivo* studies have shown that GO films not only serve as a suitable platform for delivering MSC therapies but also has neurogenic potential as a possible surface coating additive to neural conduit and wrap designs for nerve healing applications.

From this chapter it is clear that many approaches to designing different neural wraps using synthetic polymers and GO coating modifications are possible, with many iterations still unexplored. It is the goal of this study to design a 3D neural wrap composed of PCL synthetic biomaterial and surface coat with GO as a platform suitable to grow hADSC cultures. The function of this design is focused towards bridging critical size nerve defects to assist in axon guidance and stimulate nerve healing. It is also designed as a deliver platform to transport hADSC cultures to the injury site for further assist by providing immunomodulation and release of neurotrophic factors. By manufacturing this material and testing its cytocompatability towards supporting hADSC cultures *In-vitro* and tests its ability to assist in neural healing *In-vivo,* this should provide data that will determine this designs potential in providing assistance in nerve healing applications.

References

1. Black J. Biological performance of materials. In: Black J, editor. In Fundamentals of Biocompatability. Boca Raton, FL: CRC Press-Taylor & Francis; 2006.

2. Gu X, Ding F, Williams DF. Neural tissue engineering options for peripheral nerve regeneration. Biomaterials. 2014;35: 6143–6156.

3. Williams DF. Definitions in biomaterials. In Proceedings of a Consensus Conference of the Europeans Society of Biomaterials (1986). Chester: Elsevier; 1987.

4. Buddy D. Ratner FJS. Chapter II.3.2 The Concept and Assessment of Biocompatibility. In: Buddy D. Ratner, Allan S. Hoffman, Frederick J. Schoen, Jack E. Lemons, editor. Biomaterials Science: An Introduction to Materials in Medicine. 225 Wyman Street, Waltham, MA 02451, USA: Elsevier Inc; 2013. pp. 588–592.

5. Jinku Kim, Abiraman Srinivasan, and Jeffrey O. Hollinger. Chapter 8: In Vitro Testing of Biomaterials. In: Hollinger JO, editor. An Introduction To Biomaterials. 6000 Broken Sound Parkway NW, Suite 300, Boca Raton, FL, 33487-2742: Taylor & Francis Group; 2012. pp. 137–155.

6. Michael F. Wolf, Kelly P. Coleman, Gregory M. Lewerenz. Chapter II.3.3 In Vitro Assessment of Cell and Tissue Compatability. In: Buddy D. Ratner, Allan S. Hoffman, Frederick J. Schoen, Jack E. Lemons, editor. Biomaterials Science: An Introduction to Materials in Medicine. 225 Wyman Street, Waltham, MA, 02451, USA: Elsevier Inc; 2013. pp. 593–608.

7. Vidal MNP, Granjeiro JM. Cytotoxicity Tests for Evaluating Medical Devices: An Alert for the Development of Biotechnology Health Products. JBiSE. 2017;10: 431–443.

8. Jiao G, He X, Li X, Qiu J, Xu H, Zhang N, et al. Limitations of MTT and CCK-8 assay for evaluation of graphene cytotoxicity. RSC Adv. The Royal Society of Chemistry; 2015;5: 53240–53244.

9. Wang P, Henning SM, Heber D. Limitations of MTT and MTS-based assays for measurement of antiproliferative activity of green tea polyphenols. PLoS One. 2010;5: e10202.

10. Ng KW, Leong DTW, Hutmacher DW. The challenge to measure cell proliferation in two and three dimensions. Tissue Eng. 2005;11: 182–191.

11. Carlberg B, Axell MZ, Nannmark U, Liu J, Kuhn HG. Electrospun polyurethane scaffolds for proliferation and neuronal differentiation of human embryonic stem cells. Biomed Mater. 2009;4: 045004.

12. Nair LS, Laurencin CT. Biodegradable polymers as biomaterials. Prog Polym Sci. 2007;32: 762–798.

13. Christenson EM, Patel S, Anderson JM, Hiltner A. Enzymatic degradation of poly(ether urethane) and poly(carbonate urethane) by cholesterol esterase. Biomaterials. 2006;27: 3920–3926.

14. Tsuji H, Eto T, Sakamoto Y. Synthesis and Hydrolytic Degradation of Substituted Poly(DL-Lactic Acid)s. Materials . 2011;4: 1384–1398.

15. Lucas N, Bienaime C, Belloy C, Queneudec M, Silvestre F, Nava-Saucedo J-E. Polymer biodegradation: mechanisms and estimation techniques. Chemosphere. 2008;73: 429–442.

16. Tamariz E, Rios-Ramrez A. Biodegradation of Medical Purpose Polymeric Materials and Their Impact on Biocompatibility. In: Chamy R, editor. Biodegradation - Life of Science. InTech; 2013.

17. M.E. Marti, A.D. Sharma, D.S. Sakaguchi, and S.K. Mallapragada. Nanomaterials for neural tissue engineering. In: A.K. Gaharwar, S.Sant, M.J. Hancock and S.A. Hacking, editor. Nanomaterials in tissue engineering Fabrication and applications. 1518 Walnut Street, Suite 1100, Philadelphia, PA: Woodhead Publishing Limited; 2013. pp. 275–300.

18. Petrova ES. Injured Nerve Regeneration using Cell-Based Therapies: Current Challenges. Acta Naturae. 2015;7: 38–47.

19. Kehoe S, Zhang XF, Boyd D. FDA approved guidance conduits and wraps for peripheral nerve injury: a review of materials and efficacy. Injury. 2012;43: 553–572.

20. Nectow AR, Marra KG, Kaplan DL. Biomaterials for the development of peripheral nerve guidance conduits. Tissue Eng Part B Rev. 2012;18: 40–50.

21. Vasita R, Shanmugam I K, Katt DS. Improved biomaterials for tissue engineering applications: surface modification of polymers. Curr Top Med Chem. 2008;8: 341–353.

22. Curran JM, Chen R, Hunt JA. The guidance of human mesenchymal stem cell differentiation in vitro by controlled modifications to the cell substrate. Biomaterials. 2006;27: 4783–4793.

23. John AA, Subramanian AP, Vellayappan MV, Balaji A, Jaganathan SK, Mohandas H, et al. Review: physico-chemical modification as a versatile strategy for the biocompatibility enhancement of biomaterials. RSC Adv. Royal Society of Chemistry; 2015;5: 39232–39244.

24. Siemionow M, Brzezicki G. Chapter 8: Current techniques and concepts in peripheral nerve repair. Int Rev Neurobiol. 2009;87: 141–172.

25. Menorca RMG, Fussell TS, Elfar JC. Nerve physiology: mechanisms of injury and recovery. Hand Clin. 2013;29: 317–330.

26. Pfister BJ, Gordon T, Loverde JR, Kochar AS, Mackinnon SE, Cullen DK. Biomedical engineering strategies for peripheral nerve repair: surgical applications, state of the art, and future challenges. Crit Rev Biomed Eng. 2011;39: 81–124.

27. Grinsell D, Keating CP. Peripheral nerve reconstruction after injury: a review of clinical and experimental therapies. Biomed Res Int. 2014;2014: 698256.

28. Sunderland S. Nerves and nerve in juries. Edinburgh: Livingsstone1972. 1978;201. Available: http://www.sosmain.eu/data/uploads/pdf/bibliotheque/N%20dossier%2007/nervesandnerve_397.pdf

29. Hasirci V, Arslantunali D, Dursun T, Yucel D, Hasirci N. Peripheral nerve conduits: technology update. MDER. 2014; 405.

30. Misra UK, Kalita J, Nair PP. Diagnostic approach to peripheral neuropathy. Ann Indian Acad Neurol. 2008;11: 89–97.

31. Isaacs J, Browne T. Overcoming short gaps in peripheral nerve repair: conduits and human acellular nerve allograft. Hand . 2014;9: 131–137.

32. Osbourne A, Medicine 5th Year. Peripheral Nerve Injury and Repair.

33. M F G, M M, S H, Khan WS. Peripheral nerve injury: principles for repair and regeneration. Open Orthop J. 2014;8: 199–203.

34. Reichert F, Saada A, Rotshenker S. Peripheral nerve injury induces Schwann cells to express two macrophage phenotypes: phagocytosis and the galactose-specific lectin MAC-2. J Neurosci. 1994;14: 3231–3245.

35. Purves D, Lichtman JW. Principles of neural development. Sinauer Associates Sunderland, MA; 1985.

36. Zou X, Zhang L, Wang Z, Luo Y. Mechanisms of the Antimicrobial Activities of Graphene Materials. J Am Chem Soc. 2016;138: 2064–2077.

37. Szunerits S, Boukherroub R. Antibacterial activity of graphene-based materials. J Mater Chem B Mater Biol Med. The Royal Society of Chemistry; 2016;4: 6892–6912.

38. Perreault F, de Faria AF, Nejati S, Elimelech M. Antimicrobial Properties of Graphene Oxide Nanosheets: Why Size Matters. ACS Nano. 2015;9: 7226–7236.

39. Nava MM, Raimondi MT, Pietrabissa R. Controlling self-renewal and differentiation of stem cells via mechanical cues. J Biomed Biotechnol. 2012;2012: 797410.

40. Zhao C, Tan A, Pastorin G, Ho HK. Nanomaterial scaffolds for stem cell proliferation and differentiation in tissue engineering. Biotechnol Adv. 2013;31: 654–668.

41. Zigmond RE. Cytokines that promote nerve regeneration. Exp Neurol. 2012;238: 101–106.

42. Das S, Wajid AS, Bhattacharia SK, Wilting MD, Rivero IV, Green MJ. Electrospinning of polymer nanofibers loaded with noncovalently functionalized graphene. J Appl Polym Sci. 2013;128: 4040–4046.

43. Wang K, Ruan J, Song H, Zhang J, Wo Y, Guo S, et al. Biocompatibility of Graphene Oxide. Nanoscale Res Lett. 2011;6: 8.

44. Mendes RG, Koch B, Bachmatiuk A, Ma X, Sanchez S, Damm C, et al. A size dependent evaluation of the cytotoxicity and uptake of nanographene oxide. J Mater Chem B Mater Biol Med. The Royal Society of Chemistry; 2015;3: 2522–2529.

45. Ou L, Song B, Liang H, Liu J, Feng X, Deng B, et al. Toxicity of graphene-family nanoparticles: a general review of the origins and mechanisms. Part Fibre Toxicol. 2016;13: 57.

46. Hong SW, Lee JH, Kang SH, Hwang EY, Hwang Y-S, Lee MH, et al. Enhanced neural cell adhesion and neurite outgrowth on graphene-based biomimetic substrates. Biomed Res Int. 2014;2014: 212149.

47. Shah S, Yin PT, Uehara TM, Chueng S-TD, Yang L, Lee K-B. Guiding stem cell differentiation into oligodendrocytes using graphene-nanofiber hybrid scaffolds. Adv Mater. 2014;26: 3673–3680.

48. Hundepool CA, Nijhuis THJ, Mohseny B, Selles RW, Hovius SER. The effect of stem cells in bridging peripheral nerve defects: a meta-analysis. J Neurosurg. 2014;121: 195–209.

49. Jiang Y, Jahagirdar BN, Reinhardt RL, Schwartz RE, Keene CD, Ortiz-Gonzalez XR, et al. Pluripotency of mesenchymal stem cells derived from adult marrow. Nature. 2002;418: 41–49.

50. Pittenger MF, Mackay AM, Beck SC, Jaiswal RK, Douglas R, Mosca JD, et al. Multilineage potential of adult human mesenchymal stem cells. Science. 1999;284: 143–147.

51. Samsonraj RM, Rai B, Sathiyanathan P, Puan KJ, Rötzschke O, Hui JH, et al. Establishing criteria for human mesenchymal stem cell potency. Stem Cells. 2015;33: 1878–1891.

52. Neirinckx V, Coste C, Rogister B, Wislet- S. Neural Fate of Mesenchymal Stem Cells and Neural Crest Stem Cells: Which Ways to Get Neurons for Cell Therapy Purpose? In: Wislet-Gendebien S, editor. Trends in Cell Signaling Pathways in Neuronal Fate Decision. InTech; 2013.

53. Barnabé GF, Schwindt TT, Calcagnotto ME, Motta FL, Martinez G Jr, de Oliveira AC, et al. Chemically-induced RAT mesenchymal stem cells adopt molecular properties of neuronal-like cells but do not have basic neuronal functional properties. PLoS One. 2009;4: e5222.

Chapter 2: PCL Electrospin Film with GO Surface Modification as a Platform for hMSC

Abstract

Critical size neural defects have a devastating impact on people's wellbeing and has a substantial component in the overall health care cost of both acute and chronic pain patients. The current gold standard for repair of critical nerve defects has limitations that require alternative solutions to address these. This has expressed much interest in the development of new biomaterials that can provide support and protect new axonal growth as a component of a stable film or mesh known as a neural wrap device. It is suggested that a new neural wrap design composed of electrospun PCL with the addition of surface coating of GO and potential to support hADSC cultures to deliver stem cell therapies could have the potential for assisting the repair of critical nerve defects In-vivo. In this study, the ability to manufacture this type of material and its biocompatibility towards MSC lines and ability to support hADSC cultures under neural stimulation is determined. Thru our collaboration with the University of Arkansas Little Rock, we were able to manufacture graphene coatings of different oxygen content for biocompatibility assessment and create different PCL films to assess how hADSC cultures behave on its surface under normal and neural induction conditions. The results of the proliferation and viability assay of rat ADSC cultures on graphene coatings showed GO coating had the largest proliferation and viability levels compared to all other graphene iterations tested. We applied GO coating to the smooth surface and fibrous surface PCL platforms and assessed the prescence and neural expression of S100β on hADSCs at day 1 incubation and the presences and morphology of hADSC cultures at day 6 incubation using vimentin staining. Results showed that PCL fiber mesh surfaces modified with GO could support hADSC cultures under normal and neural induction In-vitro environments. Slightly more impressive cell morphology and organization was detected on PCL platforms of nanofiber topographies, suggesting that PCL fiber meshes with GO surface modifications is the preferred material composition to use moving forward to test the materials potential in a critical nerve defect model.

2.1 Neural Wrap Manufacturing

2.1.1 Introduction

Peripheral neuropathy (PN) is a condition of the peripheral nerve system that currently affects over 20 million US citizens, with a prevalence of 3% in all trauma patients showing some form of peripheral neuropathy. Neurotmesis is the most severe type of peripheral injury where the nerve segment is completely transected cutting of the action potential to all sensory and motor functions. Often classified as a grade 4 or 5 on the Sunderland nerve injury classification scheme [1–3]. Patients with neurotmesis will often experience symptoms of both acute and chronic motor weakness and abnormal sensory function that overall diminish the quality of life for patients [4]. Almost all neurotmesis injuries require surgical intervention to ensure the nerve heals properly to regain most of its functionality. Severe neurotmesis involves significant gaps (>2-3 cm) that require surgical placement of neural grafts to insure proper guidance of axons as they grow across the gap [5]. Currently, the gold standard for repair of severe neurotmesis is the use of autograft nerve segments taken from the patient [6,7]. However, this method is limited in the degree of healing possible at the damage site [8]. Surgical protocols require precise matching and orientation of the graft at the two ends of the gap which is very difficult given the nature of microsurgery. The suturing of the graft can rupture or pierce the perineurium around the fascicles, causing scar tissue to form which can cause further problems at the site as iatrogenic peripheral neuropathy. The outcome of this strategy usually involves the following implications: donor-site morbidity, sensory loss, scarring at the donor site, neuroma formation, pain, and in the case of allografts long periods of host immunosuppression [9,10]. The low quality of recovery for neurotmesis cases results in a surplus of patients affected by chronic peripheral neuropathy symptoms, contributing to an overall decrease in the wellbeing of the population and an increase in the health care costs utilized for repair and management of these symptoms which are currently estimated at around $150 billion annually. This presents a pressing need to research new alternative strategies to autografts for nerve repair that addresses these limitations while minimizing the onset of new ones.

Tissue regeneration is currently a topic extensively studied within the field of both human and animal medicine that has potential for improving the rate and quality of healing damaged tissue. One important field of study in this topic is the use of scaffolds composed of biomaterials designed to support and promote activation of cell lines committed towards assisting in the healing of damaged tissue. Studies have shown that mesenchymal stem cells (MSC) can improve the healing of damaged tissue by differentiating into multiple cell lineages that can promote the healing of damaged tissues. Studies have also shown that graphene oxide (GO) as a thin film material has low cytotoxicity, excellent cell absorption properties, and can support cultures of adipose derived stem cells (ADSC) over extended periods of time. For the application of nerve regeneration therapy, it would be advantageous to combine these two approaches into

a scaffold design that can support neural differentiated ADSC cultures while enhancing nerve regeneration at the site of healing. One important aspect of this design is selecting an appropriate biomaterial as a platform that can support GO films and ADSC viability over an extended period of time. Biocompatible synthetic polymers such as polycaprolactone (PCL) have been shown to be acceptable materials for supporting both thin films and ADSC for extended periods of time *In-vivo*. To our knowledge, the design of a PCL wrap has not yet been explored as a suitable platform to support GO thin film in combination with hADSC cultures to assist in peripheral nerve repair.

2.1.2 3D Fabrication of Neural Wrap

Previous studies have looked at the inclusion of PCL as a synthetic platform for assisting peripheral nerve healing with studies finding that PCL remains mechanically stable during the period of repair in small animal models and as a polymer with high solubility to organic compounds it can be utilized in a variety of manufacturing techniques to tailor fit a design that meets the design criteria of a successful neural wrap**.** It also is classified by the FDA as a biodegradable polymer of up to 2 years before hydrolytic degradation renders the design mute with the only residuals having little to no toxic effects to the physiological surroundings. Previous studies have also found that biomaterials with certain micro or nano- surface topographical feature are better suited to assisting in peripheral nerve stability and guidance during repair. Surfaces of high surface area that conform to groves or channels have been found to enhance neural cell migration and differentiation under the right conditions compared to smooth surface platforms. A novel method that has been used extensively in polymer-based manufacturing to produce surfaces saturated in micro channels and groves electrospinning of polymers into nanoscale fibers that act as channels or tracks that are preferred adhesion points for newly regenerating nerves.

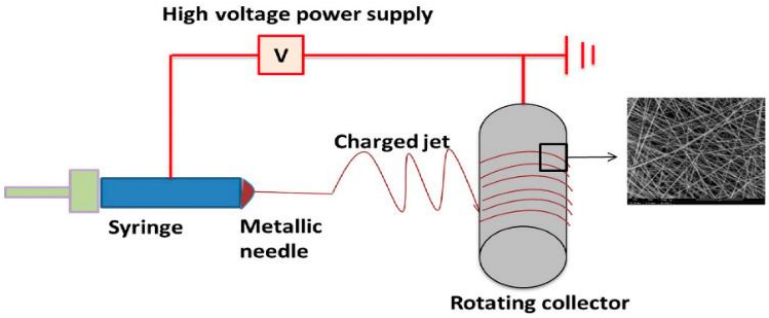

Figure 2.1 Common horizontal electrospinning apparatus setup

Source: Kadavil, Hana, Moustafa Zagho, Ahmed Elzatahry, and Talal Altahtamouni. 2019. "Sputtering of Electrospun Polymer-Based Nanofibers for Biomedical Applications: A Perspective." Nanomaterials (Basel, Switzerland) 9 (1). https://doi.org/10.3390/nano9010077.

Electrospinning is a technique that involves drawing charged polymers in solution towards a grounded collecting plate using electro repulsion forces. If polymers are successfully suspended in a compatible soluble solution and the solution is capable of holding a charge then it has the potential for electrospinning manufacturing. If the solution is charged by a generator and a grounded collector is located a distance from the solution reservoir, electro repulsive forces created from the opposite charges will attract and pull the solution and its monomer components towards the collector. The process of pulling the charged polymer solution from its reservoir towards the collecting plate until the forces exceed the surface tension forces of the solution to create the jetting effect is called the Taylor cone, and is an effect that should be present for successful solution spinning. As the solution and monomers are pulled across the air medium, the monomers align together as the solution evaporates and cross links them into a continuous fiber strand [11]. By changing the polymer percentage solution, voltage, tip-to -collector distance, and solution pump rate the diameter of the fibers can be tailored to specific fiber diameter, surface topography, and porosity specifications.

The development of neural scaffolds using synthetic electrospun polymers that provide both cellular and mechanical support at the site of healing and can be designed to biodegrade after its therapy has finished without inducing any adverse immune or cytotoxic effects [12]. This technique has gained much interest for addressing the limitations of autografts while providing the advantages of tailoring biocompatibility, biodegradation, mechanical properties, and surface architectures of the scaffold based on the materials used. This provides opportunities to test a variety of different materials in the hopes of creating the ideal scaffold design [13]. Currently, synthetic polymer scaffolds by themselves still underperform when compared to the current gold standard for defects greater than 1 cm. To address this challenge, many studies have begun to look at combining multiple TE techniques together in the scaffold design such as stem cell support, anisotropy surface architecture, and surface coatings to improve the limitations of synthetic scaffolds [14]. The majority of these *In-vivo* studies show a significant improvement in neural repair, with successful bridging of neural defects up to 3 cm in length being reported. We are particularly interested in developing synthetic neural scaffold designs that incorporate stem cell therapy and surface coatings to improve the quality of severe neurotmesis recovery.

2.1.3 Graphene Family Nanomaterial Inclusion

We are interested in studying the application of using graphene-based materials as a thin film coating applied to the surface of scaffolds to potentially enhance growth, survival, and rate of differentiation of hADSC for promoting tissue healing [15]. Graphene is a single atom thick honey comb lattice structure of carbon bonds that consist of SP_2 and SP_3 hybridizations. Graphene has been studied for its potential as a biomaterial and graphene functionalized with oxidative compounds known as graphene oxide has been

found to be one of the most promising candidates as a biocompatible substrate. Both graphene oxide thin films and hADSC have been studied extensively for their potential to enhance the repair of damaged peripheral nerve [16–18]. Results show a marked improvement of neural repair in the presence of hADSC, graphene-based materials, or both. Current studies have also shown that by treating the surface of biomaterials with carbon based thin film coatings, we can enhance the growth, survival, and differentiation of mesenchymal stem cells, supporting the notion that combining graphene-based thin films with ADSC cultures to our neural scaffold might enhance nerve repair [19,20].

2.1.4 Objective

The objective of this project is to determine whether electrospun PCL platform surfaces coated with graphene nanomaterial is a suitable platform to support MSC cultures differentiated towards a neural phenotype. This objective is the first iteration of *In-vitro* tests that will assess the cytotoxicity, and potential to support hADSC artificially stimulated towards Schwann-like cell phenotypes as the first initial set of data for support in progressing our novel therapeutic design towards *In-vivo* assessment studies that will result in the design of a 3D neural wrap functioned to support and guide peripheral nerve healing. We hypothesize that PCL films coated with GO nanomaterial films will successfully attach to the PCL film iterations and that they will show a high potential for supporting hADSC and neural differentiated hADSC cultures compared to controlled PCL films without GO coatings.

2.2 Experimental Neural Wraps

2.2.1 Graphene Solution Preparation

With a joint collaboration between the University of Tennessee's CVM department and the University of Arkansas Little Rock (UALR) Nanotechnology center, we created graphene and PEG coated coverslips using techniques originated from the work of UALR as described in (Majeed, Waqar, 2017). 8 iterations of graphene solutions and PEG solution were created based on the surface coat non-tissue glass cover slips to determine the optimal surface coating to use on PCL meshes for supporting MSC cell lines. N002-PDR PG (Angstron Materials) with x-y dimensions of 10µm and ≤2.5% oxidative group content, single-layered GO (Cheap Tubes) with x-y dimensions 300-800 nm and 35-45% oxidative group content, and PEG of 8,000 molecular weight (Bioworld) where acquired. 0.1mg/ml PG solution was created by adding 3.0mg N002-PDR PG with 18MΩ deionized water. High-Oxygen Graphene (HOG) solutions used N002-PDR PG for their preparations. Both solutions were oxidized using similar volume ratios of concentrated sulfuric acid (H_2SO_4) to concentrated nitric acid (HNO_3)- $3H_2SO_4$: $1HNO_3$. For the HOG solution, the acid volume ratio was added to 3.0 mg N002-PDR PG for 24 hours and 18MΩ deionized water was added to dilute the

solution to $3H_2SO_4$: $1HNO_3$: $1H_2O$ ratio prior to filtration. 0.1mg/ml single-layered GO solution was created by adding 3.0mg single-layered GO with 18MΩ deionized water. All graphene solutions were vacuum filtered and washed with 18MΩ deionized water several times to collect graphene precipitants. All graphene iterations solutions with the inclusion of PEG (HOG+PEG, GO+PEG) follow the same protocol as discussed previously with the inclusion of 8,000 molecular weight PEG at 0.1mg/ml. all solutions had 30 ml of 18MΩ deionized water added. All solutions where tip sonicated for 2 hours after filtration step.

2.2.2 Air Spray Surface Coating (24-Well Plate)

Thin film surface coating of graphene solutions onto glass cover slips and PCL meshes was achieved using a Paasche series airbrush kit. Under chemical fume hood conditions, two 24-well plates aligned next to each other was placed on a hot plate set to 50-55˚ C. Glass cover slips were taped to the bottom of each well to prevent cover slips from being up lifted from the wells during spraying. The last 12 wells on each end of the plates were taped off to prevent cross contamination during coating phase (**Figure 2.2**). All solutions were bath sonicated 30 min to evenly disperse graphene oxide films in solution that have settled to the bottom of the container after 24 hours or more in storage before being used to coat the materials. 10ml were used from each graphene and PEG solution to coat 24 wells per plate. Solutions were sprayed at 21 psi. A total of 10 plates for graphene and PEG iterations including positive control plates with cover slips and a total of 2 plates for graphene and PEG iterations including positive and negative control plates with smooth and fiber PCL films. Plates were covered with parafilm after coating and UV sterilized for 4 hours under cell culture sterile hood prior to culturing cells.

Figure 2.2 Air spray setup for graphene coatings on 24-well plates

Note: 24-well plates on hot plate chemical fume hood conditions for manufacturing graphene/ PEG surface coated glass cover-slips, and PCL fiber and drop coated films.

2.2.3 Electrospinning

Poly-caprolactone of 80,000 molecular weight (Sigma Aldrich) was used to create PCL solutions for both electrospinning and drop coating manufacturing techniques. Electrospinning solution of 10% wt. PCL was created using 1.5mg PCL powder to 15ml 1:1 ratio of Methylene Chloride (MC) to Dimethylformamide (DMF). Electrospinning apparatus was setup under chemical fume hood conditions with an Aladdin-6000 multi-barrel programmable 6 syringe pump (World Precision Instrument), a 5ml syringe, 19 gage needle head, voltage generator attached to the needle head, and a rotating mandrel collector wrapped with aluminum foil grounded to the fume hood box. Electrospinning parameters were set to 16-17.5 kV charge with the needle tip-to-collector distance set to 7 in and the solution pumping rate set to 1 ml/hr. 15mm non-tissue culture treated glass cover slips were attached to the collector. Each electrospin process used 4 ml of the 10% wt. PCL solution to create thick PCL meshes of random fiber orientation. PCL meshes were deposited on the surface of cover slips making it easy to separate into individual circular sections that fit into non–tissue culture treated 24-well culture plates for cytotoxicity assessment. PCL meshes along with 24 well plates were placed under UV sterilization for 4 hours prior to culturing cells.

2.2.4 Drop Coating

Drop coating solution of 5% wt. PCL was created using 0.75mg PCL powder to 15ml Chloroform. Under chemical fume hood conditions, glass cover slips were placed on top of leveled glass plates. A 200 µl pipette was used to load PCL solutions onto cover slips. A beaker was placed on top of the cover slips while chloroform evaporated. Smooth PCL films remained once all chloroform evaporated and placed into 24-well culture plates. PCL smooth films were placed under UV sterilization for 4 hours prior to culturing cells.

2.2.5 Rat/ Human ADSC Culture

Passage 3 rADSCs and hADSCs cell lines were acquired from The University of Tennessee Medical Center Laboratory for Regenerative Medicine headed by Dr. Tom Masi and Dr. Stacy Stephenson. Both cell lines were previously assessed for mesenchymal cell quality by observing their potential for differentiation towards cell lineages expected of cells that follow a mesenchymal cell pathway (tri-lineage testing), cell surface marker profile, and proliferation capacity under normal culture conditions. Non-tissue culture 24 well plates with glass cover slips surface coated with graphene and PEG iterations were seeded with rADSC culture for MTS and Calcein AM/PI assessment of cell viability. All wells were seeded with a cell density of 20,000 cells/well, suspended in 500 µl of DMEM-F12 cell culture media (DMEM-F12 +10% fetal bovine serum+1% L-glutamine+ 1% penicillin streptomycin). Wells were kept in incubator set to 5% CO_2 and 37˚C during the culture period. Regular media changes were scheduled at day 3 and 5.

Non-tissue culture 24 well plates with both electrospun (fiber) and drop (smooth) coated PCL films with surface coated graphene and PEG iterations were seeded with hADSC cultures for cell differentiation and protein expression assessment. It has been observed in previous studies that during neural regeneration that there is a marked increase in cAMP messenger proteins in axons as a result of membrane depolarization of Ca ion channels, thus regulating neurotrophic growth factors and axon extension during repair[21,22]. Our protocol for elevating intracellular cAMP to artificially induce hADSC towards cells with neural like characteristics was similar to the methods used in[23,24]. Primary induction medium consisted of 0.5 mM 3-isobutyl-1-methylxanthine (IBMX) and 1 mM dibutyl cyclic adenosine monophosphate (db-cAMP) per well with the addition of 500µl of DMEM-F12 cell culture media. Wells were kept in incubator set to 5% CO_2 and 37˚C during the culture period. Regular media changes were scheduled at day 3 and 5.

2.2.6 MTS Assay

Tetrazolium is a redox indicator commonly used to quantify the number of viable cells in a controlled area. The compound is positively charged in its initial form and when combined with negatively charged phenazine methosulfate it becomes a stable macromolecule in aqueous solution. It is permeable to the cellular and mitochondrial membrane for most cell types, giving tetrazolium easy access to metabolically active sites of cells. When tetrazolium is positioned in the mitochondria it is bio reduced by dehydrogenases enzymes. The electron from NADH or NADPH is passed to the tetrazolium molecule and yields a compound called formazan. The formazan compound is a chemically stable dye that will bind to the cell surface and is soluble in aqueous solution. By measuring the absorbance of light from the dye we can quantitatively determine how many viable cells are in a given culture area and over time observe if the number of cells increase or decrease as an indicator of cell growth or death. Each coating had a sample size of n=5 wells for culture time points day 3, 5, and 7 with 1 negative control blank well at each time point to normalize MTS values from background absorption given off by the wells material and the culture media MTS cell proliferation quantitative analysis was carried out at these time points using CellTiter 96 Aqueous one solution (Promega). At each time point, the old media was removed and replaced with fresh media. MTS reagent was added to each well at a 1/5 dilution ratio. Well plates were left in 5% CO_2 and 37˚C incubator for 3 hours to allow ample time for MTS reagent to react with cells. Using an Epoch Biotek micro-plate reader set to detect 490nm UV-Vis absorption, we quantified the formazan intensity of each coating and compared them to positive control tissue culture treated glass cover slips.

2.2.7 Calcein AM, Propidium Iodine Live Stain

Calcein AM is a fluorescent dye that is permeable to live cell membranes. Intracellular esterase removes acetoxymethyl esters from Calcein AM which reduces to the fluorescent calcein dye expressed at 485 nm

excitation and 520 nm emission. Commonly utilized as a visual indicator of live cells and for temporary tracking of live cells in culture. Propodeum Iodine is a red fluorescent dye that is impermeable to live cells, which makes it useful in labeling and tracking dying cells present in a culture area. The dye will bind with DNA by intercalating between base pairs, where the dye is expressed at 488 nm excitation and 617 nm emission. Both reagents were acquired as Cell Trace Calcein green AM 5µg/µl (ThermoFisher), and Propidium Iodine 1.0mg/ml (ThermoFisher). A combined solution of calcein AM (5µg/ml HBSS) and PI (0.5 µg/ml HBSS) was created. Old media from the well at each time point was removed and washed twice with HBSS to remove any floating dead cells or debris that could obstruct visualization of the dyes. 0.5 ml of calcein/ PI solution were dispensed into wells and left in 5% CO_2 and 35˚C incubator for 30 min to allow ample time for reagents to react with cells. Using a Light Fluorescence Microscope, we visualized surface area coverage of calcein AM and PI fluorescence on coverslips.

2.2.8 Immunofluorescence

Vimentin is an intermediate filament protein highly concentrated in the cytoplasm of mesenchymal based cell lines as a primary component of the cytoskeletal structure for cell mobility and spreading and therefore can act as a quality control marker during immunofluorescence protocols [25]. DiI is a lipophilic stain that labels the bilayer of the cellular membrane of live cells. It is often used as a cell tracking stain that will label the cells for long periods of time without impacting normal cellular physiology. This will allow for tracking of hADSC cultures seeded on biomaterials during the entire differentiation period. S100 protein are responsible for regulating Ca^{+2} levels, which are involved with different cellular pathways that regulate cell growth, cytoskeletal activities, and inflammatory responses. S100β protein is a subsidiary of the S100 family and is specific to glial cells, particularly astrocyte cells that function to regulate axon proliferation and neurite extension by controlling Ca^{+2} intracellular levels [26,27]. Vimentin present in hADSC cultures is expected to show changes in morphology similar to that of neural based cells by day 6 when stimulated with this specific neural induction media. Changes in S100β expression is expected in hADSC by 24 hours post neural induction with this specific neural induction media as an indicator of neural differentiation.

Immunolabeling was performed on MSCs plated on coated glass coverslips. 24 well-plates were divided into 2 equal sections with wells that received normal DMEM F-12 media and wells that received neural stimulant media. DiI staining of all immunofluorescence wells was performed on the same day of cell seeding to track cell growth over the culture period. Cells were fixed at 24 hours post-cell seeding at 6 days post-cell seeding. Cells were fixed in 4% Paraformaldehyde for 10 minutes. Washed wells with HBSS containing 0.1% Triton X-100 and let sit at RT for 10 min. wash twice with HBSS and blocked with 1:10 protein block for 30 min at RT. Wells fixed at day 1 were then incubated with 1µg (4µl) Unconjugated Purified mouse 0.25µg/ml (BD Pharmingen) Purified Mouse S100B-antibody while wells fixed at day 6

were incubated with 1µg (2µl) Unconjugated Purified mouse anti-vimentin, 0.5µg/ml (BD Pharmingen) at 1µg/well. Primary antibodies were added to 1:10 protein block solution at 500 µl/well and left overnight at 4°C. Primary antibody solutions were removed from wells and washed twice with HBSS. Secondary antibody AlexaFluor 488 Donkey, anti-mouse IgG, 2mg/ml, (Invitrogen) at 4µg/well (2µl) to 1:10 protein block solution at 500 µl/well and incubated for 30 min at RT. Wash wells with HBSS before mounting samples onto glass slides using 1 drop of DAPI Prolong Gold antifade reagent (Molecular Probes).

2.3 Results

2.3.1 MTS Analysis

MTS results of HOG and HOG+PEG coating showed significant increase in formazan fluorescence from day 3 to day 5, with fluorescence intensity leveling off at day 7 for HOG coating and a continued linear proliferation projection for HOG+PEG towards day 7. GO, GO+PEG, and PEG coatings showed continued significant increase in formazan fluorescence at each culture time period reaching a peak proliferation intensity at day 7 statistically similar to that of the positive control coverslips. HOG and HOG+PEG coatings appear to have moderate viability potential with proliferation reading showing significantly less formazan intensity at day 7 compared to positive control coverslips. GO, and GO+PEG was the only graphene-based coatings that showed significantly similar levels of rADSC viability at day 7 compared to the control coverslips (**Figure 2.3**).

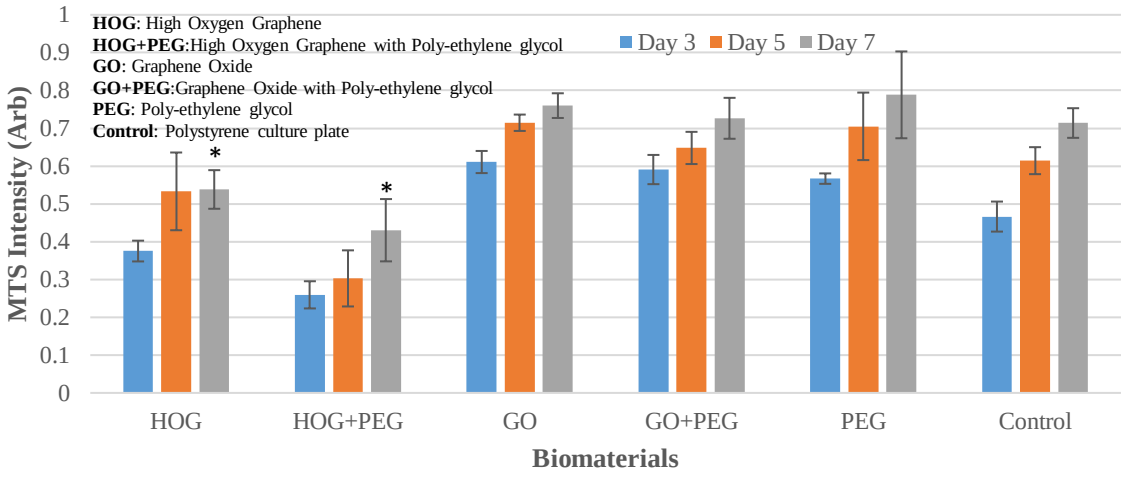

Figure 2.3 Rat ADSC MTS Analysis on Graphene Iterations

Note: Sample size n=5 per group per day, ANOVA analysis of day 7 MTS values relative to control groups. *P ≤ 0.05

2.3.2 Live/Dead Calcein AM Propidium Iodine Stain

Calcein AM and PI Live/dead stains were analyzed under fluorescent microscope with images taken at the center of each 24-well. Minimal PI dye was detected on each coating iteration most likely due to the process of washing each surface coating twice with HBSS solution before applying staining solution, thus removing any loosely adhered or floating dead rat MSCs to stain with PI. The images of positive Calcein AM staining for all coatings at day 7 are shown in (**Figure 2.4**). The qualitative assessment of these images indicates that live rADSC cultures are present on each iteration of graphene coating at day 7. Quantitative assessment of the intensity of calcein stains was performed using ImageJ by grey scaling the green fluorescence of calcein and measuring the total area coverage of the stain at five random locations at day 7 5X images with no replicates (**Figure 2.5**). Quantitative assessment showed that positive control material had significantly higher positive calcein coverage at day 7, compared to all other coating iterations.

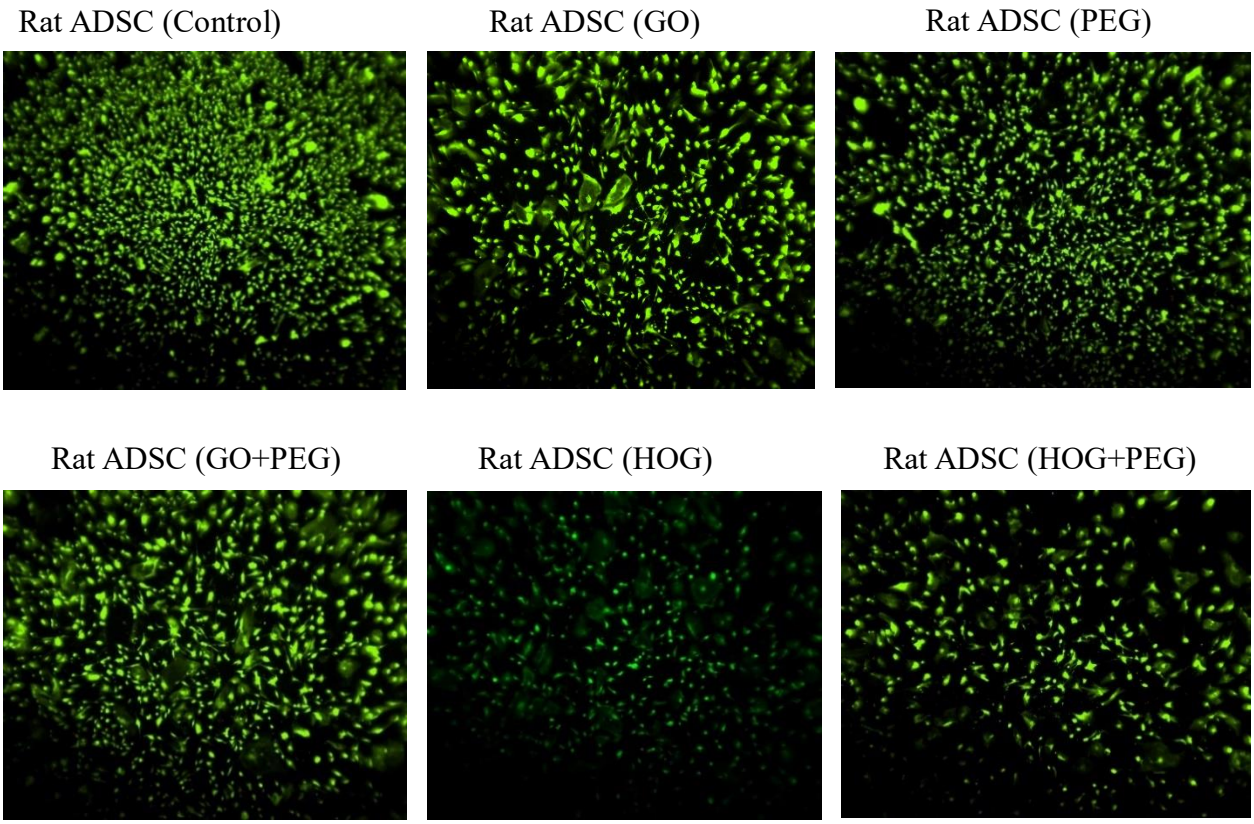

Figure 2.4 Calcein AM staining of hADSC cultures on graphene iterations

Note: Day 7 single 24-well sample of each Graphene/PEG surface coating iteration thru air spray techniques. 5x magnification using fluorescent microscope directed at center position of each 24-well. Calcein AM stained green as an indicator for viable cells present on surface coating iterations.

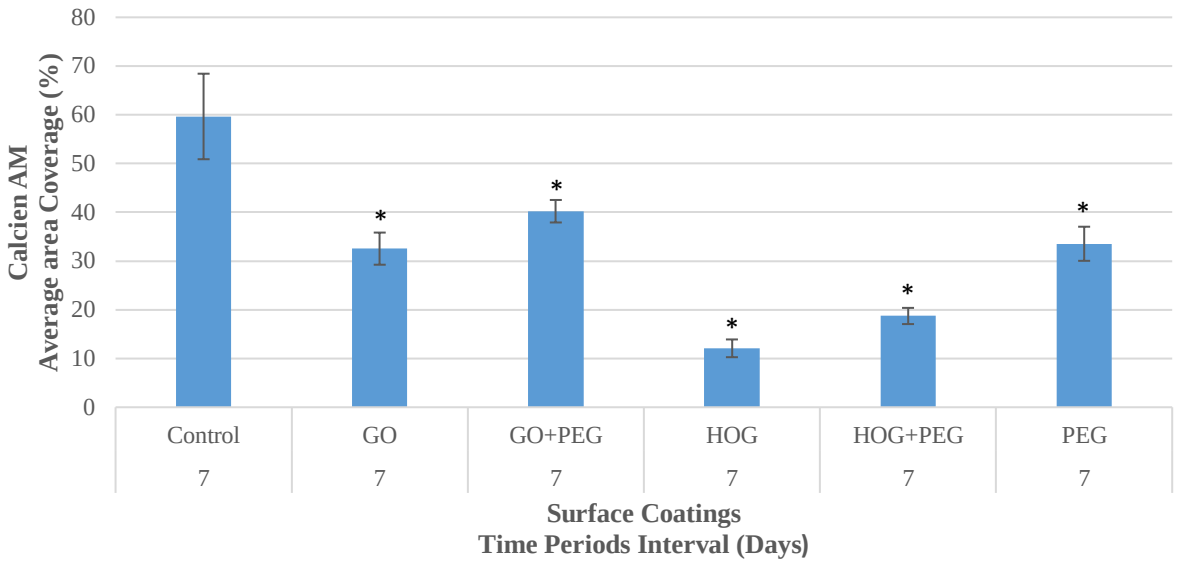

Figure 2.5 Day 7 Calcein AM average area coverage quantification

Note: Day 7 Calcein Am staining for GO and HOG coating iteration and PEG surface coating as an indicator of cell viability. Surface area coverage measurements were taken at n=5 random locations selected on each 5X magnification using ImageJ. ANOVA analysis of day 7 calcein coverage relative to the control well. *$P \leq 0.05$

2.3.3 Day 6 Immunofluorescence-Vimentin

Vimentin proteins were visualized on day 6 of hADSC culture period using a fluorescent microscope. Images were taken at 20X magnification (**Figure 2.6**).

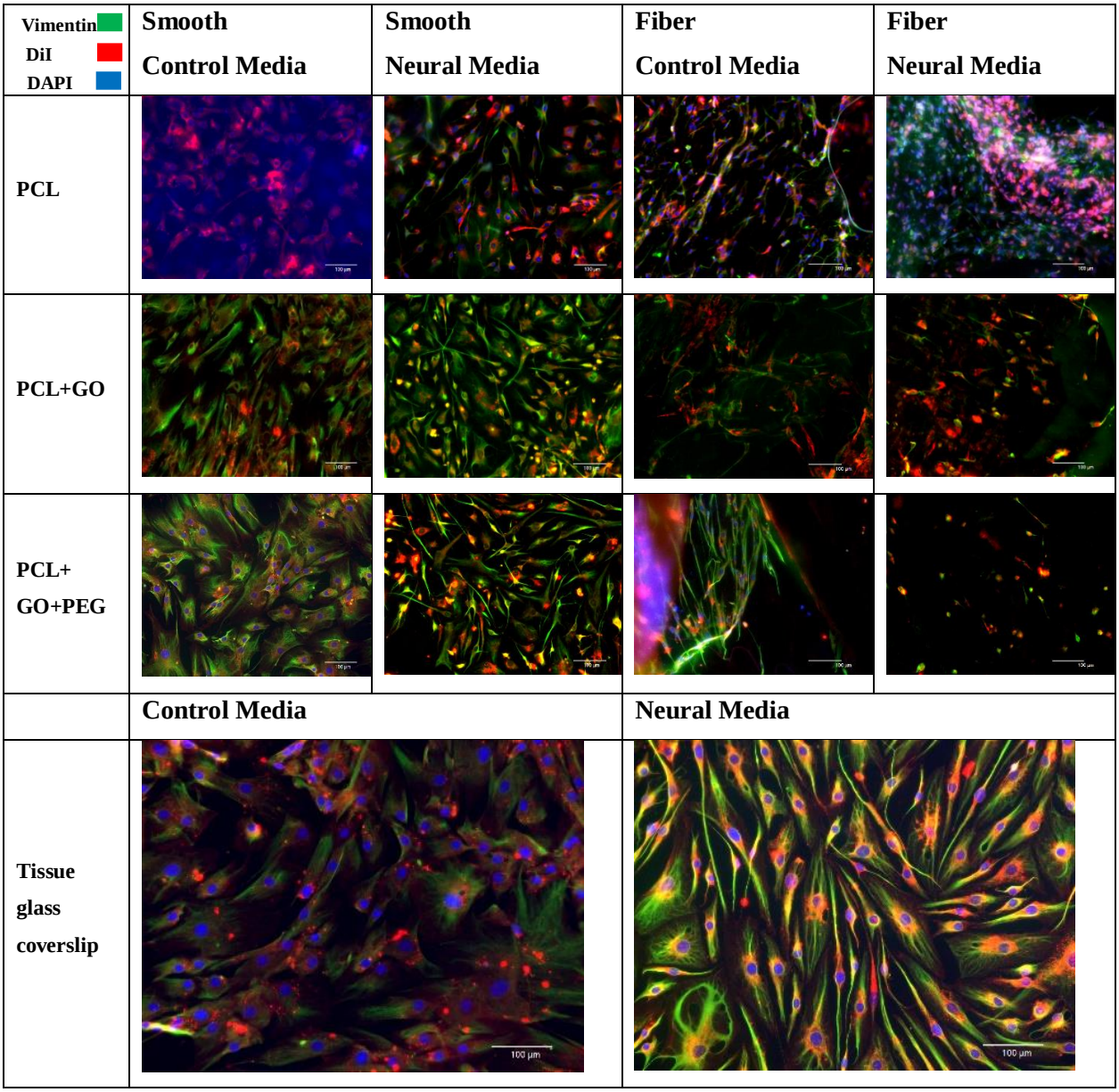

Figure 2.6 Day 6 1µg vimentin/well. Counter cytoplasm stain DiI and nuclear stain DAPI

Vimentin along with its counter DiI and DAPI showed positive on positive control glass cover slips under both neural and control induction media. smooth PCL under control media did not show positive expression of vimentin counter stained with positive DiI and DAPI at day 6 culture, while this material under neural induction media did show positive expression of vimentin counter stained with DiI and DAPI at day 6. Both the smooth PCL+GO and smooth PCL+GO+PEG iterations under neural and control media at day 6 showed positive expression of vimentin counter stained with DiI.Control media showed cellular spreading morphology, while neural induction showed profound extensions of the cell from the nucleus similar to bipolar cell morphologies. All fiber mesh iterations showed either negative expression of vimentin or vimentin expressions difficult to make out cell morphologies even when countered stained with DiI and DAPI. Vimentin and DiI staining showed that clear stable cell morphologies were profound on PCL platforms with smooth surface topography by day 6 culture period, while PCL fiber mesh platforms showed little indication of morphology or cell culture presence on the mesh surface.

2.3.4 Day 1 Immunofluorescence-S100β

S100β protein expression was visualized on day 1 of hADSC culture period using a fluorescent microscope. Images were taken at 20X magnification. S100β along with its counter DiI and DAPI showed positive on positive control glass cover slips under both neural and control induction media at day 1 culture. PCL material of both smooth and fiber topography induced by neural or control media showed low or negative expression of S100β at day 1, while smooth PCL showed positive counter stain of DiI and DAPI and fiber PCL showed positive DAPI expression at day 1. Both smooth PCL+GO and smooth PCL+GO+PEG iterations under neural and control media showed positive expression of S100β counter stained with DiI at day 1. Control media showed cellular spreading morphology, while neural induction showed profound extensions of the cell from the nucleus similar to bipolar cell morphologies. fiber PCL+GO meshes showed positive expression S100β counter stained with DiI under neural and control media at day 1. Profound elongation of hADSC along with parallel orientation and organization of cells relative to each other is present on Fiber PCL under neural and control media at day 1. Results show positive expression of S100β on PCL+GO, PCL+GO+PEG smooth films and PCL+GO fiber mesh platforms with clear different cellular morphologies detected from DiI staining at day 1 culture period. Induction of hADSC cultures towards neural-like cells might be happening on these PCL platforms (**Figure 2.7**).

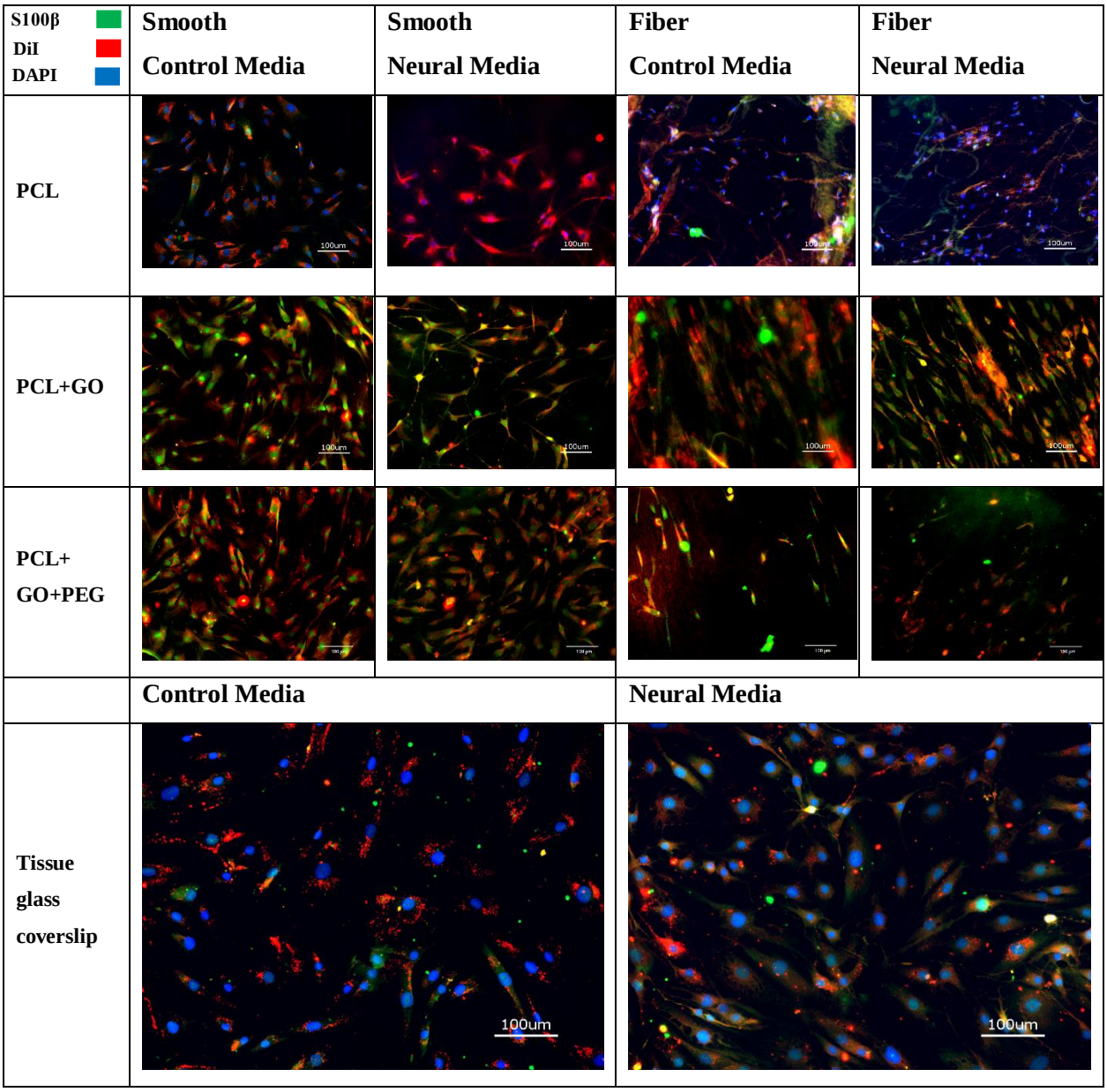

Figure 2.7 Day 1 1µg S100β/well. Counter cytoplasm stain DiI and nuclear stain DAPI

2.3.5 Day 1 S100β Intensity

Quantitative assessment of S100β intensity of hADSC cultured on both smooth PCL+GO films and fiber PCL+GO meshes at day 1 post- neural induction media was performed using ImageJ by grey scaling the green fluorescence of S100β and measuring the maximum intensity of the stain across the length of 10 randomly selected hADSC cell bodies in 5X images (**Figure 2.8**). Analysis showed that the intensity of S100β expression on control glass exposed to control media induction was significantly similar only to the PCL+GO fiber meshes exposed to control media. All other iterations had S100β intensities significantly greater than the control glass under control media. Under neural induction media, Fiber PCL+GO meshes showed similar S100β intensities to that of the control under neural induction media, while all media iterations on smooth PCL+GO films had the highest S100β intensities compared to all other groups. Results indicate that fiber PCL+GO mesh S100β intensities under neural induction at day 1 are comparable to that of the positive control material under neural induction media at day 1 (**Figure 2.9**).

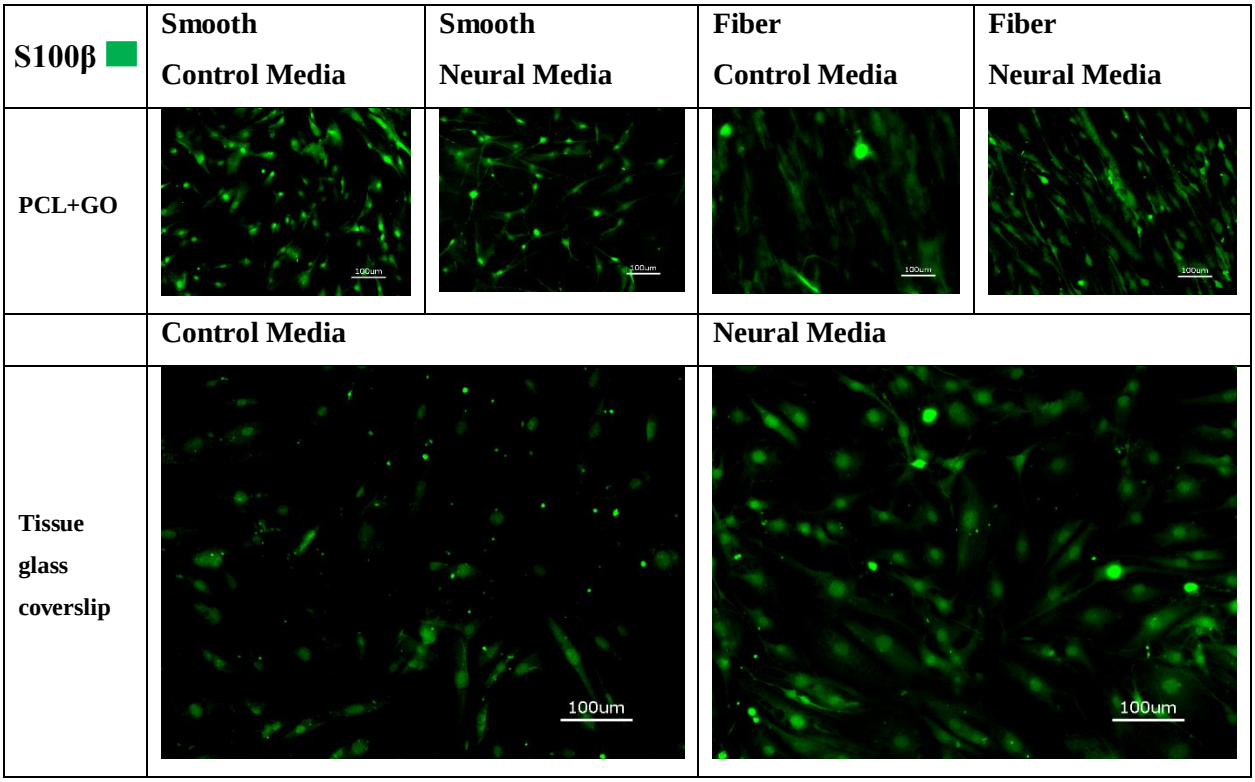

Figure 2.8 Day 1 1µg S100β/well 5X magnification.

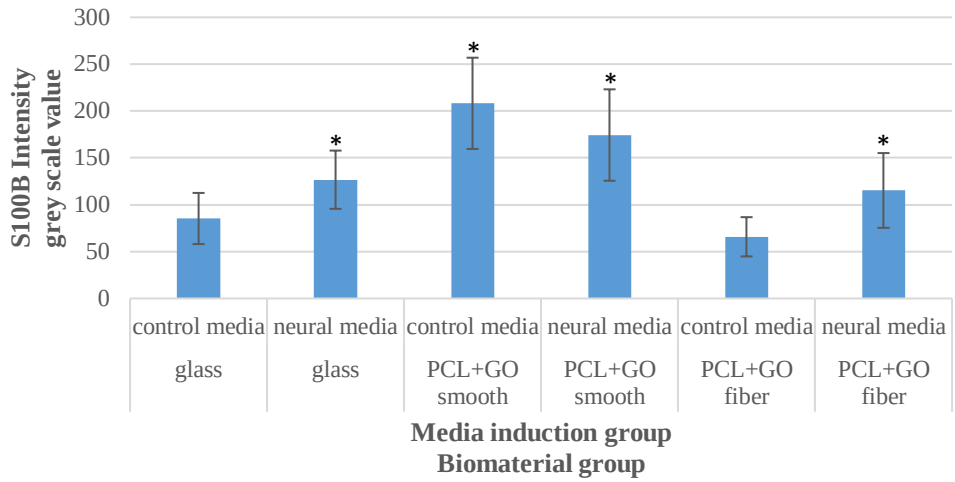

Figure 2.9 S100β intensity profile for hADSC

Note: hADSCs cultured under normal and neural induction media on PCL fiber and smooth platforms surface coated with GO. ANOVA analysis *P ≤ 0.05

2.4 Discussion

Electrospinning and drop coating techniques resulted in thin film surfaces of PCL biomaterial composition with either nanofiber or smooth surface topographies to be tested as platforms for delivering hADSC therapy *In-vivo*.

In the MTS Profile, coating with graphene of higher oxygen content was shown to have similar formazan intensity towards MSC cell model rADSC cultures compared to the control material (GO, GO+PEG, and PEG only) while HOG, and HOG+PEG had significantly smaller formazan intensity compared to the control at day 7. Since this study is interested in utilizing graphene based materials as a coating additive and the GO-based coatings showed similar cytocompatibility to rADSC to that of the control it was decided to continue further *In-vitro* studies using GO-based coatings on PCL platforms, even though PEG-only coating showed the same degree of cytocompatibility to that of the GO-based materials. Positive expression of calcein stain on graphene surfaces showed rADSC cultures at day 7. The coverage of calcein AM staining at day 7 images for each graphene coating shows a similar quantitative projection to that of the formazan intensity detected thru MTS suggesting that there might be a correlation of formazan fluorescence intensity to that of calcein fluorescence when determining the number of live cells present in culture wells with coating iterations.

Observable differences in cell morphology and S100β expression intensity was detected between coatings of different media and surface topography groups. Immunofluorescence expression of DiI, S100β, and DAPI for positive control glass coverslips under neural and control media induction at day 1 culture period was positive, indicating correct immunofluorescence protocol. Control material showed low intensity of S100β under control media compared to neural media group, indicating a low expression of S100β in undifferentiated normal hADSC cultures compared to neural induced hADSC cultures. Fiber mesh and smooth film samples for PCL+GO showed positive expression of S100β and DiI staining. Fiber PCL+GO mesh showed similar S100β intensity profile to that of the control material under different media groups. Smooth PCL+GO showed a higher intensity of S100β under control media group compared to the neural media group. This difference in S100β intensity between the media groups could be attributed to background expression of S100β, or might be attributed to the difference in surface topographies between the PCL film and mesh groups. While the control material and smooth PCL materials showed general spreading under control media and profound extensions under neural media, the fiber PCL materials under both media groups showed additional parallel orientation and organization that we would expect to b present during endogenous nerve repair. While most iterations of human mesenchymal stem cells show very little to no expression of S100β in undifferentiated form, in the presence of GO coating, specific surface topographies and, neural stimulants could account for the differences seen in S100β and the cellular morphologies in those groups. This indicates that PCL materials with fiber surface textures and coated with GO has potential to not only support neural differentiated hADSC but stimulate specific growth patterns of hADSC during differentiation.

Immunofluorescence expression of DiI, vimentin, and DAPI for positive control glass coverslips at day 6 culture period was positive, indicating correct immunofluorescence protocol and antibody concentrations in 24-well plates. Our experimental nerve wrap material PCL+GO, and PCL+GO+PEG expressed positive for vimentin along with counter stain DiI. DAPI was found to be difficult to image on materials coated with GO but the presence of cell spreading and extensions by cells expressed by vimentin and DiI confirmed the presence of these cells on the material surface. Slight difference in cell morphology can be detected between the media cultures, with neural induction cells showing longer extensions from the nucleus with some showing a bipolar shape reminiscent of a neuron, while control media shows cell with overall large spreading on the platform but no profound extensions as noted in the neural media. Cell morphologies showed profound spreading on PCL smooth film iterations while fiber surface iterations showed cell morphologies with profound extensions and bipolar stretching exceeding past their original size as well as signs of mobility and communication with surrounding cells to orient their cell bodies parallel to each other. These characteristics were further enhanced by either induction by control media or neural media were control media had profound spreading and neural induction had cultures with profound cell extensions.

Although vimentin expression of hADSC cultures were not profound in fiber PLC+GO meshes compared to smooth PCL+GO or PCL+GO+PEG by day 6 culture period, S100β expression along with DiI staining on fiber PCL+GO meshes was the only sample that showed positive S100β with profound cellular extensions oriented parallel to each other at day 1 culture period. This more closely compliments the neural development and organization that we want our design to incorporate *In-vivo*. Also, these results share some aspects of hADSC morphological changes at certain time points during neural induction recorded from studies that have referenced using this particular neural induction media recipe to assess cell morphology and neural potential by staining for S100β/ vimentin protein expression in hADSC [28].

Based on both direct and in-direct proliferation assays on MSC lines on different graphene iterations and the performance of these coatings to support hADSC cell lines stimulated towards neural-like differentiation *In-vitro*, GO nanomaterial films might have potential as a surface modifier of PCL fiber meshes for delivering stem cell and biomaterial therapies to assist in the repair of critical neural defects. It is also suggested from these results that the next step is to develop a functional 3D prototype of this biomaterial mesh design that can be implemented in a small-animal to determine initial compatibility of this design in critical nerve defect repair sites.

2.4.1 Implications/ Challenges

Neural Wrap Coating Characterization UALR's Nanotechnology group previously characterized these specific graphene solutions of varying oxygen group content used in this study. In their study, UALR was able to identify the oxygen content and the presence of graphene on coverslips using X-ray Photoelectron spectroscopy (XPS) and Raman Spectroscopy techniques that identified the molecular signature of graphene and the oxidative group bonds as well as their percent ratios in order to identify different graphene iterations produced by UALR's manufacturing methods [29]. A collaboration with the UALR Nanotechnology group was established to assist in replicating these graphene solutions and coating techniques for this study. No characterization assessment tests were performed on this studies batch of graphene coating iteration to determine with certainty that coating was successful or confirm the oxygen content of the coatings. By using UALR's controlled lab environment, equipment, and protocols used in their previous study, it is assumed that the manufacturing of graphene coating iterations will have minimal variation in characterization variables from the graphene coatings created in UALR's previous study. This study's only means of determining successful graphene coating on material surfaces is subjective visual confirmation of color changes on the material surface, most commonly changes towards a dark black or brown confirms that the graphene coating was applied and was present on the material surface.

Manufacturing While air spraying both 24-wells and PCL materials with graphene solutions by hand, it is difficult to maintain consistency of equal amounts of solution sprayed onto each material sample or well when spraying for long periods of time. Under heated conditions using a hot plate, it is difficult to regulate the temperature the sample is exposed to so that it will not melt the PCL films but will not allow graphene solution droplets to form during spraying creating a nonhomogeneous coating of graphene materials. It is suggested that we translate UALR's air spray and graphene solution protocols to our lab to improve our efficiency in creating prototypes of our material for the next study phase. While comparing the manufacturing process of this study with protocols used by UALR's group, there is a high risk for variability in manufacturing when translating protocols of one lab to another. To minimize this, we manufactured our coatings by modifying the manufacturing protocols of UALR for this study to ensure that they are compatible with our lab protocols. We do not expect much variability in manufacture results due to these protocols being new to our lab or closely mimicking similar protocols that we utilize in our lab.

Electrospinning process involves many variables that must be considered to tailor the specific mechanical and functional qualities of your fiber mesh. Altering theses variables will produce fibers with very different characteristics than what is expected. It was noted that the electrospinning parameters often required immediate changes during the spinning process in order to maintain jetting for the intended period of spray. These and other complications such as polymer hardening in the needle head, and solution blockages will have caused variations in the type of fibers that we manufactured for immunofluorescence testing. Any changes in the electrospinning process will alter the texture of the material surface and thus directly impact cell behavior on its surface as a possible explanation for unexpected cell behaviors.

Proliferation Assays The use of soluble MTT (MTS) assays to quantitate cell viability in well conditions is a well-documented and popular indirect proliferation assay. However, the potential for indirect assays to cross react with other compounds suspended with cells such as biomaterials or for biomaterials to affect the cells physiology that results in false expression of MTS regents is a real concern. With graphene-based materials the primary toxicity concern is its ability to stimulate over production of reactive oxygen species in many cell lines that both directly and indirectly impacts the metabolic conditions inside the cells. This could provide a false positive in activation of tetrazolium salt to fluorescent formalin as an indicator for of good cell viability when in reality the cell is under stress. Therefore, it is suggested that direct proliferation assays and other indirect proliferation assays be used in conjunction with MTS to determine if a potential problem exist in the biomaterial [30,31].

The result from this study concerning viability of lower oxygen graphene materials appears to contradict previous studies concerning the use of graphene with lower concentrations of oxygen groups as a platform to support ADSC lines [15,32,33]. This is not uncommon when it comes to assessing the toxicity potential

of graphene-based materials. *In-vitro* and *In-vivo* studies can often contradict each other due in part to the lack of standards for *In-vitro* and *In-vivo* towards assessing nanomaterials and the need to further understand the multiple forms and iterations of graphene-based materials that might play a role in other toxicity pathways. Graphene as a nanomaterial does not yet have a complete toxicity profile to establish with certainty what other toxic mechanisms it might play a role in, such as previously discussed concerning the possible limitations of using MTS proliferation assays on graphene and the advantages to using multiple assays in tandem with each other.

While it is standard to use an appropriate immortalized cell line as a model for assessing cytotoxicity on biomaterial, it was felt for the purposes of determining the efficacy of our biomaterial platform to support ADSCs, rat ADSC were chosen as the model for assessing cytotoxicity of PCL+GO biomaterials towards MSC lines. However, this study could have further benefited from using cell lines intended for cell therapeutic delivery in neural defects with hADSC lines. This would give the study a more accurate assessment of our materials ability to support the proposed therapy provided by hADSC lines. While the two cell lines are similar in general function and role, they play in mammalian physiological systems they have different configurations of organelles, surface markers, and membrane channels that activate specific functions that might not be found in a xenogeneic cell line. Statistical Confidence in the quantitative assessment of Calcein AM intensity could be improved with the addition of multiple replicates instead of a single well set for each time point during the MTS read out.

Immunofluorescence While a positive control material was selected to assess hADSC lines ability to adhere to a pro-adhesion surface, a positive control cell line to assess the positive expression S100β protein in cell lines where it should be highly expressed was not used. A cell line where S100β protein is highly expressed should have been used to determine if our primary secondary antibody protocol would work as intended. While previous studies have shown expression of S100β in ADSC lines it is not often certain of a positive expression or if the signal can even be labeled as positive. A better cell line to use and compare in tandem to hADSC lines would be a glial based cell line, either astrocytes, oligodendrocytes, or the most preferred in the case of peripheral nerves Schwann cells.

There were difficulties in manipulating the PCL fiber mesh iterations when suspended in media solution for visualizing cultured cells. Films were very flimsy and the surface charge of the material as well as the current of the media and the presence of cells on its structure made it easy for the film to fold and collapse in on itself. This made it difficult to straighten out on microscope slides to visualize cell morphology and protein expression. An alternative method for ensuring static movement of the film when suspended in media for the entire culture period would be advantageous and would benefit future studies involving these films.

PCL films coated with our GO surface coatings appeared to either block or absorb DAPI blue light under fluorescence microscope. It has been shown that GO compounds can decrease the intensity of fluorescence given off from other compounds such as DAPI. This process is known as quenching compounds in fluorescence compounds[34]. Other alternative neural stains can be utilized on this type of graphene to visualize the nucleus of cells adhered to its surface such as using Propidium Iodine dead staining that fluoresces in the red spectrum when it binds to the nucleus of dead cells.

2.5 Conclusion

We have described the first initial set of *In-vitro* data supporting our hypothesis as a step towards further developing a novel synthetic 3D nerve wrap that can assist in healing critical neurotmesis injuries. Our assessment determined that PCL platforms of nano-fiber architecture with additional surface coating of GO films can support both native hADSC and hADSC pre-differentiated towards neural-like cell lineages. Both indirect and direct methods respectively MTS and Calcein AM/ PI live stain confirmed a higher degree of MSC viability when rADSC cultures were seeded on GO coatings. This was further supported when PCL meshes on both smooth and fiber architectures showed hADSC with characteristic morphology changes such as cell adhesion and spreading during the culture period when staining with cytoplasm tracker DiI. Distinct differences in cell morphology and S100β expression between the different media and surface architecture groups for each coating iteration suggests that cells were beginning to differentiate in response to media and surface chemical and mechanical niches. Films surfaces with fiber architecture showed a higher degree of organization from that of smooth film surfaces. hADSCs with long extensions would often align themselves to each other in parallel formation on fiber surfaces, while these same cells would often be spread out in chaotic fashion on smooth surfaces. Majority of GO surface coatings showed excellent culture of native and differentiated hADSC cultures compared to positive glass coverslips and PCL only films. Both GO+PCL and GO+PCL+PEG coating showed similar cell response during the culture period suggesting that the addition of unfunctionalized PEG surface coating dose not significantly improve or is detrimental to the effect that graphene has on hADSC cultures.

The results of this study suggest that GO surface coating on PCL fiber mesh is an excellent platform for culturing hADSC lines. We plan to move into the next phase of *In-vivo* assessments using a rodent small animal model to create critical neurotmesis and assess the potential of our surface coated 3D wrap to assist in its repair. The success of these techniques used to manufacture PCL coated platforms at UALR has suggested plans to translate UALR's manufacturing technology and setup to our lab at UT CVM for more precise and rapid production of 3D nerve wraps when designing prototypes for our further planned *In-vitro* studies.

References

1. Fex Svennigsen A, Dahlin LB. Repair of the Peripheral Nerve-Remyelination that Works. Brain Sci. Multidisciplinary Digital Publishing Institute; 2013;3: 1182–1197.

2. Pfister BJ, Gordon T, Loverde JR, Kochar AS, Mackinnon SE, Cullen DK. Biomedical engineering strategies for peripheral nerve repair: surgical applications, state of the art, and future challenges. Crit Rev Biomed Eng. 2011;39: 81–124.

3. Hasirci V, Arslantunali D, Dursun T, Yucel D, Hasirci N. Peripheral nerve conduits: technology update. MDER. 2014; 405.

4. Misra UK, Kalita J, Nair PP. Diagnostic approach to peripheral neuropathy. Ann Indian Acad Neurol. 2008;11: 89–97.

5. Isaacs J, Browne T. Overcoming short gaps in peripheral nerve repair: conduits and human acellular nerve allograft. Hand . 2014;9: 131–137.

6. Menorca RMG, Fussell TS, Elfar JC. Nerve physiology: mechanisms of injury and recovery. Hand Clin. 2013;29: 317–330.

7. Osbourne A, Medicine 5th Year. Peripheral Nerve Injury and Repair.

8. Grinsell D, Keating CP. Peripheral nerve reconstruction after injury: a review of clinical and experimental therapies. Biomed Res Int. 2014;2014: 698256.

9. Griffin MF, Butler PE, Seifalian AM, Kalaskar DM. Control of stem cell fate by engineering their micro and nanoenvironment. World J Stem Cells. 2015;7: 37–50.

10. Wolford LM, Stevao ELL. Considerations in nerve repair. Proc . 2003;16: 152–156.

11. Sampath UGTM, Ching YC, Chuah CH, Sabariah JJ, Lin P-C. Fabrication of Porous Materials from Natural/Synthetic Biopolymers and Their Composites. Materials . 2016;9. doi:10.3390/ma9120991

12. Will J, Detsch R, Boccaccini AR. Chapter 7.1 - Structural and Biological Characterization of Scaffolds. In: Bandyopadhyay A, Bose S, editors. Characterization of Biomaterials. Oxford: Academic Press; 2013. pp. 299–310.

13. Subramanian A, Krishnan UM, Sethuraman S. Development of biomaterial scaffold for nerve tissue engineering: Biomaterial mediated neural regeneration. J Biomed Sci. 2009;16: 108.

14. Petrova ES. Injured Nerve Regeneration using Cell-Based Therapies: Current Challenges. Acta Naturae. 2015;7: 38–47.

15. Elkhenany H, Amelse L, Lafont A, Bourdo S, Caldwell M, Neilsen N, et al. Graphene supports in vitro proliferation and osteogenic differentiation of goat adult mesenchymal stem cells: potential for bone tissue engineering. J Appl Toxicol. 2015;35: 367–374.

16. Lopatina T, Kalinina N, Karagyaur M, Stambolsky D, Rubina K, Revischin A, et al. Adipose-derived stem cells stimulate regeneration of peripheral nerves: BDNF secreted by these cells promotes nerve healing and axon growth de novo. PLoS One. 2011;6: e17899.

17. Jones S, Eisenberg HM, Jia X. Advances and Future Applications of Augmented Peripheral Nerve Regeneration. Int J Mol Sci. 2016;17. doi:10.3390/ijms17091494

18. Jiang L, Jones S, Jia X. Stem Cell Transplantation for Peripheral Nerve Regeneration: Current Options and Opportunities. Int J Mol Sci. 2017;18. doi:10.3390/ijms18010094

19. Marycz K, Marędziak M, Grzesiak J, Fryczkowski R, Laska J. Polyurethane/Polylactide-Based Electrospun Nonwovens as Carriers for Human Adipose-Derived Stromal Stem Cells and Chondrogenic Progenitor Cells. Polym Plast Technol Eng. Taylor & Francis; 2016;55: 1897–1907.

20. Ruiz ON, Fernando KAS, Wang B, Brown NA, Luo PG, McNamara ND, et al. Graphene oxide: a nonspecific enhancer of cellular growth. ACS Nano. 2011;5: 8100–8107.

21. Chierzi S, Ratto GM, Verma P, Fawcett JW. The ability of axons to regenerate their growth cones depends on axonal type and age, and is regulated by calcium, cAMP and ERK. Eur J Neurosci. Wiley Online Library; 2005;21: 2051–2062.

22. Verma P, Chierzi S, Codd AM, Campbell DS, Meyer RL, Holt CE, et al. Axonal protein synthesis and degradation are necessary for efficient growth cone regeneration. J Neurosci. 2005;25: 331–342.

23. Deng J, Petersen BE, Steindler DA, Jorgensen ML, Laywell ED. Mesenchymal stem cells spontaneously express neural proteins in culture and are neurogenic after transplantation. Stem Cells. 2006;24: 1054–1064.

24. Ning H, Lin G, Lue TF, Lin C-S. Neuron-like differentiation of adipose tissue-derived stromal cells and vascular smooth muscle cells. Differentiation. 2006;74: 510–518.

25. Robinson-Bennett B, Han A. 30 - Role of Immunohistochemistry in Elucidating Lung Cancer Metastatic to the Ovary from Primary Ovarian Carcinoma. In: Hayat MA, editor. Handbook of Immunohistochemistry and in Situ Hybridization of Human Carcinomas. Academic Press; 2006. pp. 537–545.

26. Kingham PJ, Kalbermatten DF, Mahay D, Armstrong SJ, Wiberg M, Terenghi G. Adipose-derived stem cells differentiate into a Schwann cell phenotype and promote neurite outgrowth in vitro. Exp Neurol. 2007;207: 267–274.

27. Donato R, Cannon BR, Sorci G, Riuzzi F, Hsu K, Weber DJ, et al. Functions of S100 proteins. Curr Mol Med. 2013;13: 24–57.

28. Alghazali KM, Newby SD, Nima ZA, Hamzah RN, Watanabe F, Bourdo SE, et al. Functionalized gold nanorod nanocomposite system to modulate differentiation of human mesenchymal stem cells into neural-like progenitors. Sci Rep. 2017;7: 16654.

29. Majeed W, Bourdo S, Petibone DM, Saini V, Vang KB, Nima ZA, et al. The role of surface chemistry in the cytotoxicity profile of graphene. J Appl Toxicol. 2017;37: 462–470.

30. Wang P, Henning SM, Heber D. Limitations of MTT and MTS-based assays for measurement of antiproliferative activity of green tea polyphenols. PLoS One. 2010;5: e10202.

31. Jiao G, He X, Li X, Qiu J, Xu H, Zhang N, et al. Limitations of MTT and CCK-8 assay for evaluation of graphene cytotoxicity. RSC Adv. The Royal Society of Chemistry; 2015;5: 53240–53244.

32. Akhavan O, Ghaderi E, Akhavan A. Size-dependent genotoxicity of graphene nanoplatelets in human stem cells. Biomaterials. 2012;33: 8017–8025.

33. Mendes RG, Koch B, Bachmatiuk A, Ma X, Sanchez S, Damm C, et al. A size dependent evaluation of the cytotoxicity and uptake of nanographene oxide. J Mater Chem B Mater Biol Med. The Royal Society of Chemistry; 2015;3: 2522–2529.

34. Povedailo VA, Ronishenko BV, Stepuro VI, Tsybulsky DA, Shmanai VV, Yakovlev DL. Fluorescence Quenching of Dyes by Graphene Oxide. J Appl Spectrosc. 2018;85: 605–610.

Chapter 3: Biometric Data Comparison Between Lewis and Sprague Dawley Rats

Abstract

Pressure mapping systems are a commonly utilized instrument for indirect assessment of the repair of critical defect in small-animal models. For the purposes of our study we are interested in utilizing Tekscans VH4 pressure map system for assessing the degree of critical size repairs in real time during the healing process with rodent models. Previous studies have reported normal kinematic data from common rat species. However, there does not appear to be any literature that compares the normal gait pattern of Sprauge Dawley rats to Lewis rats using a Tekscan VH4 pressure mat system. The purpose of this study is to assess the gait profile of Lewis and Sprauge Dawley rats generated by Tekscan's VH4 system to detect similarities and/or differences gait parameters involving both force and temporal variables to prepare for future critical defect *In-vivo* models that require careful selection of animal participants based on gait profile. The gait profile of 14 Lewis and 14 Sprauge Dawley rats was recorded and gait parameter data was normalized and compared for statistical variance between the two rodent strains. The results showed that the temporal and normalized force parameters were not significantly different between the two strains. Variation in some of these parameters were considered due to the significant difference in overall body size between the two strains and how each rodent act as its own independent group. For future critical size *In-vivo* models, either rodent strain would be acceptable for assessing critical repair in any model that uses the Tekscan VH4 pressure map system since the base line gait profile recorded from both strains were found to be statistically similar to each other.

3.1 Introduction

Animal models are the primary component in the establishment of acceptable *In-vivo* testing of implantable medical devices. Animal models have been designed to assess the standard clinical requirements expected of class II or III medical devices and a focused assessment of the functional properties of the device. This is for the purpose of studying the different variations of the device's actual performance in a physiological system similar to that of humans compared to its expected or intended performance in order to prepare the device for consideration for clinical trials. In order for a class II or III medical device to be considered for clinical evaluation in human trials, the data collected from *In-vivo* studies must be quantifiable in order to be normalized to human physiologic parameters when translating from an animal model [1–3]. Biometric data comparing changes in gait profiles is a critical step when using animal models to study musculoskeletal and peripheral nerve injury. Assessment tools used in the measurement of the biometrics of locomotion are common tools for quantitatively assessing the quality of tissue repair [4–6]. Depending on the animal model and species selected, the tissues being studied to determine the performance of the device, and the tools for collecting and assessing gait parameters, the biometric data can be included as quantitative evidence for support of a class II or III device prior to human clinical trials. It is therefore important to fully understand the normal gait pattern for any animal species used in an animal model were gait parameter data will be recorded for the purposes of assessing implant performance as a prerequisite for approval to begin clinical trials in humans.

While the types of animal species used and the specific tissues assessed in critical size defect models has changed by a small margin, the tools and techniques used to assess gait patterns and report quantitative data has markedly improved [7–9]. This is due, in part, to the inclusion of novel technologies that can more precisely and accurately detect specific gait parameters with minimal background noise, the augmentation of previous methods by combining different technologies together creating instruments capable of producing a more extensive gait profile, and the increased practice of using exogenous gait biometric data from previous tissue repair studies as an acceptable control standard for quantifying implant performance *In-vivo*. Rats are one of the most common animals used in critical defect models for preclinical testing of class II and III medical devices [10–12]. As the instrumentations for assessing gait parameters continues to develop new technologies, it is important that normal gait parameters of different species of rats are determined to provide data upon which to plan experiments. It is also valuable to compare normal gait biometrics between different species of rats that use similar gait assessment tools in order to evaluate differences among species used for specific defect models. This is especially relevant for biometric tools that find significant differences in the gait parameters between different strains of rats, where one species gait pattern is more consistent and less varied for a particular tissue defect model than other species. A more

predictable gait pattern could have a greater advantage in profiling tissue repair in specific critical defect models *In-vivo*.

Recently, pressure sensing mat technology has been developed as a more accurate and precise tool for quantifying gait [13–15].We aimed to utilize a commonly used pressure sensing mat tool to measure the kinematic and timing variables in both the forelimb and hindlimbs of two species of rats. Studies that have utilized the VH4 system have reported excellent calibration reliability of the 5101 sensors in *In-vivo* studies of 1.2–4.4%, well within the established acceptable cut-off range of 5%. A previous study also reported this as an acceptable range when reporting sensor reliability ranges of 3–4% [16]. Two of the most common rat species used in *In-vivo* critical defect testing are Sprague Dawley and Lewis rats [17,18]. While previous studies have reported normal kinematic data from these rat species, there does not appear to be any literature that compares the normal gait pattern of Sprauge Dawley rats to Lewis rats using a pressure mat system [19–22]. In this study we will be comparing the gait parameters between Sprauge Dawley and Lewis rats. The type of data output from pressure mat systems concerns both temporal and force gait data. Temporal data analyzed in this study includes stance time (how long each limb makes contact with mat), swing time (the time it takes between two hits on the mat with the same hindlimb), stride time (the time it takes between right forelimb and left hindlimb to make contact with the mat at the same time as well as the opposite limb pattern), stride length (distance between right forelimb and left hindlimb as well as its opposite limb pattern) stride velocity, stride acceleration, and limb surface area coverage. Force data assessment includes the limb forces generated on the mat with respect to pressure difference, normalized force data to the body weight of each rodent, impulse force in each hindlimb.

We hypothesized that the normal walking gait motion between the two species would be similar. The objective is to comparing the gait parameters between Sprauge Dawley and Lewis rats. The type of data output from pressure mat systems concerns both temporal and force gait data. Temporal data analyzed in this study includes stance time (how long each limb makes contact with mat), swing time (the time it takes between two hits on the mat with the same hindlimb), stride time (the time it takes between right forelimb and left hindlimb to make contact with the mat at the same time as well as the opposite limb pattern), stride length (distance between right forelimb and left hindlimb as well as its opposite limb pattern) stride velocity, stride acceleration, and limb surface area coverage. Force data assessment includes the limb forces generated on the mat with respect to pressure difference, normalized force data to the body weight of each rodent, impulse force in each hindlimb and its normalized version to the rodent bodyweights, and the peak pressure generated in each hindlimb. The system is also capable of comparing specific limbs to each other as a ratio profile for maximum force generation, stance time, stride time, stride length, and stride velocity variables. These ratios concern 4 areas of comparison towards these variables: forelimbs to hindlimbs, all

limbs on the right side of rodent to all limbs on the left side, right forelimb to left forelimb, and right hindlimb to left hindlimb.

3.2 Methods

The study was approved by the Institutional Animal Care and Use Committee (IACUC) at the University of Tennessee, Knoxville (IACUC# 2574-0318). Lewis and Sprague Dawley rats were selected for use in the study of gait biometrics. Sprague Dawley and Lewis rats used in this study were eight-week old males (n=14, each) and allowed to acclimate to their environment for one week before gait assessment. Animals were directed to walk two passes on the pressure mat during each testing period before the testing began in order for the animals to get familiar to the mat and become comfortable with handling and being directed across the mat.

3.2.1 Pressure Sensing Mat Specifications

Gait patterns were analyzed using a pressure sensor mat (Tekscan VH4, Tekscan, Boston, MA). This mat is composed of four 5101 high-resolution pressure sensor matrix grids layered in series to each other. The sensing area uses rows and columns of sensels and converts the change in electrical resistance to a force based on calibration to known applied weight. Each sensor has a grid of 44 columns and 44 rows (11.2 cm x 11.2 cm) of sensels, creating 176 sensel columns x 44 sensel rows for a total area of 11.18 cm x 44.7 cm (499.75 cm2) with a 0.127-cm gap between sensels in each row and column. The total grid has 7,744 sensels at a density of 15.5 sensels/cm2. The sensors/handles were aligned to place the origin (0,0) in the upper left corner of the sensel grid [23]. For the purpose of this experiment, The gait testing unit was modified to include a tinted Plexiglas tunnel (width 17.0 cm, height 17.0 cm, length 44.7 cm) and a Styrofoam side wall (width 2.54 cm, height 2.54 cm, length 44.7 cm) for the purpose of guiding the rats across the mat and to insure that the rats remained in the sensel area so that the rats would perform normal walking gait patterns across the entirety of the mat. This minimized false data recordings from animal miss-steps on the edges or outside the sensor matrix area (**Figure 3.1**).

The pressure sensing mat was calibrated using a phantom device designed to support a known mass (2,006.8 g; 4.42 lb.; 19.7 N). The instrument was programmed to record gait parameters at a sample rate of 50 frames/sec, with start and stop recordings being manually controlled. Calibration accuracy was tested by comparing five repeated measures of the phantom weight. Tekscan software records the raw data of each gait variable as an average mean value for each trial walk in an ASCII file format. Each limb must record at least 3 footfalls (“hits”) on the mat to calculate an average value, otherwise the software will record an N/A for the calculated variable.

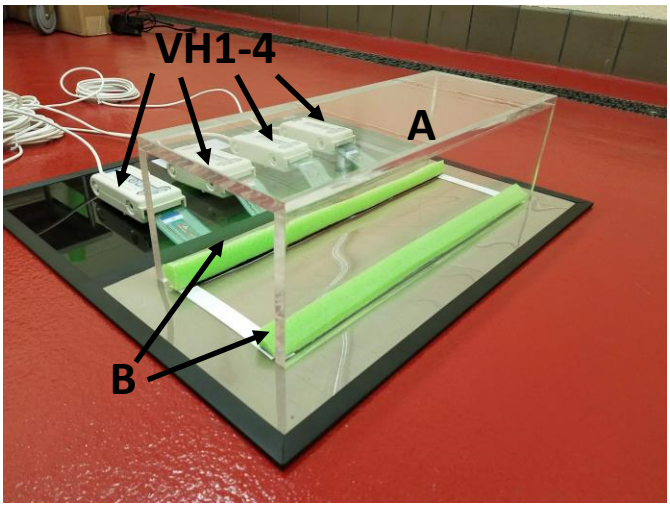

Figure 3.1 Tekscan VH4 Pressure-mat system setup.

Note: Testing apparatus consists of a tinted Plexiglas tunnel (A). The tunnel is positioned over the Tekscan pressure mat aligned to Styrofoam borders placed at the edges of the sensel area (B). Four sensors (VH1–4) connect the four 5101 sensors to the Tekscan mat.

3.2.2 Gait Testing Protocol

Calibration of the pressure sensors was carried out before each use of the device. Each rat was weighed using a digital scale before starting walk trials on the mat. The rats were released on either side of the pressure mat facing the open end of the transparent Plexiglas tunnel centered over the sensel area on the mat. The tunnel was designed with dimensions that encompassed the Styrofoam walls attached to the mat without making contact with the sensel area. After the rats had been acclimated to their environment for at least 1 week and body weights were recorded, the rats were positioned and held by the operator at either end of the tunnel openings and released when the test was initiated by manually starting the recording procedure in the software by the operator. The animal then traversed the length of the tunnel until they reached the other end at which time the recording was stopped manually for either a successful trial or an incomplete trial as determined by the software operator.

Criteria for a successful walk across the mat was determined if the rats were able to walk continuously from one end of the mat to the other with minimal to no pause in gait motion and at least three strikes were detected for each limb as confirmed by reviewing video recording of the measured biometric data on the software. All data recorded for the gait parameters were average values from each successful trial. The procedure was repeated for each animal until 2 successful trials were achieved, giving a total of 28 data sets per rodent group. Data was reported as the average peak measures of each gait variable and for each limb

as recorded by the sensels and identified as either the right forelimb (RF), left forelimb (LF), right hindlimb (RH), or left hindlimb (LH) as a whole for the trial.

A video camera was attached to a strip located directly above the Plexiglas tunnel and synced to the gait profile to capture the motion of the animals as they walked across the mat to observe the subject's behavior and match the limbs with the corresponding limb strikes in the gait profile. The operator had to use video synchronization in order to identify any software selection of the wrong limb strike box and when it the software was unable to discern multiple limb strikes at a single location during the trials due to ipsilateral forelimb and hindlimb contact which often overlap each other. This made it necessary to manually correct boxes by following the subject's motion on both the camera and gait force profile for corrected gait assessment (**Figure 3.2**).

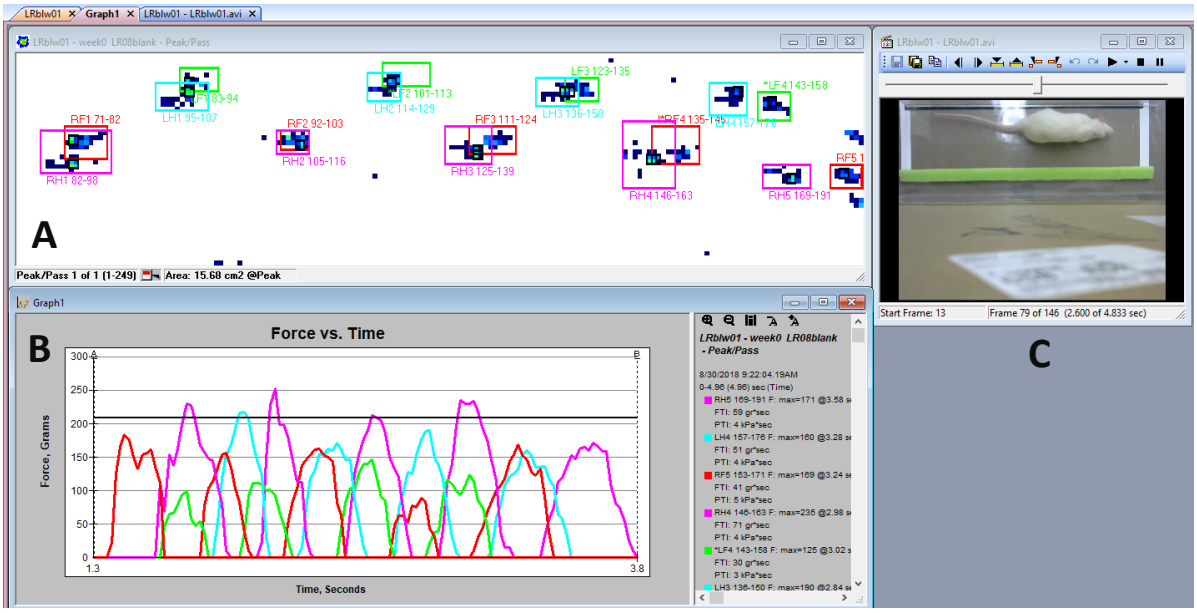

Figure 3.2 Tekscan software display.

Note: A: Example gait force profile during the subjects walk from right to left. Visual display of right forelimb (red), left forelimb (green), right hindlimb (pink), and left hindlimb (blue) contact sensor boxes is represented as the summation of sensels activated and their corresponding limbs recording location on the mat, time, and gait variables. B: Graph of force vs. time for the example gait profile of force peaks with their respective limbs. C: Logitech camera visual output.

Gait temporal variables measured included average stance time, swing time, stride time, stride length, stride velocity, and stride acceleration based on the location of the limb strikes relative to the sensel area and another subsequent limb strikes. Contact variables included contact area derived from the maximum number of sensels loaded. Force generation parameters included contact force, impulse force, and contact pressure derived from the maximum sensor readings at the time of impact. Contact pressure, impulse force and contact force were normalized to the weight of the animals on the date of testing (average value divided by body weight). Time variables (stance time, stride time, stride length, and stride velocity) and maximum force were normalized to specific limb orientations (forelimbs to hindlimbs, left side limbs to the right sided limbs, left forelimb to right forelimb and left hindlimb to right hindlimb) and compared for statistical significance.

3.2.3 Statistical Analysis

All successful trials were included from each rodent group. Analysis of variance was used to compare all 28 data sets per rodent group as a means comparison for each gait variable. Two-way analysis of variance for comparisons between the groups followed by Bonferroni's post-hoc analysis. Significance was set at $P \leq 0.05$.

3.3 Results

3.3.1 Normal Gait Assessment

All 28 rodent subjects from the Sprague Dawley (n=14) and Lewis (n=14) rat groups completed two successful walk trials. This resulted in a total of 28 successful gait trials per group, giving a total of 56 data sets to assess mean values of gait parameters for rodent groups. The body weight of each rat was recorded before beginning trials. Significant difference was detected in the initial body weight of the rat groups, with the Sprauge Dawley rat group having a mean body weight 26.1% greater than the Lewis rat group (**Figure 3.3**).

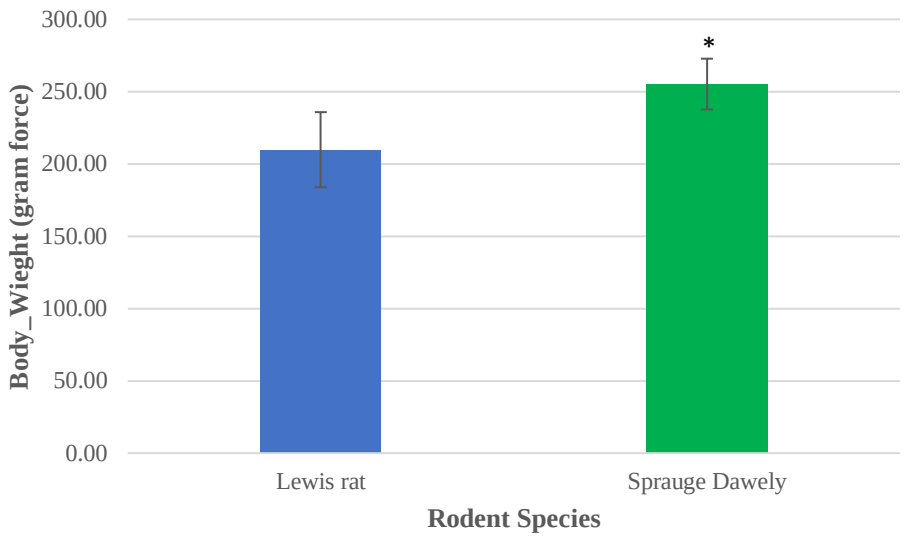

Figure 3.3 Mean Body weight distribution between Lewis and Sprauge Dawley Rats

Note: ANOVA analysis *P ≤ 0.05

3.3.2 Gait Analysis: Ratio Temporal Parameters

The ratio means values indicate the degree of variance between different limbs for specific temporal variables (**Figure 3.4**). The mean and standard deviations applicable for each gait variable assessed are presented as follows: Sprague Dawley Rat (SD), Lewis Rat (LR), Stance Time forelimb/hindlimb (Stance TF/H), Stride Time forelimb/hindlimb (StrideTF/H), Stride Length forelimb/hindlimb (StrideLF/H), Stride Velocity forelimb/hindlimb (StrideVF/H), and Maximum Force forelimb/hindlimb (MFF/H), Stance Time Left side/Right side (Stance TL/R), Stride Time Left side/Right side (StrideTL/R), Stride Length Left side/Right side (StrideLL/R), Stride Velocity Left side/Right side (StrideVL/R), and Maximum Force Left side/Right side (MFL/R), Stance Time Left forelimb/Right forelimb (Stance TLF/RF), Stride Time Left forelimb/Right forelimb (Stride TLF/RF), Stride Length Left forelimb/Right forelimb (Stride LLF/RF), Stride Velocity Left forelimb/Right forelimb (StrideVLF/RF), and Maximum Force Left forelimb/Right forelimb (MFLF/RF), Stance Time Left hindlimb/Right hindlimb (Stance TLH/RH), Stride Time Left hindlimb/Right hindlimb (StrideTLH/RH), Stride Length Left hindlimb/Right hindlimb (StrideLLH/RH), Stride Velocity Left hindlimb/Right hindlimb (StrideVLH/RH), and Maximum Force Left hindlimb/Right hindlimb (MFLH/RH).

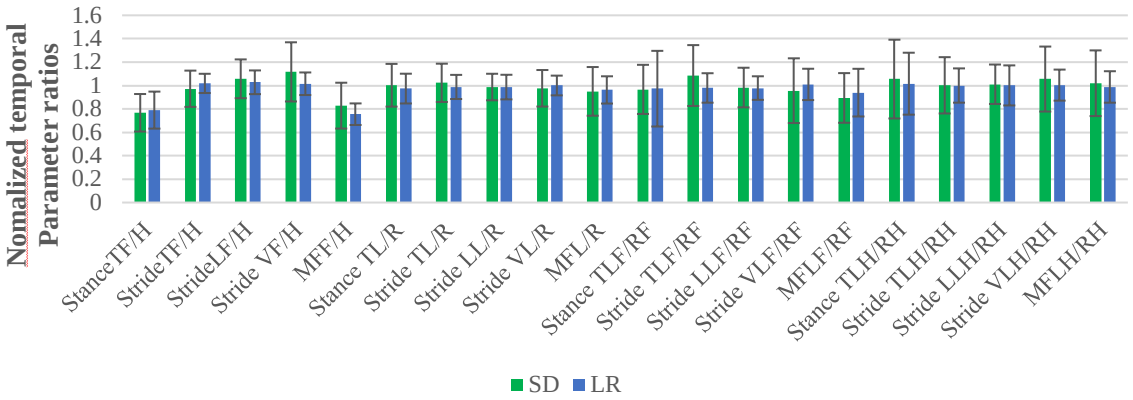

Figure 3.4 Ratio temporal and force parameter values

Note: ANOVA analysis. *P ≤ 0.05

Table 3.1 Ratio values for normalized temporal parameters

Species	StanceTF/H	StrideTF/H	StrideLF/H	Stride VF/H	MFF/H
SD	0.77±0.16	0.97±0.155	1.06±0.166	1.12±0.25	0.83±0.2
LR	0.79±0.16	1.02±0.08	1.03±0.101	1.02±0.1	0.76±0.09
Species	Stance TL/R	Stride TL/R	Stride LL/R	Stride VL/R	MFL/R
SD	1.00±0.18	1.02±0.16	0.99±0.11	0.98±0.16	0.95±0.21
LR	0.97±0.13	0.988±0.10	0.99±0.105	1.0±0.08	0.96±0.12
Species	Stance TLF/RF	Stride TLF/RF	Stride LLF/RF	Stride VLF/RF	MFLF/RF
SD	0.97±0.21	1.08±0.26	0.98±0.17	0.96±0.28	0.894±0.21
LR	0.97±0.32	0.98±0.13	0.98±0.1	1.01±0.13	0.94±0.204
Species	Stance TLH/RH	Stride TLH/RH	Stride LLH/RH	Stride VLH/RH	MFLH/RH
SD	1.06±0.34	1±0.24	1.01±0.17	1.06±0.28	1.02±0.28
LR	1.02±0.26	1±0.15	1±0.17	1±0.13	0.99±0.13

Note: Stance Time, Stride Time, Stride Length, Stride Velocity, and Maximum Force comparative analysis based on limbs. The closer the mean values are to 1.0, the less variance there is between limbs of the animals

Table 3.2 Values for # of Stance, Gait time, Gait Distance, Gait Velocity, Gait Cycle Time, Cycle min

Species	No_Stance	Gait_Time (sec)	Gait_Distance (cm)	Gait_Velocity (cm/sec)	Gait_Cycle_Time (sec)	Cycles_min (sec)
SD	14.43±2.3	1.88±0.86	30.47±5.64	19.85±9.8	0.62±0.233	110.43±39.5
LR	17.93±1.94	2.04±0.57	37.32±3.67	19.85±6.2	0.5±0.104	125.3±25.45

Table 3.3 Values based on specific limbs for both species.

Species	Extremity	Stance_time (sec)	Swing Time (sec)	Stride_time (sec)	Stride_length (cm)	Stride_velocity (cm/sec)	Stride_Acc (cm/sec²)
LR	LF	0.30±0.142	0.2175±0.076	0.493±0.112	9.37±1.41	20.27±6.44	-2.05±26.93
	LH	0.4±0.15	0.129±0.05	0.49±0.119	9.22±1.48	19.8±5.57	2.81±36.63
	RF	0.32±0.109	0.212±0.052	0.51±0.109	9.62±1.27	20.21±6.30	1.15±24.38
	RH	0.408±0.184	0.136±0.23	0.491±0.099	9.34±1.42	19.88±5.64	14.8±35.85
SD	LF	0.356±0.133	0.295±0.174	0.629±0.235	10.58±2.29	19.73±9.63	5.93±25.34
	LH	0.499±0.2	0.181±0.077	0.63±0.275	10.54±2.28	19.3±8.08	-8.95±20.7
	RF	0.368±0.13	0.249±0.16	0.60±0.257	10.96±2.24	21.73±10.44	5.12±32.47
	RH	0.486±0.2	0.178±0.075	0.651±0.252	10.33±1.88	18.94±10.01	13.4±35.93

Species	Extremity	MF_BW (%)	MF (gr)	Impulse_BW (%)	Impulse (gr)	MPr (kPa)	Cont_Area (cm²)	Adj_Pr (g/cm²)/BW
LR	LF	61.93±10.53	133.9±29.83	10.86±3.06	23.64±8.25	47.7±9.74	0.508±0.08	1.3±0.353
	LH	84.71±9.7	183.6±37.17	20.09±7.86	44.46±22.52	55.53±9.74	0.611±0.1	1.46±0.26
	RF	67.02±10.55	144.3±26.82	12.2±3	26.57±8.49	49.04±7.9	0.515±0.07	1.35±0.203
	RH	86.55±10.52	187.3±35.34	20.5±6.27	44.8±17.1	56.2±10.1	0.633±0.12	1.441±0.253
SD	LF	63.64±13.17	161.0±33.93	12.7±4.54	31.93±10.73	51.75±9.56	0.568±0.11	1.127±0.203
	LH	84.48±15.0	215.9±43.05	24.57±9.53	62.96±25.73	61.4±6.96	0.704±0.14	1.215±0.174
	RF	74.83±19.3	189.8±45.03	14.18±5.45	35.86±12.66	56.46±9.95	0.611±0.112	1.225±0.225
	RH	85.29±16.63	217.9±46.1	24.6±12.14	63.11±32.71	64.07±8.45	0.726±0.133	1.19±0.214

3.3.3 Gait Analysis: Force and Temporal Parameters

Force and temporal parameter values specific to the four limbs that make up the gait profile of each animal group (**Figure 3.5**). Mean variance analysis showed that there were no significant differences for both the Sprague Dawley and Lewis rat groups in the stride velocity and stride acceleration temporal parameters for each limb. The analysis also determined that the normalized maximum and impulse forces in the groups for each limb were statistically similar. Stride length, impulse force, maximum force, contact area, and normalized pressure showed statistical differences between the groups for each limb tested. Swing time, and stride time showed statistical differences between the groups for the hindlimbs and the left forelimb while the right forelimb showed no significant difference. The stance time showed a significant difference for the left hindlimb only. The maximum peak force showed significant differences for all limbs except the left forelimb.

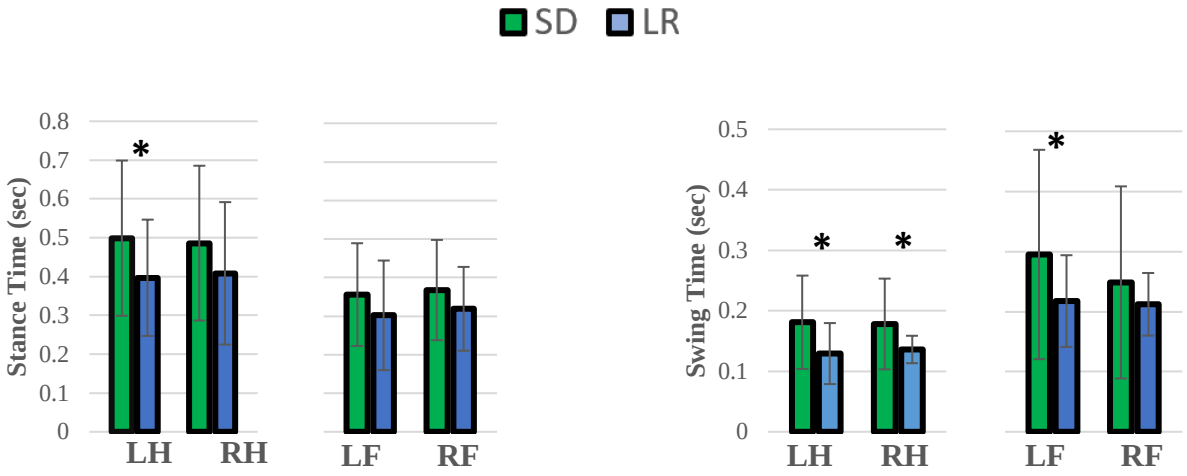

Figure 3.5 Analysis of variance of gait variables

Note: Two-way ANOVA Bonferroni's post-hoc and Tukey's grouping analysis. Statistical comparison of values between Lewis Rats (LR) and Sprague Dawley rats (SD), subcategorized by left forelimb (LF), right forelimb (RF), and left hindlimb (LH), and right hindlimb (RH). All values are presented as group means and SD error bars. *P < 0.05.

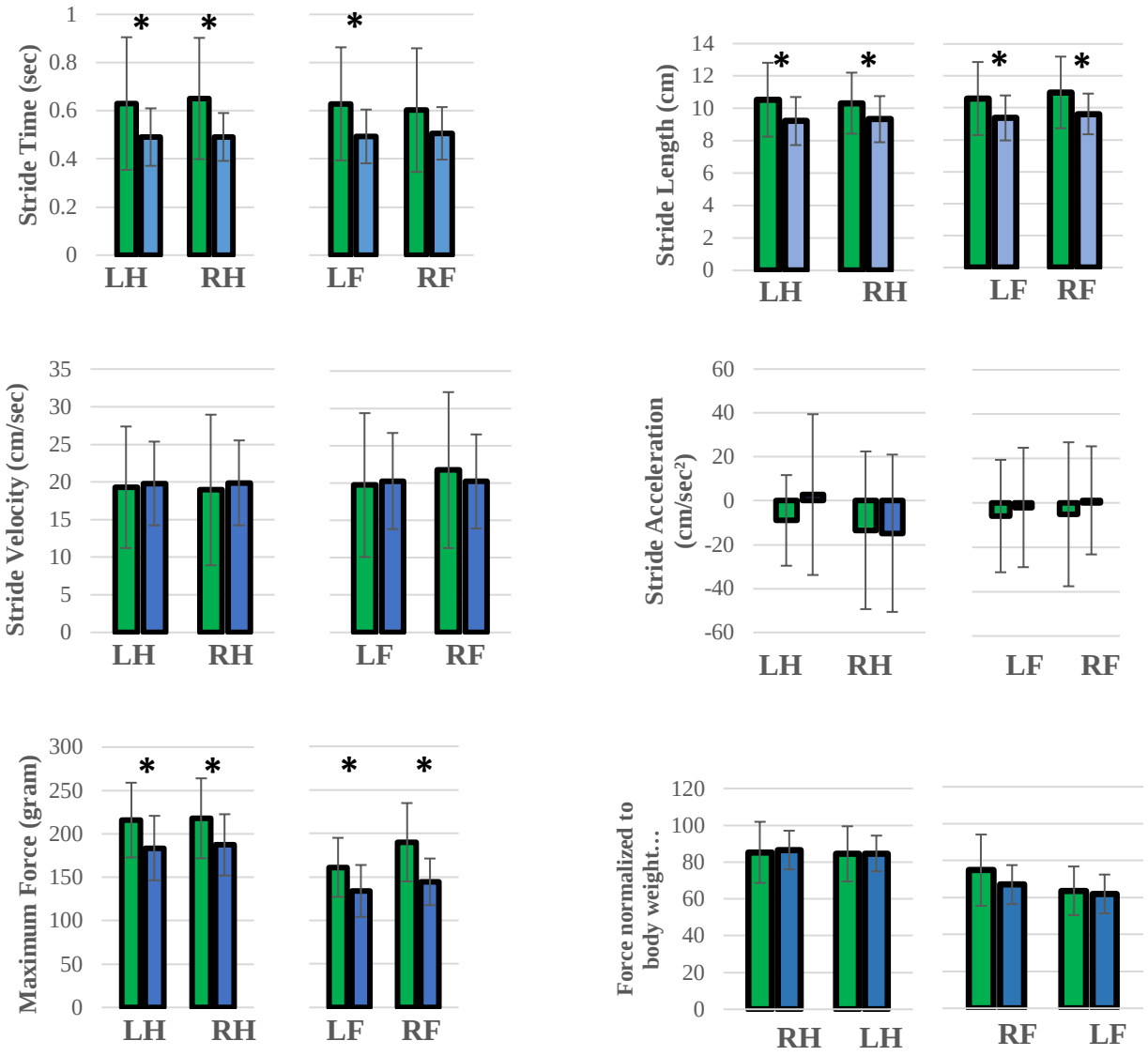

Figure 3.5 Continued

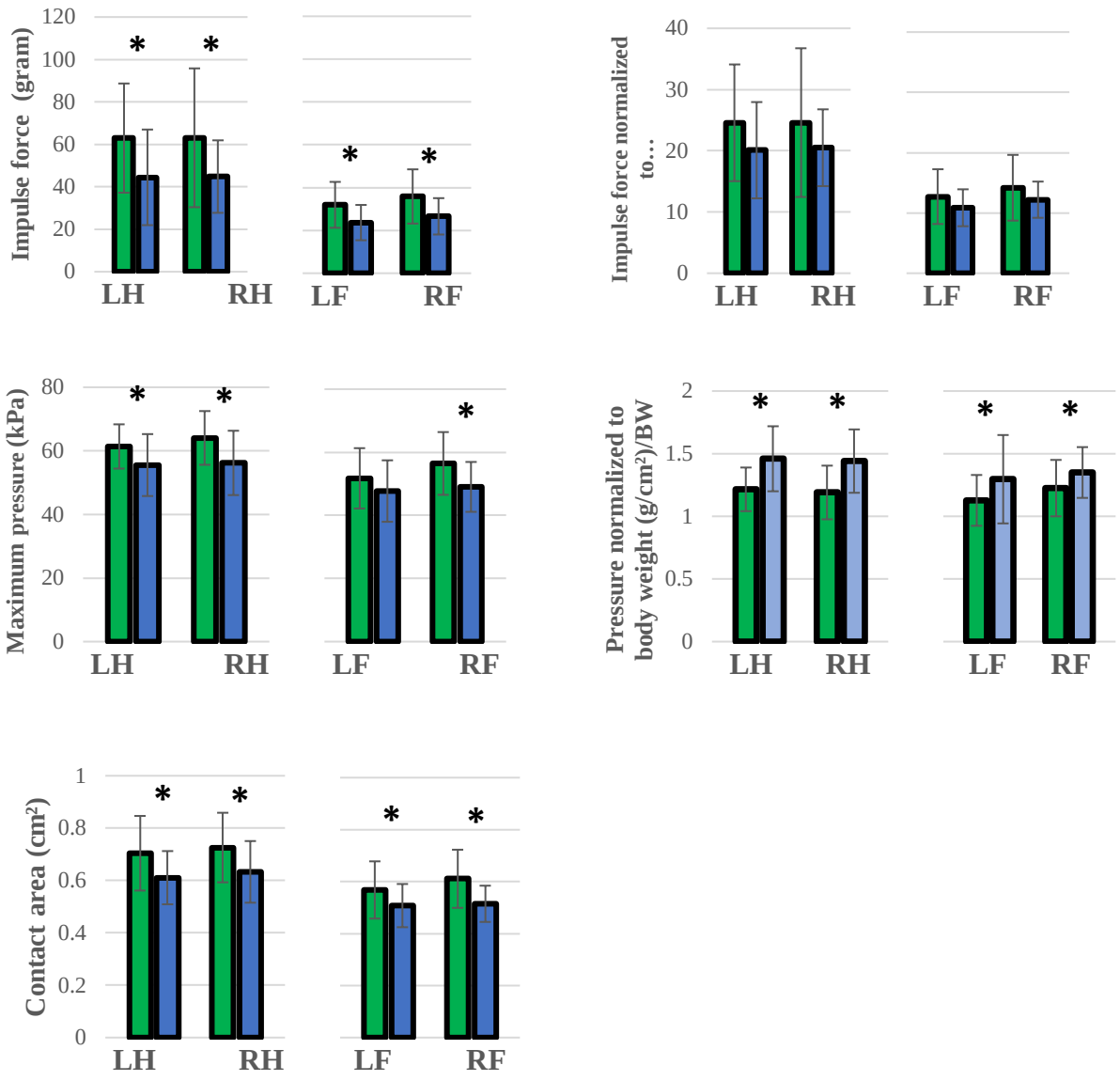

Figure 3.5 Continued

Gait parameters recorded from left and right hind limbs were also assessed for mean variance grouping between the limbs for each rat group to determine how similar the mean force and temporal values are compared to each limb. In the Lewis group stride time, stride length, stride velocity, stride acceleration, and normalized pressure in each limb were found to be statically similar to each other. Swing time, maximum force, normalized maximum force, impulse force, normalized impulse force, and contact area showed statistical differences between the forelimbs and the hindlimbs with the hindlimb mean values having a higher value compared to the forelimb. Maximum pressure and stance time mean variables for Lewis limbs were grouped based on their statistical mean variance from each other.

Similar to the Lewis group, the Sprague Dawley group stride time, stride length, stride velocity, stride acceleration, and normalized pressure in each limb were found to be statically similar. Stance time, impulse force, normalized impulse force, and contact area showed statistical differences between the forelimbs and the hindlimbs with the hindlimb mean values having a higher value compared to the forelimb. Swing time, maximum pressure, maximum force, and normalized force mean variables for Sprague Dawley limbs were grouped based on their statistical mean variance from each other.

Mean temporal parameters concerning gait distance and gait cycle time were found to be significantly different between the two groups, while all other variables cycle min, gait velocity, gait time, and number stance were found to not be significantly different between the two groups.

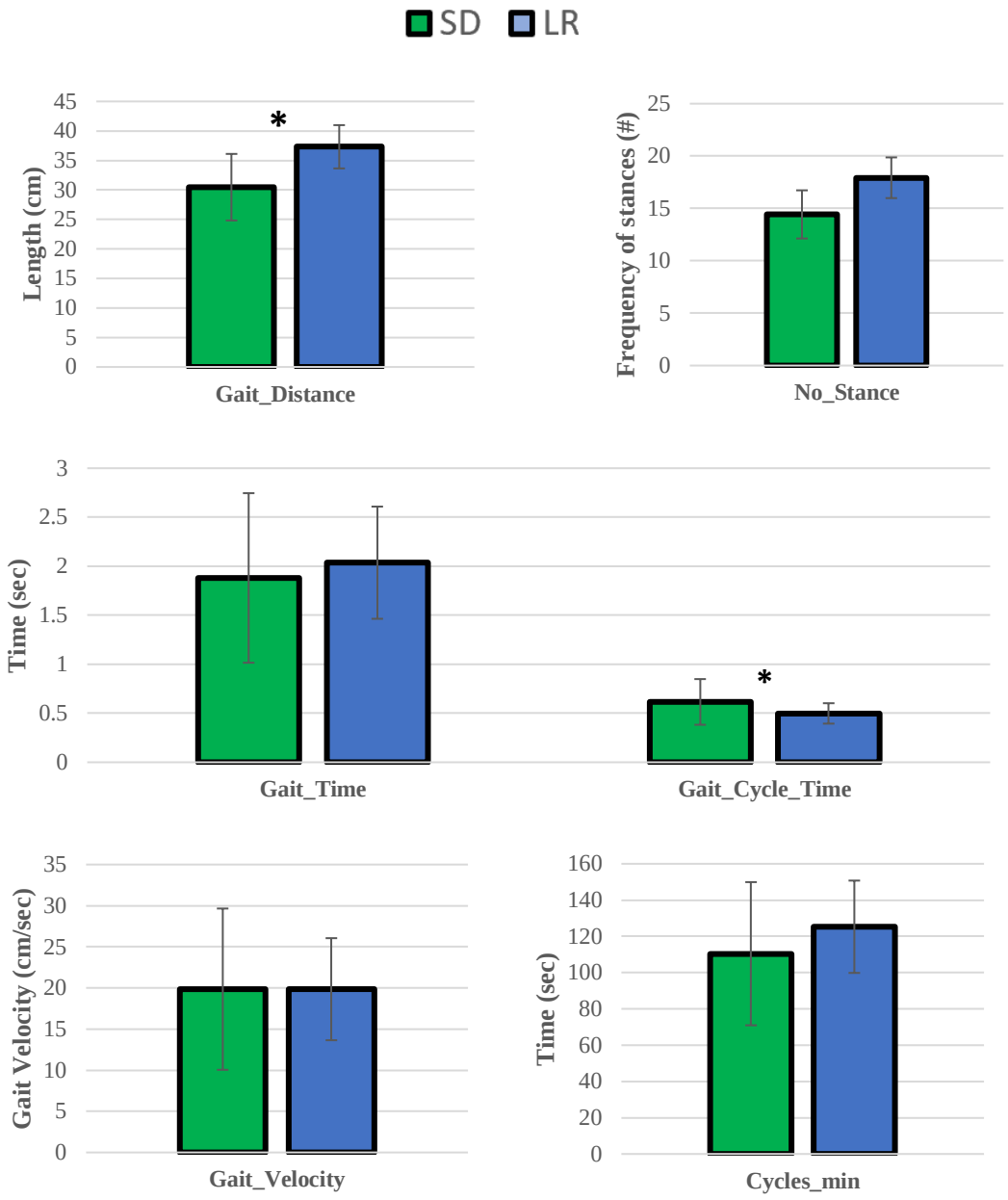

Figure 3.6 Mean temporal parameter values

Note: Sprauge Dawley (SD) and Lewis (LR) rats -ANOVA analysis. *P ≤ 0.05

3.4 Discussion

To our knowledge, this is the first study to compare the gait pattern between Sprague Dawley and Lewis rat species using the pressure mapping system. We have identified specific differences in the gait pattern between these rat species that might be a factor to consider when choosing appropriate rodent species for critical defect models. Large variances were detected in both the Sprauge Dawley and Lewis rat groups when comparing the forelimbs to the hindlimbs for variables concerning the maximum force and stance time. All other limb iterations and variables assessed showed mean values with variances that did not exceed deviations greater than 0.12, indicating small differences in gait temporal values between the limbs of the rats. ANOVA analysis of each gait variable was assessed between the animal groups, these results are identified in **Table 3.4**.

Table 3.4 Mean values statistical comparison between Sprauge Dawley and Lewis groups based on limbs.

Species	Stance_time (sec)	Swing Time (sec)	Stride_time (sec)	Stride_length (cm)	Stride_velocity (cm/sec)	Stride Acceleration (cm/sec²)
LF	0	1	1	1	0	0
LH	1	1	1	1	0	0
RF	0	0	0	1	0	0
RH	0	1	1	1	0	0

Species	MF_BW (%)	MF (gr)	Impulse_BW (%)	Impulse (gr)	Max_Peak_Pressure (Pa)	Cont_Area (cm²)	Adj_Pr (g/cm²)/BW
LF	0	1	0	1	0	1	1
LH	0	1	0	1	1	1	1
RF	0	1	0	1	1	1	1
RH	0	1	0	1	1	1	1

Note: Sprague Dawley rats (SD), subcategorized by left forelimb (LF), right forelimb (RF), and left hindlimb (LH), and right hindlimb (RH). 1= ($P < 0.05$), 0= ($P \geq 0.05$)

Variables concerning speed, acceleration and normalized forces generated in each limb of Sprague Dawley and Lewis rats are expected to have similar values and variations given the conditions of the rat population studied. The analysis also showed expected differences between the groups concerning the unadjusted impulse force, maximum force, contact area, stride length, and adjusted pressure values detected in each limb. The temporal parameters concerning stance time, swing time, and stride time were unexpected in that the results indicated similar swing and stride times for the right forelimb yet significant difference in the stance time for the left hindlimb between the two groups. The most likely cause for these differences between the two groups is the presence of some rats with gait patterns that favor a particular limb over the others, creating an uneven gait kinematics and locomotion during normal gait motion. This theory is corroborated when grouping the mean values of the limbs for each group (**Table 3.5 and Table 3.6**) which showed swing and stances times which had different mean grouping profiles between the limbs for each group indicating partial unevenness to the normal gait of these groups. This has been confirmed from previous studies that have noted similar observations in the normal gait pattern of rodents.

Table 3.5 Lewis mean value group comparison between limbs

Lewis	Stance_time (sec)	Swing Time (sec)	Stride_time (sec)	Stride_length (cm)	Stride_velocity (cm/sec)	Stride Acceleration (cm/sec²)
LF	1	1	0	0	0	0
LH	1, 2	2	0	0	0	0
RF	1, 2	1	0	0	0	0
RH	2	2	0	0	0	0

Lewis	MF_BW (%)	MF (gr)	Impulse_BW (%)	Impulse (gr)	Max_Peak_Pressure (Pa)	Cont_Area (cm²)	Adj_Pr (g/cm²)/BW
LF	1	1	1	1	1	1	0
LH	2	2	2	2	2, 3	2	0
RF	1	1	1	1	1, 2	1	0
RH	2	2	2	2	3	2	0

Note: Right forelimb (RF), and left hindlimb (LH), and right hindlimb (RH). 1, 2, 3= individual groups for mean variance, 0= similar mean variance group

Table 3.6 Sprague Dawley mean value group comparison between limbs

Sprague Dawley	Stance_time (sec)	Swing Time (sec)	Stride_time (sec)	Stride_length (cm)	Stride_velocity (cm/sec)	Stride Acceleration (cm/sec²)
LF	1	1	0	0	0	0
LH	2	2	0	0	0	0
RF	1	1, 2	0	0	0	0
RH	2	2	0	0	0	0

Sprague Dawley	MF_BW (%)	MF (gr)	Impulse_BW (%)	Impulse (gr)	Max_Peak_Pressure (Pa)	Cont_Area (cm²)	Adj_Pr (g/cm²)/BW
LF	1	1	1	1	1	1	0
LH	2	2	2	2	2, 3	2	0
RF	1, 2	1, 2	1	1	1, 2	1	0
RH	2	2	2	2	3	2	0

Note: Right forelimb (RF), and left hindlimb (LH), and right hindlimb (RH). 1, 2, 3= individual groups for mean variance, 0= similar mean variance group

Forward motion variables such as velocity and acceleration were consistent between both groups, including the additional analysis of individual limbs regarding these variables. This would indicate that the motion of each of the limbs of the rats was the same for both groups. Due to the difference in animal size between the groups, swing time and stride length variables were statistically different between the two groups, where the Sprauge Dawley rats showed greater stride length and swing time than the Lewis rats [24]. This also explains why the Sprague Dawley group had on average a lower mean value of stances number, gait length, and gait time compared to the Lewis group. As expected, normalized maximum and impulse forces were consistent between both groups. Meaning that the force generated in each limb during both deceleration and acceleration of the limbs on the mat were the same between both groups when normalized to the weight distribution of the rats in each of their respective limbs. This was further confirmed when grouping the mean values of the limbs for each group, which showed statistically similar stride velocity and acceleration for each limb while normalized force and contact area values remained statistically different between forelimbs and hindlimbs. Previous studies have used rodents as a control group for normal gait motion and have described this gait pattern were the hindlimbs will support more of the rodent's weight compared to the forelimbs due to the unequal distribution of the rodent weight across the body frame from the front end to the back end [7,21]. This also explains why the stance time variable has a large variance between the forelimbs and hindlimbs for both rodent groups, as the greater weight supported by the hindlimbs needs more time to stabilize and propel the body forward during normal gait motion. This is why during normal gait motion in rodents the hindlimbs are considered more responsible for producing forward motion, while the forelimbs are more concerned with directing forward motion in the intended direction.

3.5 Conclusion

In summary, we highlighted specific differences in the gait pattern between Sprague Dawley and Lewis rat groups using the VH4 Tekscan pressure mapping gait system. This in an effort to establish a control standard gait model to assist in selecting appropriate animals for critical defect models where animal gait biometric data is relevant and the tool for assessing gait patterns is similar to Tekscan' s VH4 model. We have shown for the first time, comparative quantitative assessment of normal gait patterns in Sprague Dawley to Lewis rats using Tekscan' s VH4 pressure-map system. Our results concerning normalized force and stride velocity/acceleration variables shows that both groups maintained statistically similar weight distributions and forward motion in each limb during normal walk patterns. Unadjusted variables concerning contact area, force and stride length showed significant differences between the two groups for each limb and fore limbs from each group having significantly different values compared to the hind limbs. We also detected irregular patterns in the swing, stride, and stance time variables between the two groups which we attribute to uneven gait motion during the trial due to favoring or odd sensation from one or more limbs.

This data would suggest that the gait pattern for Sprague Dawley rats are statistically similar to that of the gait pattern of Lewis rats when using Tekscan' s VH4 model pressure mat system. Careful consideration must be taken for possible variations in the temporal data due to specific rodent biometric specification, asymmetrical gait patterns due to limb sensations or favoritism, and the rodent's behavior and degree of training prior to testing on the pressure mat. This would indicate that for the purposes of collecting gait biometric data as a quantitative assessment of tissue repair in critical size defect models that the use of either Sprauge Dawley or Lewis rat normal gait patterns might both be used interchangeably as acceptable positive gait control models. Certain limitations to this study should be considered such as a much-focused set of rodent specifications that might overlook other biometric variables that have a larger impact on normal rodent gait patterns such as male vs female and other rodent species, the time and form of training and conditioning prior to test, ease and difficulty to house and handle, and potential physiological changes brought on by stress or pathogens. Comparison of the Tekscan VH4 model results with other highly sensitive pressure mat systems results might be prudent to help establish control rodent gait patterns for other commonly utilized gait assessment tools. The statistical power of this study could also be improved by amending the number of trials performed by each rat to a higher number than 2 or by increasing the number rodents acquired for the study.

Moving forward with assessing the performance of our neural wraps in a sciatic nerve defect model *In-vivo*, rodents are the most commonly used animal model for assessing nerve regeneration in critical nerve defects

[25]. While both Lewis and Sprague Dawley rats are considered active rodent strains suitable for gait analysis for assessing nerve repair, it is suggested that Lewis rats are used as the subjects in critical nerve defect models over other alternative rodent strains due to minimal occurrence of autotomy behavior after an extended period post transection of the sciatic nerve gap. This is supported by previous studies that have highlighted the physiological behavior changes in different rodent strains after induction of critical size nerve defects [26,27].

References

1. Baker R, McGinley JL, Schwartz MH, Beynon S, Rozumalski A, Graham HK, et al. The gait profile score and movement analysis profile. Gait Posture. 2009;30: 265–269.

2. Vivek Raut, Thomas Patterson, Joseph Wenke, Jeffrey Hollinger, George Muschler. Chapter 9 Assessment of Biomaterials: Standardized In-Vivo Testing. In: Hollinger J, editor. An Introduction to Biomaterials. Boca Raton: Taylor & Francis Group; 2012. pp. 157–172.

3. James Anderson FS. Chapter II.3.4 In Vivo Assessment of Tissue Compatibility. In: Buddy D. Ratner, Allan S. Hoffman, Frederick J. Schoen, Jack E. Lemons, editor. Biomaterials Science: An introduction to Materials in Medicine. Waltham: Elsevier; 2013. pp. 609–617.

4. Lambert CS, Philpot RM, Engberg ME, Johns BE, Kim SH, Wecker L. Gait analysis and the cumulative gait index (CGI): Translational tools to assess impairments exhibited by rats with olivocerebellar ataxia. Behav Brain Res. 2014;274: 334–343.

5. Coulthard P, Pleuvry BJ, Brewster M, Wilson KL, Macfarlane TV. Gait analysis as an objective measure in a chronic pain model. J Neurosci Methods. 2002;116: 197–213.

6. Górska T, Chojnicka-Gittins B, Majczyński H, Zmysłowski W. Changes in forelimb-hindlimb coordination after partial spinal lesions of different extent in the rat. Behav Brain Res. 2013;239: 121–138.

7. Boyd BS, Puttlitz C, Noble-Haeusslein LJ, John CM, Trivedi A, Topp KS. Deviations in gait pattern in experimental models of hindlimb paresis shown by a novel pressure mapping system. J Neurosci Res. 2007;85: 2272–2283.

8. S. JTB, Arts PIIL. Advancing Clinical Gait Analysis Through Technology and Policy [Internet]. Available: https://dspace.mit.edu/bitstream/handle/1721.1/53326/501813998-MIT.pdf;sequence=2

9. Nandikolla VK, Bochen R, Meza S, Garcia A. Experimental Gait Analysis to Study Stress Distribution of the Human Foot. J Med Eng Technol. 2017;2017: 3432074.

10. McCarthy TJ, Baxter DVM. Animal Models in Medical Device Development and Qualification. 2014; Available: http://dx.doi.org/

11. Kaplan HM, Mishra P, Kohn J. The overwhelming use of rat models in nerve regeneration research may compromise designs of nerve guidance conduits for humans. J Mater Sci Mater Med. 2015;26: 226.

12. Mohanty CB, Bhat DI, Devi BI. Use of animal models in peripheral nerve surgery and research. Neurol India. 2019;67: S100–S105.

13. Mendes CS, Bartos I, Márka Z, Akay T, Márka S, Mann RS. Quantification of gait parameters in freely walking rodents. BMC Biol. 2015;13: 50.

14. Zammit GV, Menz HB, Munteanu SE. Reliability of the TekScan MatScan(R) system for the measurement of plantar forces and pressures during barefoot level walking in healthy adults. J Foot Ankle Res. 2010;3: 11.

15. Nakamura A, Funaya H, Uezono N, Nakashima K, Ishida Y, Suzuki T, et al. Low-cost three-dimensional gait analysis system for mice with an infrared depth sensor. Neurosci Res. 2015;100: 55–62.

16. Bachus KN, DeMarco AL, Judd KT, Horwitz DS, Brodke DS. Measuring contact area, force, and pressure for bioengineering applications: using Fuji Film and TekScan systems. Med Eng Phys. 2006;28: 483–488.

17. Kornfeld T, Vogt PM, Radtke C. Nerve grafting for peripheral nerve injuries with extended defect sizes. Wien Med Wochenschr. 2018; doi:10.1007/s10354-018-0675-6

18. Vajgel A, Mardas N, Farias BC, Petrie A, Cimões R, Donos N. A systematic review on the critical size defect model. Clin Oral Implants Res. 2014;25: 879–893.

19. Sarikcioglu L, Demirel BM, Utuk A. Walking track analysis: an assessment method for functional recovery after sciatic nerve injury in the rat. Folia Morphol . 2009;68: 1–7.

20. Cai X, Wong YF, Zhou H, Xie Y, Liu ZQ, Jiang ZH, et al. The comparative study of Sprague-Dawley and Lewis rats in adjuvant-induced arthritis. Naunyn Schmiedebergs Arch Pharmacol. 2006;373: 140–147.

21. Jacobs BY, Lakes EH, Reiter AJ, Lake SP, Ham TR, Leipzig ND, et al. The Open Source GAITOR Suite for Rodent Gait Analysis. Sci Rep. 2018;8: 9797.

22. Yu P, Matloub HS, Sanger JR, Narini P. Gait analysis in rats with peripheral nerve injury. Muscle Nerve. 2001;24: 231–239.

23. Tekscan, Inc. Medical Sensors 5101QL. In: Tekscan [Internet]. 011719 [cited 25 Mar 2019]. Available: https://www.tekscan.com/products-solutions/medical-sensors/5101ql

24. Koopmans GC, Deumens R, Brook G, Gerver J, Honig WMM, Hamers FPT, et al. Strain and locomotor speed affect over-ground locomotion in intact rats. Physiol Behav. 2007;92: 993–1001.

25. Angius D, Wang H, Spinner RJ, Gutierrez-Cotto Y, Yaszemski MJ, Windebank AJ. A systematic review of animal models used to study nerve regeneration in tissue-engineered scaffolds. Biomaterials. 2012;33: 8034–8039.

26. Carr MM, Best TJ, Mackinnon SE, Evans PJ. Strain differences in autotomy in rats undergoing sciatic nerve transection or repair. Ann Plast Surg. 1992;28: 538–544.

27. Strasberg JE, Strasberg S, Mackinnon SE, Watanabe O, Hunter DA, Tarasidis G. Strain differences in peripheral-nerve regeneration in rats. J Reconstr Microsurg. 1999;15: 287–293.

Chapter 4: Critical Nerve Defect Model using Lewis Rat Subjects to Assess *In-vivo* Performance of PCL+GO+hADSC Fiber Neural Wrap

Abstract

The successful establishment of PCL+GO platforms and the successful *In-vitro* testing for biocompatibility towards adipose derived MSC and ability to support neural stimulated hADSC culture has provided the first round of data that supports this material as a potential biomaterial candidate for creating neural wraps to be used in the repair of critical neural defects. In this study, we have established a rodent model using Lewis rats to simulate a critical nerve defect and determine the potential of this material with hADSC cultures is at assisting in the repair of critical nerve defects *In-vivo.* 24 total Lewis rats were separated into 4 independent treatment groups. Treatment was left to provide its intended therapy for 12 weeks before being removed for histology assessment of the repair. Gait assessment of the rodent's gait pattern was also collected using a Tekscan pressure mat system as an indirect assessment for return of neural function. Results of our gait analysis indicate a significant deviation from normal rodent gait patterns after creating the neural defect in rats as expected, however data could not conclude if nerve function was beginning to return at the defect site by 12 weeks repair. Histology sections of the neural wraps at 12 weeks show new tissue growth present inside the neural wrap tubing with tissue growth expanding across the material towards the distal section of the defect. Staining shows that new tissue has similar characteristics to the tissue found in native peripheral nerves in terms of tissue layering and organization. However, we cannot yet fully identify what the new tissue is until a more specific set of staining protocols are used. Most likely these stains will search for tissue that we expect to make up a significant component of the new tissue that is growing such as axon, myelin, and Schwann cell specific stains. From this study we determined that this material has potential to grow new tissue at critical nerve defects while remaining intact for up to 12 weeks *In-vivo*. The effectiveness of the material to regenerate new neural tissue, or how effective the addition of hADSC therapies is in repairing the defect remains unknown and is the center of new studies being developed to address the limitations of this current study.

4.1 Sciatic Nerve Transection Model

4.1.1 Introduction

Neurotmesis is one of the most damaging forms of peripheral neuropathy that affects approximately 3 % of trauma patients around the globe. Severe forms of neurotmesis involves significant gaps (>2-3 cm) along peripheral nerve sections that often require surgical intervention to successfully repair. Currently, the gold standard for repair of severe neurotmesis is the use of autograft nerve segments taken from a different area of the patient were the nerve type, diameter size, and length are similar to the nerve gap. The limitations of this method are well known and the expected degree of repair from such technique are quite varied which has opened to discussions of finding alternative methods of tissue repair. The use of scaffolds to regenerate damaged peripheral nerve presents a possible solution to healing severely damaged peripheral nerve segments. For peripheral nerve injuries a preferred scaffold implant is one that can support the damaged nerve at the wound site as well as stimulate and guide the growth of new peripheral nerve tissue through the scaffold.

In our previous study, we assessed the cytocompatibility of our novel biomaterial to support hADSC in a combined therapeutic approach to assist in peripheral nerve repair using manufacturing techniques developed thru our collaboration with the University of Arkansas Little Rock (UALR) Nanotechnology group. We have also provided the methods and resources to assess the compatibility of novel biomaterials developed by UALR intended also for assisting in the repair of severe neurotmesis injuries. All iterations regarding the development of these candidate neural scaffolds have been assessed in vitro using MSC culture systems. Previous *In-vitro* analysis of cytotoxicity and stability as a cell platform have been assessed via cultures of established Mesenchymal stem cell lines (hADSC and rADSC) by evaluating cell proliferation, viability. We also have assessed the biomaterials potential to guide MSC lines in vitro towards neural-like lineages when artificially increasing cAMP messenger proteins to guide differentiation of MSCs towards a neural-like phenotype by evaluating the changes in expression intensity of proteins present during neural differentiation such as S100β.

We determined that Electrospun PCL fiber meshes surface coated with GO nanomaterials were capable of supporting hADSC lines in both their undifferentiated form and their differentiated states towards neural-like phenotypes. It is suggested from these results that *In-vivo* testing is the next reasonable step to determine the scaffolds ability to stimulate nerve regeneration, re-establish functional activity of the nerve, and return to function of tissues innervated by target nerves. This work must be done using animal models of induced nerve defects so that the biological response can be assessed [1–3]. These in vivo models also allow for study of the biocompatibility of the scaffolds to determine candidacy for clinical use. In this study

we modified the films into 3D neural wrap prototypes to be assessed *In-vivo* for their potential in assisting in actual nerve repair. We utilized a rat sciatic nerve model in which a segmental defect is made in the sciatic nerve of rats which is then repaired with our 3D neural wraps consisting of PCL fiber meshes modified with GO surface coating.

The sciatic nerve defect model utilizing rodents is the most commonly used small-animal model for evaluating neural repair. The model consists of transecting a segment of the animal's peripheral nerve on either the left or right hind limb. The segment having a gap that is considered a critical defect based on the species and size of the animal subject. The peripheral nerve gap is then connected by an open-end cylindrical conduit/wrap biomaterial or a peripheral nerve graft that is surgically aligned to the distal and proximal ends of the gap with minimal tension and impairment to new growing native tissue. The animal subject remains under observation until either partial repair or complete repair of the nerve gap is reached in order to assess the quality of tissue growth. This time variable is dependent on the animal species and the size of the nerve gap based on the expected rate of peripheral nerve growth to span the defect. The most common methods for evaluating the return of normal peripheral nerve function can use both direct (electrophysiology, muscle mass, histochemical staining) and indirect (gait analysis, pain sensation) methods. Multiple methods used in tangent with each other can assess the presence of new nerve tissue growth and whether it is functional.

Rodents are a validated, extensively published, and common model used in evaluating neural conduit or wrap *In-vivo* cytotoxicity and regenerative capability of these biomaterials due to their relevant neural physiology, ease of handling, small size and affordability, and the shortened time required to reach end points successful peripheral nerve healing. There are studies that have attempted to standardized the sciatic nerve model by controlling for specific variables present in the rodent subjects to determine the optimal rodent variables to use in the sciatic nerve model. Such variables include species, age range, sex, rodent body dimensions, and breeding vendor in an attempt to improve the precision of end-result data and quality of tissues extracted for assessment. Studies have also noted asymmetrical or abnormal behavior in rodent species in response to transection of their sciatic nerves including differences in normal gain motion. One such behavior is self-mutilation or atotomy at limbs affected by the transection of the sciatic nerve. The current consensus in the appropriate animal subjects to use for the sciatic nerve model are Lewis rats due to minimal occurrence of atotomy behavior after prolonged exposure to sciatic nerve transection compared to other common rodent species used in this model (Sprauge Daweley, Wistar). Male rodents have reported greater lengths in newly regenerating peripheral nerves compared to female, while the rate of nerve regeneration and quality of tissue in younger rodents is at a markedly higher degree than that of older rodent

populations. It is suggested that healthy male Lewis rats that fall within the demographic of 8 to 12 weeks old is the best subjects for this model.

The objective of this study is to assess the *In-vivo* potential of neural wrap designs to assist in healing critical neurotmesis defects through changes in gait parameters, and histochemical staining assessment. It is hypothesized that PCL biomaterials enhanced with the addition of GO, or Gold-nanorod thin film surface coatings with the addition of hADSC therapy can support the growth of new peripheral nerve in an *In-vivo* system. At 12 weeks post-repair of critical defect, we expect that new peripheral nerve will span the defect gap and reach the distal stump by growing along the scaffolding designs. Attention to new tissue organization compared to native peripheral nerves and the distance of new tissue growth thru the nerve scaffolding are critical for this assessment. Results of these studies will guide further research to improve the designs of these nerve scaffold prototypes and determine the functionality of any potential nerve tissue growth on these scaffolds. The end result is to create a peripheral nerve scaffold that is capable repairing severe neurotmesis cases in both humans and animals. If we can design a biomaterial platform that meets or exceeds the quality of repair achieved in autologous neural grafts, we can begin the process of establishing clinical trials for assessment in humans which will hopefully result in a successful translation of our patent into the neural graft market.

4.2 Methods

The study was approved by the Institutional Animal Care and Use Committee (IACUC) at the University of Tennessee, Knoxville (IACUC# 2574-0318). 24 Lewis rats were selected for use in the study of gait biometrics and histology assessment. Lewis rats used in this study were eight-week old males and allowed to acclimate to their environment for one week before the surgery date. Animals were organized into 6 independent groups as follows: Group 1- control only (sciatic nerve defect with no treatment of the defect, Group 2-3 represented electrospun PCL wraps with GO surface coating. and electrospun PCL wraps with GO surface coating pre-cultured with hADSC lines. Group 4- Autologous nerve graft. Each group included a sample size of n=6. Lewis rats were subjected to critical size neurotmesis nerve injury to their sciatic nerves as described in previous similar nerve models [1,4]. Animals in each group were maintained for up to 12 weeks post-surgery with gait analysis data collection at each 2-week interval from each rat.

4.2.1 Electrospinning

The creation of 3D PCL meshes of nanofibrous architecture was performed with the same solution and electrospinning parameters as discussed in Chapter 2 methods section (pg. 6) with modifications in the parameters including changing the voltage applied to 15 kV charge and altering the needle tip-to-collector distance setting to 6 inches to create PCL fiber meshes of greater rigidity and easier to manage when wetted in cell culture media. To create a thicker PCL nanofiber mesh deposit on the collector mandrel, the solution was left to spin for 4 hours which used a total of 4 ml of spinning solution per spin which created a projected film thickness of approximately 0.01 mm. The entire PCL mesh was removed from the collector plate and cut to the dimensions of 9cm x 12cm sections. The sections were attached to a 24-culture well lid using tape and pre-sterilized under UV sterilization for 4 hours prior to air spraying GO solutions onto the surface of the mesh. GO solution was prepared under the same parameters as discussed in Chapter 2 (pg. 5). GO solutions was bath sonicated for 30 min to evenly disperse graphene oxide films in solution that have settled to the bottom of the container after 24 hours or more in storage before being used to coat the materials. Under fume hood conditions, 10ml of GO solution was used to coat the surface of PCL fiber meshes using air spray technique on hot plate set to between 45-55°C. Solutions were sprayed at 21 psi. PCL meshes was removed from 24 culture-well lid and placed into sterile glass dishes with glass cover lids. Under cell-culture sterile hood conditions, PCL GO coating fiber mesh sections were cut to dimensions of 12mm x 6mm sections as appropriate to span the expected sciatic nerve defect length with a 1 mm margin of error for attaching the proximal and distal sections.

4.2.2 Animal Surgery

Prior to surgery, all neural wrap prototypes were UV sterilized for 4 hours under cell culture sterile hood prior to culturing cells. 24 hours prior to implanting the PCL nerve wraps into rodent subjects, hADSC cell lines used in the previous Chapter 2 *In-vitro* study were cultured onto the surface of nerve wraps that were placed into 30mm diameter sterile non-tissue culture polystyrene wells. $1*10^6$ total hADSC cells were seeded at a concentration of $1*10^6$ cells/ 200µl DMEM-F12 stem cell culture media to the surface of nerve wraps. The cells were left to adhere to the surface of the nerve wrap for 3 hours before adding an additional 800µl of DMEM-F12 culture media to the well to support the cell lines for the remaining 21 hours in culture period. To determine if hADSC cell lines successfully adhered to the surface of nerve wraps in 24 hours post seeding, DiI staining was used to track the remaining viable cells found on the surface of the nerve wraps. If the nerve wraps showed a majority of its surface covered with hADSC cell lines with characteristic stretching and spreading indicative of cells successfully adhered to biomaterials the wrap remained in incubation until needed for implantation. All films were transferred into sterile wells filled with sterile saline solution for transport to the surgical environment.

All subjects were initially weighed and injected with 0.03 mg/kg; subcutaneous injection of buprenorphine just before prepping for surgery. Under isoflurane anesthesia, all rats were positioned into lateral recumbency and prepped for surgery by shaving the right hind leg and sterilized using isopropanol and iodine solutions. A skin incision of 3 cm was made longitudinally to the posterior aspect of each thigh, from the greater trochanter to the knee. Blunt dissection of the gluteus maximus and biceps femoris muscles will expose the sciatic nerve directly underneath. A critical size nerve defect in rats is approximately 10 mm which was made by removing a segment of the sciatic nerve. The defect was repaired using our PCL fiber mesh coated with GO that includes with or without hADSC cultures to span the defect and attach to the proximal and distal nerve stumps using 10-0 absorbable suture material (**Figure 4.1**).

Negative control group (n=6) had 10 mm sections of sciatic nerve removed but did not receive any scaffold treatment. Positive control group (n=5) had sciatic nerve sections re-implanted to the distal and proximal stump using 10-0 vicryl sutures to mimic gold standard autologous peripheral nerve repair. The muscle tissue was returned to its original position and the skin was closed with 5-0 vicryl sutures. Each animal was administered buprenorphine (0.03 mg/kg; subcutaneous) every 6–12 hours for 72 hours and provided with free access to water containing Enrofloxacin (Baytril) oral antibiotics (100 mg/400 mL) and Gatorade powder for 72 hr. We applied E-collars to each rat for 24 hours post-surgery. This model of transecting the Sciatic nerve causes all animals to be affected by diminished use of the operated leg to various degrees over the duration of the study. This should not be interpreted as lameness or an indication of pain, but rather a result of the disability associated with the nerve model used. Signs of autotomy by the rats on the affected leg was also considered in our normal checkup of the rats as previous sciatic nerve studies have reported cases of potential self-mutilation most likely caused by abnormal sensations in the hind foot digits after transecting the sciatic nerve.

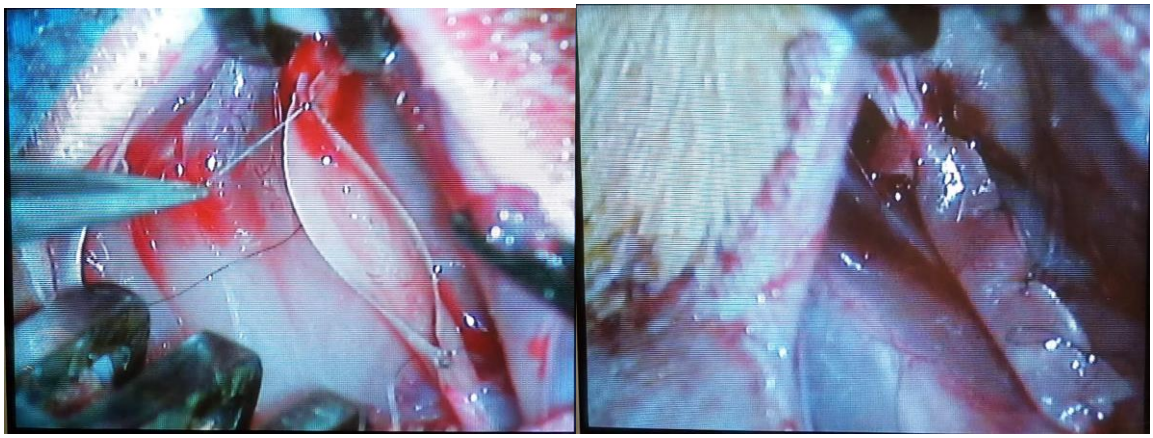

Figure 4.1 GO+PCL neural wrap repair of 10mm peripheral nerve defect in Lewis rat subject.

4.2.3 VH4 Pressure Sensing Mat Assessment

Gait patterns were analyzed using a pressure sensor mat (Tekscan VH4, Tekscan, Boston, MA) for each rat when they reach each 2-week interval post-surgery. The mat was prepared using the same tinted Plexiglas tunnel and Styrofoam borders to ensure the rats stay on the sensel areas during normal rat gait motion. The procedures for calibrating the, protocols for guiding rats to walk across the mat, and criteria for selecting successful runs are based on our previous gait comparison analysis between Sprague Dawley and Lewis rats referenced in chapter 3. All mean values for normalized body weight, and surface area contact from each successful trial was recorded to assess any changes in gait profiles that could indicate a return to function of motor and sensor endplates due to newly regenerated functional nerve tissue reaching the distal end of the sciatic nerve gap.

4.2.4 Histology

At 12 weeks, the neural scaffolds and grafts were removed from the rats and aligned on sections of cardboard before being placed in 10% formalin to preserve the tissue sections. The tissues were embedded into paraffin and sliced longitudinally for histochemical analysis of the newly regenerated nerve tissues inside the nerve scaffolds extending from the proximal start to distal end. Based on the previous methods described by Carriel, Víctor, 2011 in the use of H&E and MCOLL histology methods for labeling layers of different tissue sections present in the peripheral nerve anatomy [5]. While H&E is a common method of staining for collagen tissues and the nucleus of cells, MCOLL staining involves the combined approach of using Luxofast Blue to stain for lipoproteins that should be found on the surface of myelin sheath tissue and Picrosirus Red stain for specific staining of different collagen tissues which makes up the majority of the perineurium and epineurium sections of peripheral nerves. This combination allows for clear identification of myelin sections present in newly regenerated nerve tissue for comparing the organization of myelin sections and their dimensions to that of native peripheral nerve tissue.

4.3 Results

4.3.1 PCL Neural Wrap Extraction

96 % of the original 24 rat subjects made it to week 12 euthanasia. The study resulted in 6 Negative control rats, 5 autologous graft rats, 6 PCL+GO rats, and 6 PCL+GO+hADSC rats at week 12. One rat was removed due to complications during recovery post-surgery. No animal subjects showed any signs of discomfort of atotomy behavior caused by transecting the sciatic nerve during the 12-week study period.

Electrospun PCL+ GO **Electrospun PCL+ GO+ hADSC**

Figure 4.2 Week 12 neural wrap/conduit removal from Lewis rat subject's post-euthanasia

Note: Stance Time, Stride Time, Stride Length, Stride Velocity, Maximum Force distribution, and surface contact area based on limb.

All neural conduits and wraps extracted from animal subjects that reached week 12 in the study showed stable platforms with both ends securely attached to both the distal and proximal ends of the nerve gap. Neural wraps showed slight indications of early deterioration most likely due to hydrolyzes, on porous thin films. All neural wraps were extracted from all 12-week rats. Wraps, and autologous grafts were placed on cardboard sections then preserved in 10% formalin as histology slides.

4.3.2 Gait Assessment of Lewis Rats During 12-Week Nerve Repair

At pre-op and at each 2-week interval during nerve repair, each Lewis rat was placed on a Tekscan Pressure Mat system to assess the return of nerve function thru tracking of normal gait motion. Data pertaining to normal gait motion included maximum normalized force distribution, and surface contact area which were collected from both the right and left hind limbs as a means value. This gave us a profile of the rats' gait in each group during nerve repair.

Table 4.1 Tekscan pressure mat raw data of mean temporal parameters

Time	Group	Limb	Stance_ time	Swing Time	Stride_ time	Stride_ length	MF_BW	MF_gr	Max_ Peak_Pressure
Week 2	Negative	LH	1.00±0.65	0.16±0.087	1.03±0.65	8.60±1.72	90.95±9.92	202.80±31.07	56.57±8.84
		RH	0.92±0.67	0.26±0.13	1.01±0.71	8.24±1.91	68.87±17.7	152.20±35.9	60.30±9.52
	Autologous	LH	1.43±0.96	0.14±0.056	1.36±0.71	7.15±1.07	90.52±10.9	227.92±37.2	59.40±8.2
		RH	1.25±0.91	0.21±0.12	1.25±0.75	6.60±1.5	66.21±15.2	167.16±44.4	60.52±9.2
	PCL+GO	LH	1.06±0.43	0.11±0.062	1.10±0.51	8.18±1.89	86.81±11.5	192.40±24.37	57.03±5.77
		RH	0.82±0.31	0.30±0.24	0.99±0.49	7.73±1.62	56.97±17.82	127.03±42.14	51.60±12.44
	PCL+GO+hMSC	LH	0.84±0.52	0.13±0.037	0.83±0.57	8.32±1.25	85.12±14.11	196.0±35.18	56.17±9.61
		RH	0.67±0.4	0.24±0.11	0.75±0.44	7.62±1.58	58.78±12.85	135.17±30.32	54.37±8.68
Week 4	Negative	LH	0.99±0.38	0.13±0.044	1.11±0.45	8.60±1.36	94.44±9.62	236.03±33.44	62.63±7.92
		RH	0.81±0.36	0.25±0.17	0.99±0.43	7.73±1.91	64.92±12.4	161.3±29.32	60.83±8.05
	Autologous	LH	1.18±0.62	0.14±0.068	1.17±0.56	7.60±1.52	88.70±10.8	250.32±32.7	67.68±6.96
		RH	0.96±0.52	0.25±0.057	1.06±0.48	6.68±1.3	64.66±12.24	181.04±27.61	62.88±8.16
	PCL+GO	LH	1.38±0.85	0.12±0.04	1.34±1.06	9.35±1.78	92.32±12.8	238.47±38.03	64.63±9.75
		RH	0.97±0.73	0.31±0.21	1.07±0.88	7.79±2.35	52.69±11.92	136.10±32.42	52.60±9.5
	PCL+GO+hMSC	LH	1.05±0.6	0.12±0.056	1.13±0.76	8.41±1.83	86.43±19.12	237.43±56.6	63.17±10.62
		RH	0.84±0.46	0.21±0.11	0.89±0.51	7.25±1.83	55.32±21.1	150.17±54.5	54.43±15.0
Week 6	Negative	LH	1.17±0.57	0.13±0.061	1.20±0.64	8.17±1.78	96.02±16.74	260.77±58.7	67.43±10.83
		RH	0.84±0.51	0.26±0.21	1.01±0.54	7.08±2.17	60.96±15.62	163.40±39.9	60.60±9.83
	Autologous	LH	0.90±0.43	0.13±0.06	0.95±0.49	8.26±1.59	91.55±11.27	280.0±34.51	66.60±6.02
		RH	0.80±0.52	0.18±0.07	0.81±0.56	7.10±1.74	71.38±12.15	218.04±35.7	71.48±8.97
	PCL+GO	LH	1.70±0.99	0.13±0.1	1.89±1.26	8.94±1.67	94.01±16.47	264.97±49.24	67.83±9.77
		RH	1.31±0.95	0.28±0.17	1.56±1.19	7.28±2.25	57.63±14.6	162.0±40.9	57.50±10.8
	PCL+GO+hMSC	LH	1.24±0.77	0.12±0.05	1.26±0.7	8.55±1.66	91.23±15.93	273.07±51.14	67.83±9.16
		RH	0.95±0.71	0.27±0.13	0.96±0.56	6.67±1.3	57.66±15.2	171.67±43.09	57.63±11.7
Week 8	Negative	LH	1.34±0.64	0.15±0.11	1.33±0.59	8.40±1.92	92.20±13.35	259.80±55.8	67.30±9.52
		RH	1.26±0.73	0.24±0.084	1.31±0.72	7.81±1.79	64.52±12.75	178.67±30.24	67.50±9.24
	Autologous	LH	1.22±0.58	0.15±0.05	1.20±0.66	8.21±1.89	86.18±10.38	277.40±38.0	68.32±9.5
		RH	1.14±0.65	0.18±0.09	1.14±0.71	7.73±2.16	70.88±14.85	226.56±40.02	72.60±8.98
	PCL+GO	LH	1.54±1.02	0.10±0.03	1.57±1.17	9.41±1.58	90.83±14.15	274.0±47.14	68.70±9.0
		RH	1.22±0.88	0.24±0.08	1.26±0.91	7.77±2.16	56.73±11.45	170.37±32.5	60.37±10.34
	PCL+GO+hMSC	LH	1.01±0.47	0.11±0.043	0.89±0.56	8.99±1.75	95.87±13.9	303.90±41.61	72.03±7.98
		RH	0.79±0.35	0.25±0.17	0.77±0.41	8.53±3.28	56.70±19.65	179.70±61.7	59.83±14.73

Table 4.1 Continued

Time	Group	Limb	Stance_ time	Swing Time	Stride_ time	Stride_ length	MF_BW	MF_gr	Max_ Peak_Pressure
Week 10	Negative	LH	1.11±0.54	0.14±0.069	1.20±0.57	8.70±1.85	95.35±10.65	280.93±55.07	68.57±8.98
		RH	0.93±0.56	0.19±0.096	0.98±0.53	7.38±1.99	64.04±13.25	186.13±36.51	67.60±9.36
	Autologous	LH	0.90±0.39	0.14±0.05	0.97±0.47	9.18±1.89	91.48±8.53	308.72±35.93	71.92±7.75
		RH	0.78±0.32	0.16±0.065	0.79±0.36	7.84±1.37	72.32±9.92	243.0±29.35	75.56±8.22
	PCL+GO	LH	1.16±0.56	0.13±0.13	1.25±0.67	9.56±1.84	91.14±13	286.60±42.39	71.37±7.12
		RH	0.88±0.45	0.27±0.16	1.01±0.56	8.21±2.34	58.27±16.51	183.80±53.62	64.40±12.87
	PCL+GO+hMSC	LH	0.99±0.4	0.11±0.045	0.85±0.37	8.54±2.19	91.54±12.09	304.83±48.19	68.97±9.66
		RH	0.81±0.35	0.22±0.098	0.81±0.38	7.52±1.78	58.64±12.78	194.07±40.42	66.80±12.27
Week 12	Negative	LH	1.23±0.55	0.12±0.046	1.24±0.56	8.46±1.23	92.55±11.34	285.77±57.39	70.10±8.14
		RH	0.95±0.44	0.21±0.076	0.99±0.53	7.18±2.03	60.03±9.54	184.33±36.25	68.53±10.58
	Autologous	LH	0.81±0.32	0.14±0.064	0.86±0.43	9.10±2.05	85.44±9.63	299.76±44.91	71.36±7.63
		RH	0.62±0.26	0.16±0.11	0.68±0.31	7.23±1.26	66.58±10.3	232.56±36.86	72.80±7.39
	PCL+GO	LH	0.84±0.3	0.10±0.026	0.81±0.33	9.05±1.9	84.62±11.6	283.50±42.5	73.37±8.3
		RH	0.71±0.32	0.19±0.057	0.69±0.33	7.99±1.98	58.12±9.68	193.90±30.88	66.40±9.37
	PCL+GO+hMSC	LH	1.04±0.68	0.12±0.038	0.91±0.65	9.40±1.97	91.90±9.59	318.47±38.23	71.40±6.41
		RH	1.00±1.0	0.21±0.059	0.94±0.98	8.37±2.19	64.81±12.06	223.70±38.87	70.60±10.36

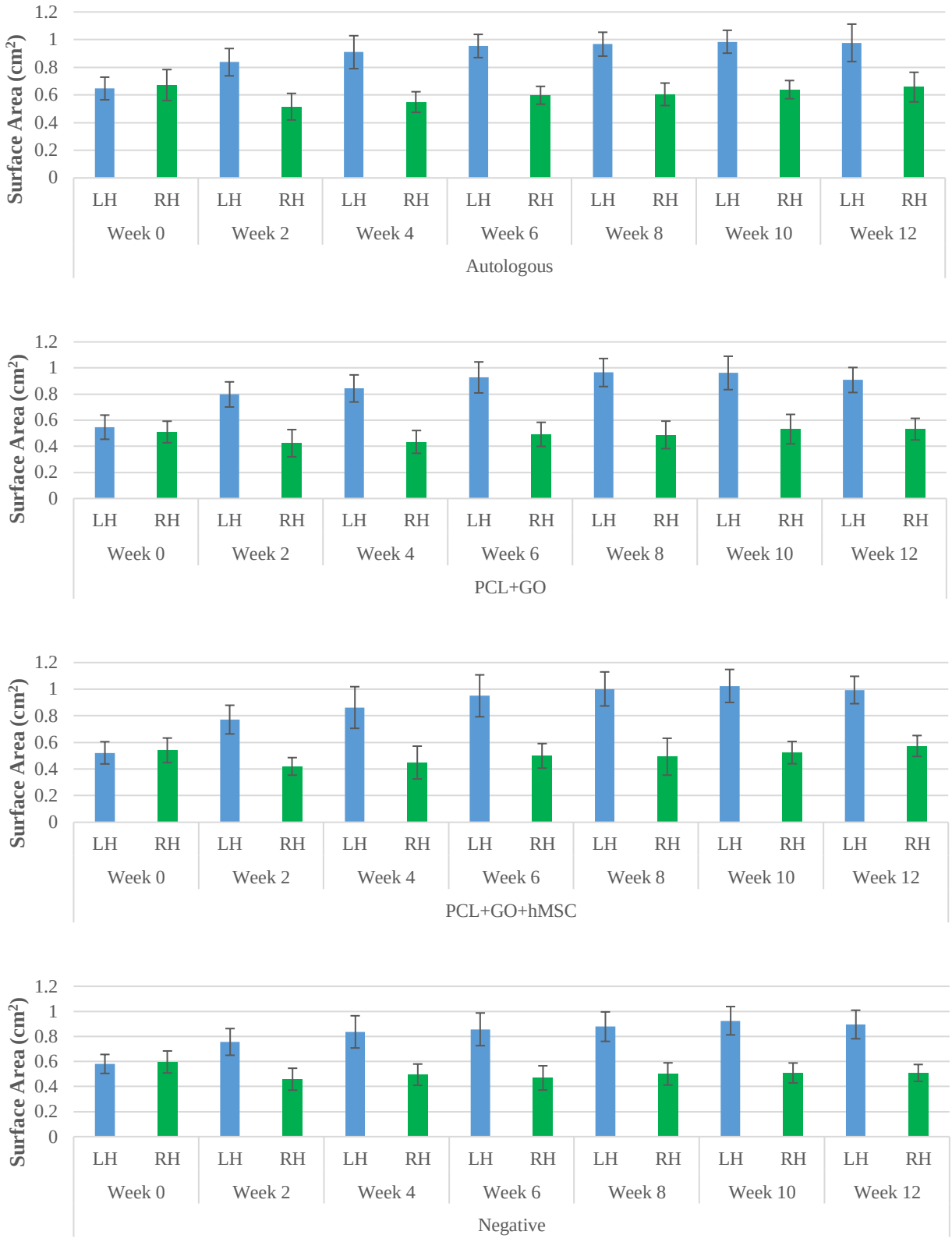

Figure 4.3 Mean surface area coverage profile of left and right hind limbs for each group.

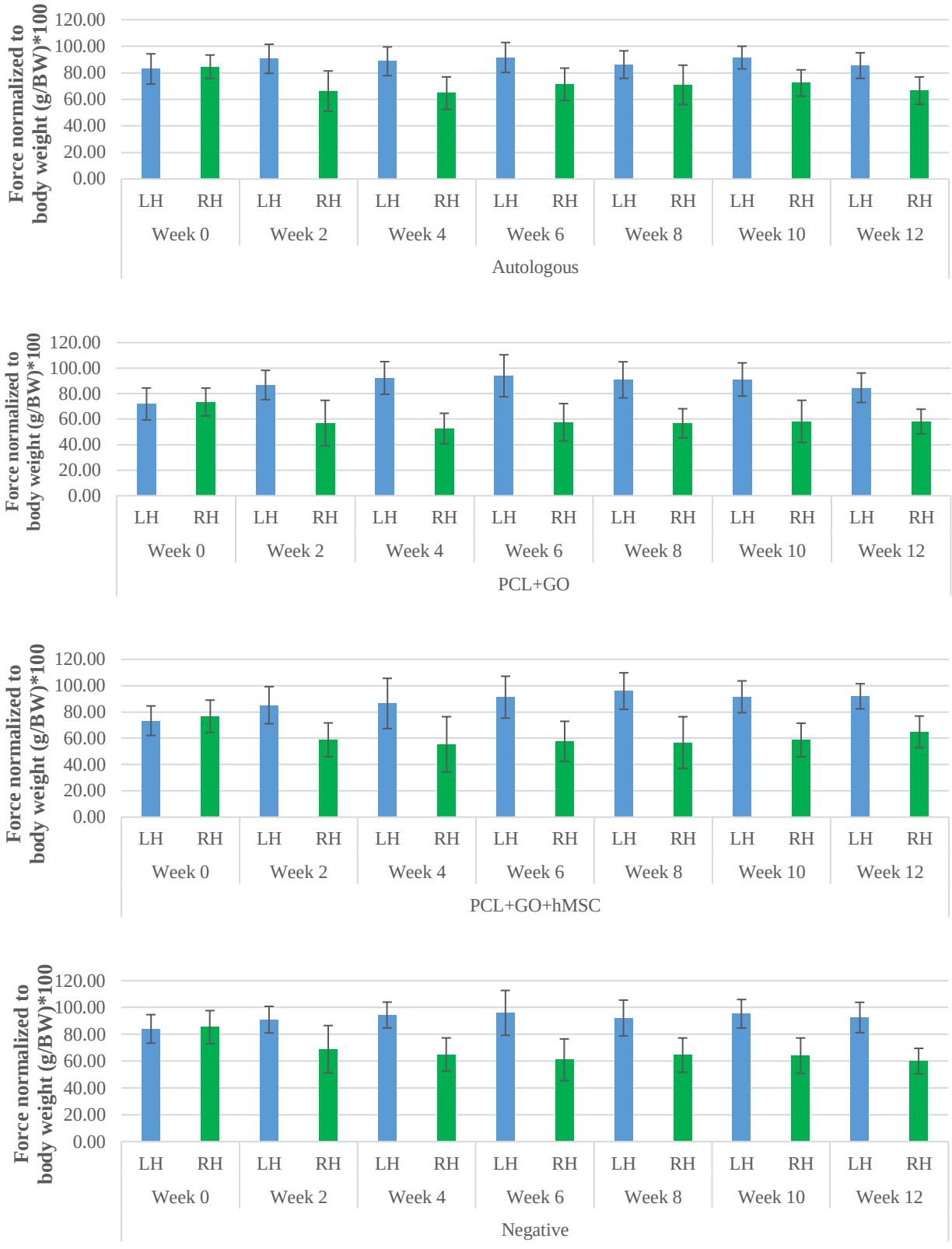

Figure 4.4 Normalized mean body weight percentage profile of left and right hind limbs for each group.

In order to compare these results between each group given that each rodent is independent from all other rodents in the sample size it is essential that we normalize the results as a ratio between the hind limbs impacted by the neural defect (right hind limb) and the control hind limb with no neural defect impact left hind limb). **Table 4.2** compares the mean surface area contact and normalized body weight ratios over the period of 12 weeks of nerve repair using the pre-surgery time point (week 0) as the base line for fully functional nerves. A value close to 0 indicates LH and RH hind limb values that are similar to each other in terms of either the surface area contacts or force distribution in the hind limbs.

Table 4.2 Mean ratios of hind limbs mean

				Autologous			
	Week 0	Week 2	Week 4	Week 6	Week 8	Week 10	Week 12
SAC	0.036766	0.624656	0.657499	0.596527	0.600062	0.542816	0.487804
BW max	0.019401	0.367206	0.371938	0.282616	0.215733	0.264808	0.283345
				PCL+GO			
	Week 0	Week 2	Week 4	Week 6	Week 8	Week 10	Week 12
SAC	0.072203	0.881526	0.944491	0.887065	0.979261	0.809786	0.708114
BW max	0.021006	0.523932	0.752135	0.631211	0.601034	0.563951	0.45587
				PCL+GO+hMSC			
	Week 0	Week 2	Week 4	Week 6	Week 8	Week 10	Week 12
SAC	0.034916	0.838589	0.921013	0.904774	1.034102	0.957124	0.734144
BW max	0.043607	0.448086	0.562425	0.582355	0.69087	0.560962	0.417867
				Negative			
	Week 0	Week 2	Week 4	Week 6	Week 8	Week 10	Week 12
SAC	0.026312	0.649361	0.690812	0.826862	0.753592	0.820436	0.759931
BW max	0.015267	0.320492	0.454587	0.57499	0.42894	0.488836	0.541729

Note: mean surface area coverage (SAC) and mean max body weight percentage (BW max): Week X (LH Week X/RH Week X)-1

4.3.3 Histology

Autologous, normal Lewis rat sciatic nerve section, and nerve wrap tissue samples were removed from 10% formalin solution and embedded in parafilm. Tissue samples were oriented in order to cut longitudinal histology sections of the tissue to visualize the organization and distance of new tissue growth thru the nerve scaffold across the length of the critical defect. MCOLL staining of longitudinal sections from each euthanized rat was carried out and images from 1 random rat subject from each group was assessed under light microscopy with images taken at 4x and 40x magnification at 5 specific areas along each tissue section. These areas were determined by establishing areas at the two ends of the longitudinal sections as the proximal and distal ends and half way in between as the center position. Areas between the two ends and the center area were labeled as proximal center and distal center positions.

	Distal	**Distal_Center**	**Center**	**Center_Proximal**	**Proximal**
Normal Sciatic nerve	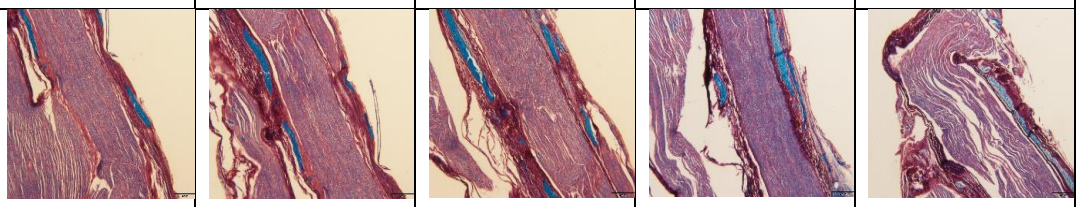				
Autologous	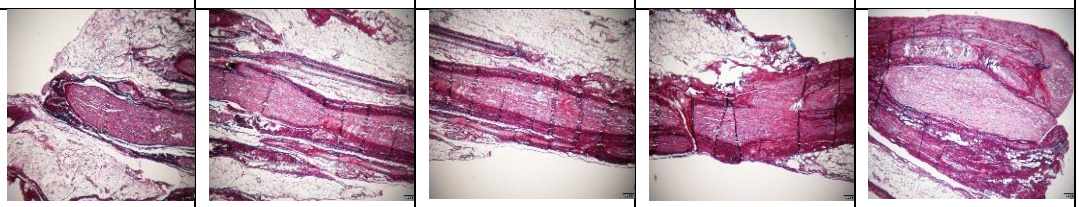				
PCL+GO	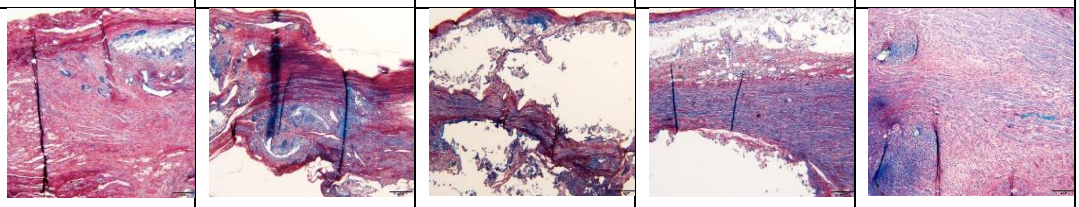				
PCL+ GO+hADSC	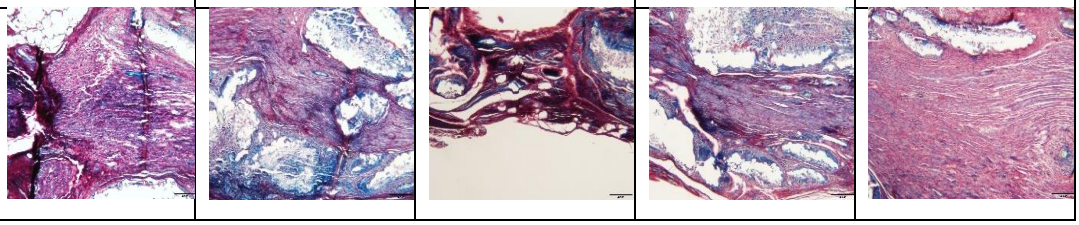				

Figure 4.5 Week 12 MCOLL staining

Note: Extracted nerve repair groups at 5 primary regions along the sciatic nerve gap.

4.3.4 Luxofast Blue Coverage/Myelin Diameter

20x magnification MCOLL images at all areas of the longitudinal histology sections excluding the distal areas were used to assess luxofast area coverage. A lack of luxofast blue staining present at the distal stump for all tissue sections besides the normal sciatic nerve tissue is most likely due to new nerve growth not having reached the distal stump by 12 weeks of nerve repair in the nerve wrap groups. 20x images from the proximal region to the distal center region was processed thru ImageJ to grey scale luxofast blue to determine its area coverage across each of these regions as a positive stain for myelin tissue (**Figure 4.6**). 5 random areas in each 20x image was selected for luxofast blue area coverage. This resulted in a total of 20 data points for 1 histology section from each repair group with no replicates. (**Figure 4.7**).

Results showed that the normal sciatic nerve had the highest luxofast blue stain coverage across the entire span of the tissue section indicating a potential large presence of myelin tissue in native Lewis rat sciatic nerves. The Gold standard autologous group showed significantly lower levels of luxofast blue coverage at 12 weeks repair compared to all other groups tested. PCL+GO and PCL+GO+hADSC experimental nerve wraps showed luxofast blue coverage significantly greater than the autologous group with the PCL+GO groups showing coverage comparable to that of the native nerve tissue.

40x magnification MCOLL images from 3 selected areas of the longitudinal histology sections excluding the distal area was selected for the presence of intense luxofast blue intensity organized into characteristic myelin sheath dimensions as described in previous studies using MCOLL staining on peripheral nerves. Using ImageJ, lines were drawn transecting the axons perpendicular to the axonal axis of the myelin sections. Diameters of myelin sections at their widest point were recorded at random areas in each 40x image to assess myelin thickness by 12 weeks nerve repair. This resulted in a total of 30 data points for 1 histology section from each repair group with no replicates. (**Figure 4.8**).

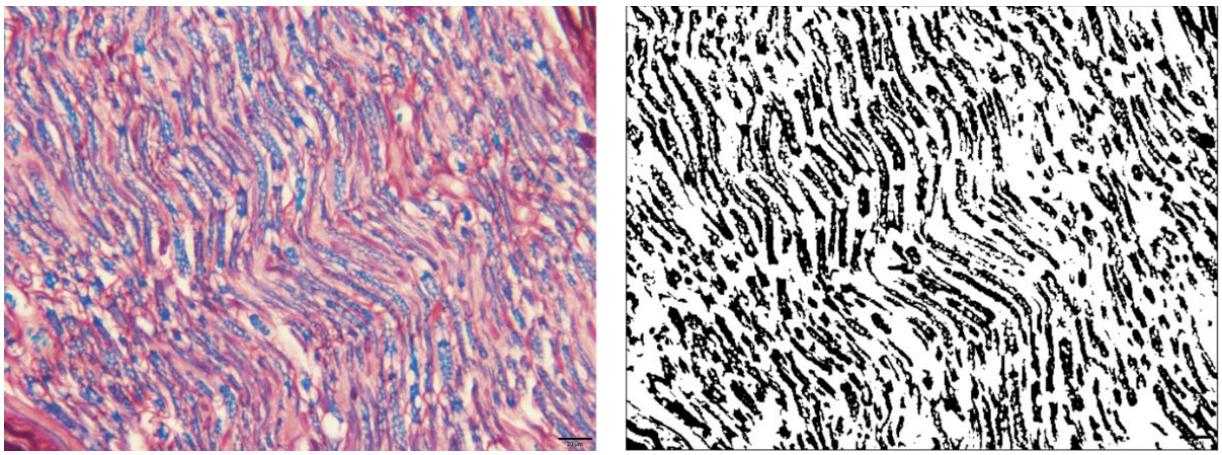

Figure 4.6 ImageJ grey scaling of luxofast blue staining of myelin sheath

Note: Quantified myelin area coverage for each group at week 12 extraction.

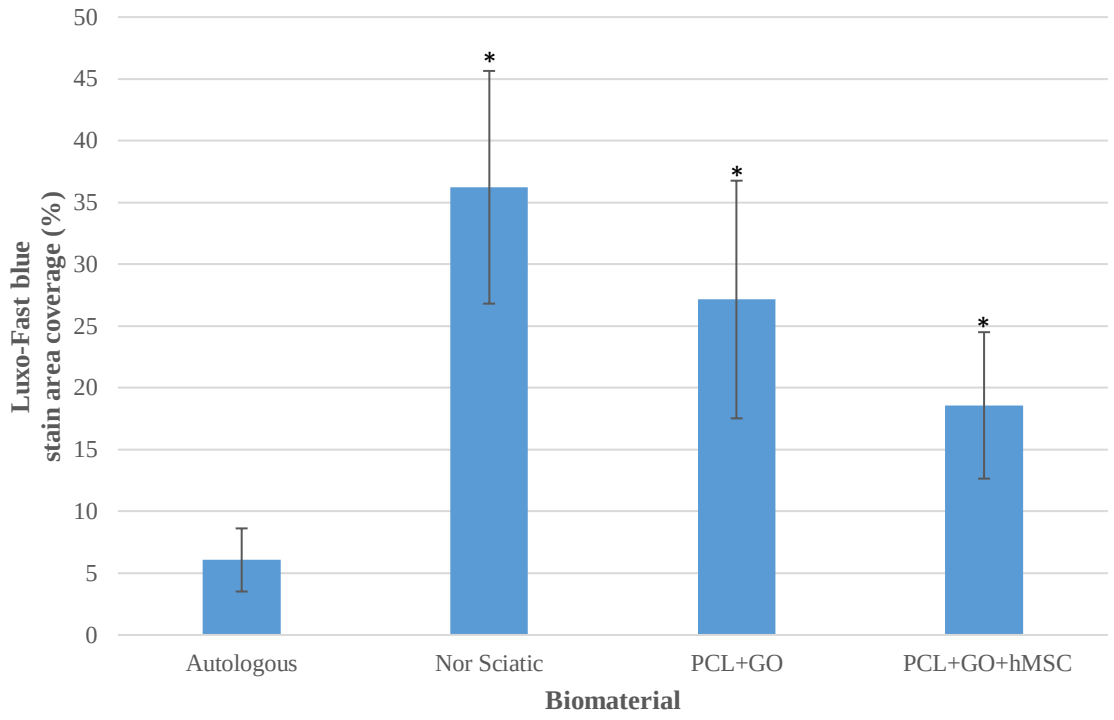

Figure 4.7 Luxofast Blue stain area coverage quantification spanning the neural defect at week 12

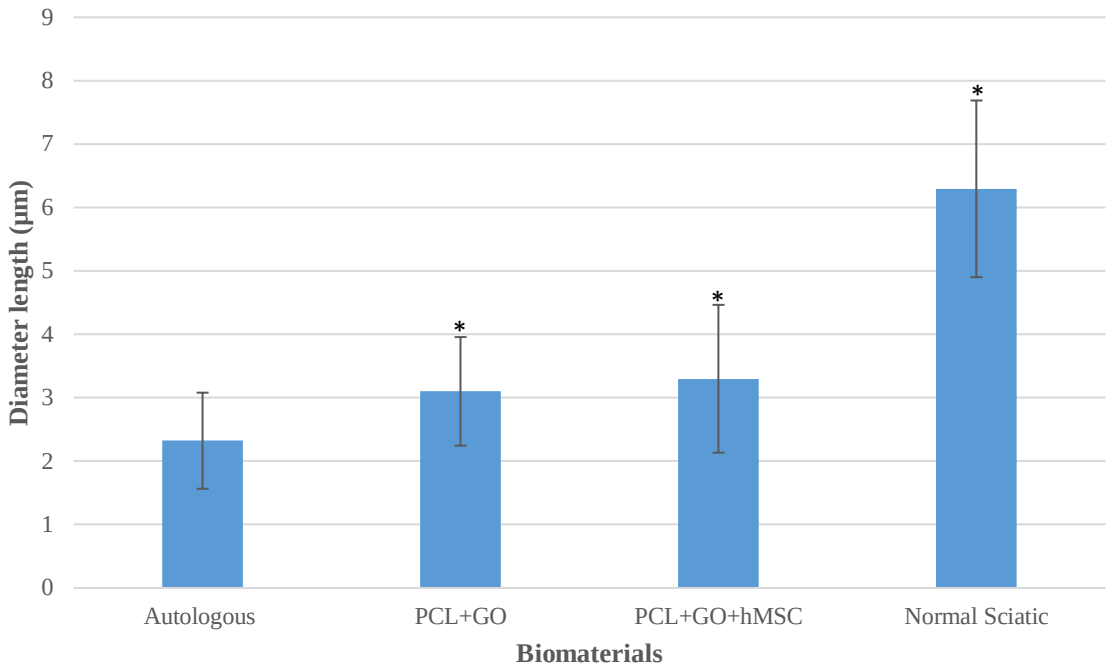

Figure 4.8 Myelin diameter assessment: tracking for presence of myelin tissue at week 12

Results showed that the normal sciatic nerve had the highest myelin sheath thickness compared to all other groups tested. The Gold standard autologous group showed significantly lower myelin thickness at 12 weeks repair compared to all other groups tested. PCL+GO and PCL+GO+hADSC experimental nerve wraps showed myelin sheath diameters significantly greater than the autologous group by week 12 with expected new immature myelin tissue to be in abundance around the experimental nerve wraps.

4.4 Discussion

3D PCL fiber meshes coated with GO were successfully created using slightly modified manufacturing protocols from previous *In-vitro* study. Films selected to support hADSC growth were confirmed to have cell culture growth thru DiI staining 24 hours prior to film implant. The study lost one Lewis rat due to complications during recovery.

Temporal data of rats did not show signs of significant changes during the 12-week period of nerve regeneration. Force distribution and surface area contact ratios between the right and left hind limbs were found to be significantly similar to each other at pre-surgery time points for all rodent groups. After sciatic nerve transection, the ratios for force distribution and surface area contact between the hind limbs was found to be significantly different to each other. These results show a similar pattern to Boyds study

involving transecting a section of the Sprague Dawley spinal cord that affected the right leg only and recorded both the pre-surgery and post-surgery changes in gait parameters for both hind limbs using the same system and software used in the study [6]. Results comparing surface area contact and body weight distribution between all experiment groups showed that by week 12 no group ratio values for either surface area contact and body weight distribution parameters was significantly similar to the base line ratios. This would suggest that the repair groups implemented to repair a 10 mm sciatic neural defect in Lewis rats did not reach full functionality by 12 weeks *In-vivo*

MCOLL staining of tissue sections showed positive staining on control normal sciatic nerve sections with clear tissue organization similar to that of previous longitudinal histology sections of peripheral nerves stained with MCOLL. This type of organization was also present along the regions of PCL+GO and PCL+GO+hADSC nerve wrap experimental groups. Identification of neural wrap tissue sections stained with luxofast blue, and picosirus red was not clear in all sample tissues stained. PCL+GO nerve wrap with and without the inclusion of hADSC showed nonspecific staining of other tissue components present in the neural defect that could not be identified at present. Peripheral nerve anatomy structures are not as pronounced as what is shown in normal sciatic nerve tissue sections. Autologous clinical gold standard showed minimal expression of luxofast blue staining across all regions indicating a potential lack of myelin tissue in new regenerating tissue by 12 weeks. High density of hematoxylin staining for cell nucleus is present in all experimental groups compared to the normal sciatic nerve groups most likely due to the intrusion of fibroblasts, Schwann cells, and macrophages to regulate endogenous nerve repair.

Quantitation of luxofast blue surface coverage in histology images showed normal sciatic nerves had the highest coverage of luxofast blue staining. This is most likely attributed to its abundance of mature and developed myelin sections present in the native peripheral nerves. Autologous showed the lowest coverage of luxofast blue, indicating that newly regenerated myelin sheath production has not started by week 12. The neural wrap design both with and without hADSC showed statistically greater coverage of the stain than the autologous group, with the neural wraps without hADSC cultures showing stain coverages almost comparable to that of normal sciatic nerve tissue. This would suggest that new myelin sheath production has started along the length of the neural wrap.

Quantitation of the diameter of myelin sections showed that normal sciatic nerves had the highest myelin sheath diameter sections. This is most likely due to that most of the myelin present in native sciatic nerve tissue is mature and well developed as a thick myelin sheath. Autologous showed the lowest myelin sheath diameter, indicating that newly regenerated myelin sheath production has not started by week 12. The neural wrap design both with and without hADSC showed statistically greater myelin sheath diameter sizes than the autologous group.

4.4.1 Implications/Challenges

Sciatic nerve defect model The selection of the animal subjects regarding strain of rats was initially using Sprague Dawley rats. However, these strains were found to be very susceptible to sensations in the hind limbs after transecting the sciatic nerve eventually leading to them self-mutilating their affected hind limbs in a behavior pattern known as autotomy. The study started out with 17 total Sprague Dawley rats following the protocols stipulated in IACUC# 2574-0318. 70.6% of the Sprague Dawley population was affected by autotomy behavior during different time points of the 12-week nerve repair. Multiple methods were considered to try and reduce the onset of autotomy behavior including the use of bitter apple and metronidazole coatings to dissuade biting at the effected hind limbs. These methods showed no indications of improving or preventing autotomy as the study progressed. It was decided to change the strain of the rat subjects to Lewis rats due to their recorded history of showing less autotomy behavior in neural defect models. 100% of the Lewis rat population showed no signs of autotomy throughout the entire duration of nerve repair.

Multiple passes were needed from each rat to achieve the required 5 successful walks to be assessed for gait analysis. The ease of handling of Lewis rats on the gait pressure mat could be improved if the rodents are given an extended period of time to adjust and trained to use the mat system to reduce the number of false walks or passes on the pressure mat during data collection. This can also be managed by making appropriate modifications to the pressure mat design by installing higher border sections at the sensel edges and smaller tunnel dimensions so that the rats can't walk off the mat or stand on their hind limbs while recording gait.

Histology While the MCOLL staining method did well in establishing the presence of new tissue growth in the biomaterial without any observable interference from the scaffold. The non-specificity of the stain makes it difficult to identify with confidence the types of tissue that stains with the MCOLL. Other more specific staining methods are needed to evaluate specific components of newly regenerated nerve tissue such as staining for specific myelin sheath protein 0 or specific axon protein markers β 3 tubulin, or GAP-43. Embedding aligned tissue sections in parafilm sections were made difficult by the thin film characteristics of the biomaterial. Longitudinal cuts of the tissue sections potentially missed large sections of tissue across the length of the neural scaffold. The additions of cross-sectional cuts would also assist in identifying the exact location of new tissue growth relative to the biomaterial. Multiple layered cuts of the tissue are needed in order to make a complete assessment of the materials potential for new tissue growth.

Histology assessment concerning data on stain intensity and tissue dimensions between different repair groups only looked at one tissue sample from each group. Need to assess the remaining tissue sections

stained with MCOLL as replicates to further improve the statistical confidence of the data. Current measurements concerning luxofast blue and myelin sheath diameter would not be publishable if they came from tissue sections of just one rat replicate. More specific measurements of the tissue sections dimensions such as tissue length and size will make locating regions on the tissue more precise as opposed to simply saying the proximal, or center region. This will also improve the precision of selecting areas in these regions for data measurements as opposed to saying the top left corner of the proximal region was assessed for myelin sheath dimensions. Quantitative intensity assessment of nonspecific luxofast blue staining was subjective with each image to maximize intensity of the myelin sections while minimizing the intensity of other nonspecific tissues stained with luxofast. This emphasizes the need to stain for specific markers rather than nonspecific surface properties to identify and measure tissues we expect to be present in regenerating nerves.

Manufacturing The initial PCL with GO surface coatings of this *In-vivo* study had similar characteristics to the PCL fiber meshes created in the manufacturing phases of the *In-vitro* study discussed in chapter 2. Similar to our discussions in this chapter, it also determined that the ease of handling these 3D biomaterials of similar fiber designs after being placed in a wetted environment was difficult to manage in both the initial assessment of visualizing hADSC cultures on the material surface after 24hours incubation and positioning the biomaterials in at the neural defect site during surgery. Slight modifications in the electrospinning protocol by reducing the voltage and reducing the distance of spinning produced PCL fiber meshes that were more rigid and less able to fold on itself making visualization and handling in surgical settings easier to manage.

Gait analysis The pressure mapping system detected differences in hind limb force distribution and surface area contact to assess the return of neural functions. As an acceptable indirect format for evaluating return of nerve function it is necessary to note that these results might not correlate well to more direct approaches to evaluating nerve function such as electrophysiology and histomorphometric analysis. One of the most common indirect methods for assessing nerve function in the sciatic nerve of rodents is the standard Sciatic Function Index (SFI). Studies have shown that the SFI is highly correlated to that of direct methods for assessing nerve function including histomorphometric analysis. It would be a beneficial component to this study to use SFI assessment in tandem with the Pressure mapping system to bridge the results of the gait analysis to that of the histology results to determine if a correlation is present.

The results from this study leave many questions concerning how the new tissue develops and grows at different time points and whether they correlate to the gait patterns at these time points as well during the nerve repair cycle. This suggests that the design of this experiment should be altered to euthanize a number of rodents from each group at different time points during the 12-week period to establish a more accurate

assessment of the how the new tissue grows on the nerve wrap and see if a correlation exist between the growth pattern and the gait pattern. It might also be prudent to extend the period of nerve repair to a further time period to see if the gait pattern of or neural wraps will eventually become significantly similar to the baseline values that would indicate a return of full functionality of the sciatic nerve.

It is also unclear what impact that hADSC therapy had at repairing the critical nerve defect in rats when cultured onto the neural wrap design. It is expected by week 12 that the exogenous hADSC cultures will have been removed by the rat physiology, but no clear indications of the cells impact at the injury site are obvious when assessing both gait and histology data. As suggested before it might be beneficial to divide rats in each group to be euthanized at early stages of nerve repair to increase the chances of observing how these cells respond in this type of environment and what immediate or lasting impact they might have on the repair of neural defects. If future studies plan to move toward this setup, it is imperative that methods for tracking these cell cultures *In-vivo* are utilized and careful extraction of the tissue so as to not disrupt any remaining live cells for analysis, such as staining for specific human markers to differentiate between cells of human origin from native exogenic tissue. The decision to keep cell cultures allogenic or exogenous must also be considered as is likely that allogenic cultures will survive longer and provide more therapeutic effects at the injury site compared to exogenous therapy.

4.5 Conclusion

We have described the first initial set of *In-vivo* data supporting our hypothesis as a step towards further developing synthetic 3D PCL fiber GO coated wraps for consideration into clinical trials. Our assessment determined that PCL platforms of thin film nano-fibers surface coated with GO in combination with or without hADSC line cultures were capable of supporting new tissue that mimics closely in tissue layering and orientation to that of native peripheral nerve tissue at different areas of the neural scaffolds. Indirect gait analysis of the rats over the period of recovery showed significant differences in the gait of the rats after transection of the sciatic nerve in terms of weight distribution and surface area contact ratios between the hind legs. By week 12 of neural repair, all repair groups showed significant differences in weight distribution and surface area contact ratios compared to the pre-surgery baseline values, indicating full recovery of sciatic nerve defects had not been reached by week 12. Pressure map systems cannot discern the potential implication of asymmetrical pattern and behavior inherent in complex physiological systems. To determine if this data is dependent or not on the nerve injury induced in the rats, the end period time point should be extended to a later date to see if these patterns persist or subside according to what is expected. Direct histochemical staining of each group confirmed the presence of new tissue at multiple sites along each neural scaffold tested. New tissue showed areas of similar organization to that of native sciatic

nerve tissue. Neural wraps had additional tissue growth that were non-specific to the MCOLL stain making areas of the tissue difficult to clearly differentiate organization that is expected in native neural tissue. All iterations of the nerve wrap showed signs of extensive growth thru the scaffolds at 12 weeks of neural healing, with potential signs of early myelin sheath production occurring along the length of the material compared to the gold standard autologous.

The results of this study suggest that PCL fiber meshes with GO surface coatings with or without the addition of hADSC cultures were successful in supporting new tissue growth and possibly assisting in guidance of new tissue across the peripheral nerve defect. Based on our histochemical nonspecific staining for myelin and collagen tissue in native peripheral nerve and the organization of this tissue leads us to suggest that the new tissue is most likely new peripheral nerves that are extending from the proximal stump with endogenous repair and support being provided by the neural wraps. It is suggested that the next phase of *In-vivo* assessments use the same rodent small animal model but extend the time of the study to ensure that new tissue reaches the distal stump, with the addition of other direct methods for assessing neural function such as electrophysiology and staining for more specific nerve markers. These additions should help us determine with a higher degree of confidence that the new tissue is in fact new peripheral nerves and whether it is active nerve segments capable of propagating their own electrical signals without assistance. This should also determine if we can correlate the pressure map system data to that of data established from direct methods for assessing neural function as new neural tissue reaches the distal stump. Further studies may involve making alterations to these scaffold designs such as improving tracking of hADSC cultures *In-vivo*, better techniques for improving the amount of MSC seeded to the PCL platforms, and improving material mechanics of neural wraps to prevent material collapse when it is wetted.

References

1. Yurie H, Ikeguchi R, Aoyama T, Kaizawa Y, Tajino J, Ito A, et al. The efficacy of a scaffold-free Bio 3D conduit developed from human fibroblasts on peripheral nerve regeneration in a rat sciatic nerve model. PLoS One. 2017;12: e0171448.

2. Niu Y, Li L, Chen KC, Chen F, Liu X, Ye J, et al. Scaffolds from alternating block polyurethanes of poly(ε-caprolactone) and poly(ethylene glycol) with stimulation and guidance of nerve growth and better nerve repair than autograft. J Biomed Mater Res A. 2015;103: 2355–2364.

3. Sabri F, Gerth D, Tamula G-RM, Phung T-CN, Lynch KJ, Boughter JD Jr. Novel Technique for Repair of Severed Peripheral Nerves in Rats Using Polyurea Crosslinked Silica Aerogel Scaffold. J Invest Surg. Taylor & Francis; 2014;27: 294–303.

4. Nepomuceno AC, Politani EL, Silva EG da, Salomone R, Longo MVL, Salles AG, et al. Tibial and fibular nerves evaluation using intraoperative electromyography in rats. Acta Cir Bras. 2016;31: 542–548.

5. Carriel V, Garzón I, Alaminos M, Campos A. Evaluation of myelin sheath and collagen reorganization pattern in a model of peripheral nerve regeneration using an integrated histochemical approach. Histochem Cell Biol. 2011;136: 709–717.

6. Boyd BS, Puttlitz C, Noble-Haeusslein LJ, John CM, Trivedi A, Topp KS. Deviations in gait pattern in experimental models of hindlimb paresis shown by a novel pressure mapping system. J Neurosci Res. 2007;85: 2272–2283.

Chapter 5: Conclusions

5.1 Final Remarks

This body of work represents the careful steps and assessments required to determine proof of concept and functionality in the early stages of developing novel tissue engineering devices. This study has resulted in the successful manufacturing of a neural wrap material composed of electrospun nanofiber PCL matrices with surfaces modified by thin coating GO films by air spray methods to support hADSC therapies. This design was pursued in an attempt to address the problem of inadequate repair of critical size defects in the peripheral nerves of trauma patients. The design was created to function as a conduit bridge across the defect gap that will deliver hADSCs to the site of injury while guide and stimulate early axon regeneration that would culminate in early and or improved tissue repair. Early *In-vitro* studies showed that this biomaterial was biocompatible to MSC cultures and could support hADSC cultures for up to 6 days in culture while hADSCs were artificially stimulated towards neural-like lineages. To assess the *In-vivo* potential of this biomaterial design a rat sciatic nerve defect model that simulates a critical size neural defect expected in patients with severe neurotmesis was utilized. The wraps were sutured to the defect site and left *In-vivo* for 12 weeks to provide assistance in repairing of the neural defect. At 12 weeks it was found that the wraps could support and guide new tissue growth along the longitudinal axis of the neural defect site both with and without hADSC cultures. This suggests that nanofiber PCL+ GO surface coating material iterations might be a suitable candidate for further preclinical studies in developing biomaterial wraps designed to assist in critical nerve defect repairs.

While this material has shown great potential in supporting new tissue growth *In-vivo*, further preclinical studies are needed to determine the materials effectiveness at specifically supporting and stimulating growth of axons as a targeted therapy approach. This involves tweaking the design of the material based on the suggested improvements and complications addressed in the *In-vivo* study, and altering the experimental design of the *In-vitro* tests to address the complications noted there. Of primary concern is to determine what type of therapy hADSC cultures have during the initial stages of nerve repair and whether their presence significantly improves or has a neutral or insignificant affect on neural regeneration. By carefully considering the appropriate neural cell line to co-culture with hADSCs and further control for specific extracellular compounds present during endogenous nerve repair, we can see how hADSC cultures will behave as an early look at what types of therapy effects hADSC cultures might express *In-vitro*. In the *In-vivo* study if we euthanize rats at earlier time points, we might be able to track the stem cells as the new nerve tissue regenerates. We can also use this time to look for specific neural markers expressed during axonal growth and improve techniques in handling rodent subjects during gait analysis and techniques for extracting and embedding neural tissue samples for histology slides.

One other complication of concern is determining whether the gait parameters measured during the *In-vivo* study can be correlated to the histology results at their respective time points. By using in conjunction to our pressure mat another indirect method that has been well established as having a high correlation to histology results when assessing a return of nerve function, there would be a greater chance of establishing a correlation pattern if one exists. The Sciatic Function Index (SFI) method is the most commonly used and reported method in conjunction with histomorphology results, with a high record of these reports stating a high correlation to histology results.

As I conclude this study, I am reminded of the prodigious responsibility that tissue engineers owe to the people we serve. While it is often enough to simply follow the standards and guidelines of assessing new devices, I feel it is our obligation to remind ourselves to why we follow them. Medical devices are some of the most dangerous items available to the market. A device specifically engineered to function with or within a system that is not yet fully understood, where stimulation from a medical device can cause a cascading effect that if not corrected could have severe acute or long-term effects on a person's health or wellbeing. These standards are in place more so to protect the customers who trust that our products will target to resolve their immediate or future medical related problems without causing complications in the form of new medical problems. As engineers, scientist, researchers, and inventors it is our duty to discover, create, and seek out new and innovative ideas/products out of the public's interest or our own, but I feel that it is our responsibility to always actively seek out and pursue faults in our ideas and designs. This is more relevant today than in any other period in history for developing medical devices. With the rate at which new technologies are being developed comes the need to revise the current standards to assess how these new technologies will impact the public's health should they be used in developing new medical devices. By critiquing ourselves, we indirectly proclaim to the public that it is in our concern for their wellbeing as the reason why we develop medical devices in the first place. This will only further our creed to create devices that will improve the public's wellbeing and thus further solidify the public's trust in us.

Vita

Richard Conlin Steiner was born in Knoxville TN, to the parents of Lori and Henry-York Steiner. He is the first of two sons and one daughter: Mitchell and Madison. He attended Olive Chapel Elementary school and continued into Apex High School in Apex NC. After graduation, he attended East Carolina University in Greenville NC, where he pursued a degree in biomedical engineering. Richard was involved in an undergraduate research project dealing with biomaterial and electrospinning mechanisms with Dr. Muller-Borer during his undergraduate studies, which furthered his interest in biomaterials and regenerative medicine. He obtained a bachelors of technology degree from University of East Carolina on May 2014, in biomedical engineering. He accepted a research assistantship from the University of Tennessee, Knoxville from the Comparative and Experimental Medicine program thru the UTCVM department. Richard graduated with a Doctoral of Philosophy in Comparative and Experimental Medicine in August 2019. He further plans to pursue research opportunities in industry involving regenerative medicine therapies.